MODELING AND OPTIMIZATION OF

FLOW-INDUCED CRYSTALLIZATION

IN POLYMER PROCESSING

By

TSUNG-CHIEH TSAI

Bachelor of Science
National Taiwan Institute of Technology
Taipei, Taiwan
1989

Master of Science
Oklahoma State University
Stillwater, Oklahoma
1992

Submitted to the Faculty of the
Graduate College of the
Oklahoma State University
in partial fulfillment of
the requirements for
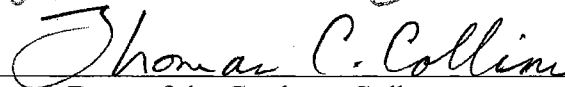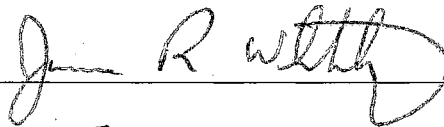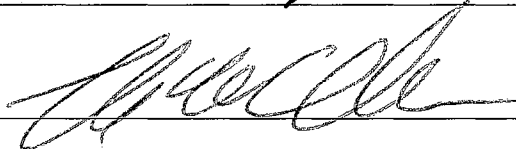the Degree of
DOCTOR OF PHILOSOPHY
July, 1997
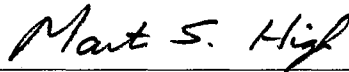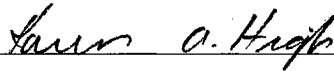
Theni
1997D
1877M

MODELING AND OPTIMIZATION OF

FLOW-INDUCED CRYSTALLIZATION

IN POLYMER PROCESSING

Thesis Approved:

_____
Thesis Advisor

_____

Marat S. High

_____

_____

_____
Dean of the Graduate College

ii

ACKNOWLEDGMENTS

TABLE OF CONTENTS

LIST OF TABLES

LIST OF FIGURES

Figures   Pages

LIST OF SYMBOLS

Roman Letters

a, b, c, d, e, f velocity components

A   Helmholtz free energy

E   maximum depth of the potential well

f_m shape factor

$f(\underline{x})$ objective function

G   linear growth rate

ΔG Gibb's free energy change

$\mathcal{H}$ Hamiltonian

ΔH enthalpy change

h   half-height of the flow cavity

II   second invariant

J   normalization constant

k   Boltzmann constant, 1.38×10^{-6} erg molecule^{-1} $^{\circ}$K^{-1}

K   growth rate

K   Avrami coefficient

L   length of the dumbbell

L   Lagrangian

M   nucleation rate

m	power-law pre-factor
$\tilde{N}$	Avogadro's number
O_x	orientation parameter with respect to the x-direction
P	pressure, dyne/cm^2
P	penalty function
P_n	the Legendre polynomial
$P_n^m s_m$, $P_n^m c_m$	spherical harmonics
r_{sep}	separation distance from the bead in the crystal
t	(present) time, s
S	flow conductance
ΔS	entropy change
S_x	relative x-direction strength
T	absolute temperature, °K
u_i	Lagrange multiplier for inequality constraints
u_x	velocity in x-direction, cm/s
u_y	velocity in y-direction, cm/s
u_z	velocity in z-direction, cm/s
u_r	radial velocity, cm/s
u_θ	radian/s
u_ϕ	azimuth velocity, radian/s
v	velocity in y-direction, cm/s
V_{avg}	average velocity at the entrance of diffuser

w_i Lagrange multiplier for equality constraints

W half width of the slit

W_1 entrance height of the diffuser

W_2 exit height of the diffuser

We   Weissenberg number

x, y, z   Cartesian coordinates, cm

z   past time, s

Greek Letters

δ_{ij} Kronecker delta

ϕ spherical azimuthal angle

ϕ_c crystal volume fraction

ϕ_∞ crystal volume fraction at infinite time

$\dot{\phi}$ time derivative of ϕ coordinate

$\dot{\gamma}$ shear rate, s^{-1}

Γ intermolecular potential

Γ_w wall boundary

Γ_I entrance boundary

Γ_C center line boundary

Γ_O exit boundary

η shear viscosity

η_s solvent shear viscosity

$[\eta]_0$ zero-shear-rate intrinsic viscosity

κ characteristic strain rate

λ time constant for the dumbbell, $\varsigma L^2/12kT$

λ step length

Λ linear operator, defined as $\left(\dfrac{\partial}{\partial \underline{u}} \cdot \dfrac{\partial}{\partial \underline{u}} \right)$

μ viscosity, g/cm·s

ν activation frequency

θ spherical polar angle

$\dot{\theta}$ time derivative of θ coordinate

Θ_i flow factor

ρ density, g/cm^3

σ distance at which potential is zero

σ_x x component of total normal stress

σ_i slack variable

ψ configurational probability distribution function

ψ_c probability of finding a molecule in the lattice site

ψ_ϕ probability of the molecule falling into the lattice site

Ψ_1 first normal stress coefficient

Ω_s linear operator for shearing flow

Ω_e linear operator for elongational flow

ζ friction coefficient

Vectors

$\underline{d}$ change in variables

$\underline{F}^{(h)}$ hydrodynamic force

$\underline{F}^{(b)}$ Brownian force

$\underline{F}^{(e)}$ external force

$\underline{g}$ difference in gradients

$\underline{n}$ outward normal unit vector

$\underline{r}_v$ position vectors at beads v with respect to a fixed arbitrary point

$\underline{R}_v$ position vectors at beads v with respect to the center of mass of molecule

$[\![\underline{\dot{r}}_v]\!]$ the momentum-space averaged velocity at bead v

$\underline{s}$ unit vector in the θ direction

$\underline{S}$ search direction vector

$\underline{t}$ unit vector in the ϕ direction

$\underline{u}$ unit vector in the r direction

$\underline{\dot{u}}$ time derivative of unit vector $\underline{u}$

$\underline{\delta}_r, \underline{\delta}_\theta, \underline{\delta}_\phi$ unit vectors in spherical coordinate system

$\underline{\delta}_x, \underline{\delta}_y, \underline{\delta}_z$ unit vectors in rectangular coordinate system

$\underline{x}$ variable vector

$\underline{\nabla}$ gradient

Tensors or Matrixes

$\underline{\delta}$ unit tensor

$\underline{\delta}_i\underline{\delta}_j$ dyadic product

$\underline{\zeta}$ friction tensor

$\underline{\underline{\kappa}}$ transpose of velocity gradient tensor, $(\underline{\nabla}\underline{v})^{\dagger}$

$\underline{\underline{H}}$ Hessian of the objective function

$\underline{\underline{B}}$ approximated Hessian matrix

CHAPTER I

INTRODUCTION

Variations in polymer processing can impart different polymer microstructures that can lead to different physical properties. Commonly processed polyethylene (PE) is very weak, while drawn PE is at least 3 orders of magnitude stronger as is shown in Table I. Polymeric materials can have the strength and stiffness to rival steel if the material is properly processed. The usual design procedure of a polymer part is to process polymeric materials under given sets of conditions, obtain samples and measure the physical properties. The selection of the proper material/process combination for a needed part is found empirically. The advantage of computer analysis tools would be to avoid expensive make-test-redesign cycles on a component. However, the iterative experimental approach cannot be totally superseded by the computer tools because the microstructure of the polymer is difficult to predict.

Polymer molecules typically consist of a large number of carbon atoms successively bonded together by strong covalent bonds to form long chains. The configuration of the polymer chain determines the bulk strength. For commonly processed polymers, Folded Chain Crystals (FCC) are formed from randomly coiled polymer chains as shown in Figure 1a. For a drawn polymer, Extended Chain Crystals (ECC) are formed

TABLE I

MATERIAL STRENGTH

Material	Tensile Modulus (Gpa)[*]	Breaking Strength (GPa)[*]
Steel	210	1-4
Commonly Processed PE	1-7	0.001
Drawn melt-crystallized PE fibers	70	1
Drawn PE gel fibers	120-220	3-6
Drawn single crystal mat of UHMWPE	200	6
Theoretical limit for PE	240-250	35

[*] $1 \text{ GPa} = 1.45 \times 10^5 \text{ psi}$
Collyer and Clegg (1986)

from the extended and highly oriented polymer chains during the drawing process as shown in Figure 1b.

The anisotropic mechanical properties are intimately related to the orientation of the extended polymer molecular crystals. During the crystallization process, the crystallization rate of ECC is greater than FCC, due to the fact that the aligned molecules diffuse to the lattice sites more readily. Notwithstanding the improvement in mechanical properties in one direction, there is also a simultaneous reduction in strength in other directions. Hence there is a need to optimize the extent and direction of flow-induced crystallization.

The research efforts in the field of flow-induced crystallization at Oklahoma State University focused on three different aspects of the crystallization process. These areas are experimental characterization, development of a mechanistic predictive model and optimization of die geometry using information from the experiment and the model.

3

Quiescent   Oriented

drawing

Folded-Chain Crystal
(Spherulites)

Extended-Chain Crystal
(Row-nucleated)

(a)   (b)
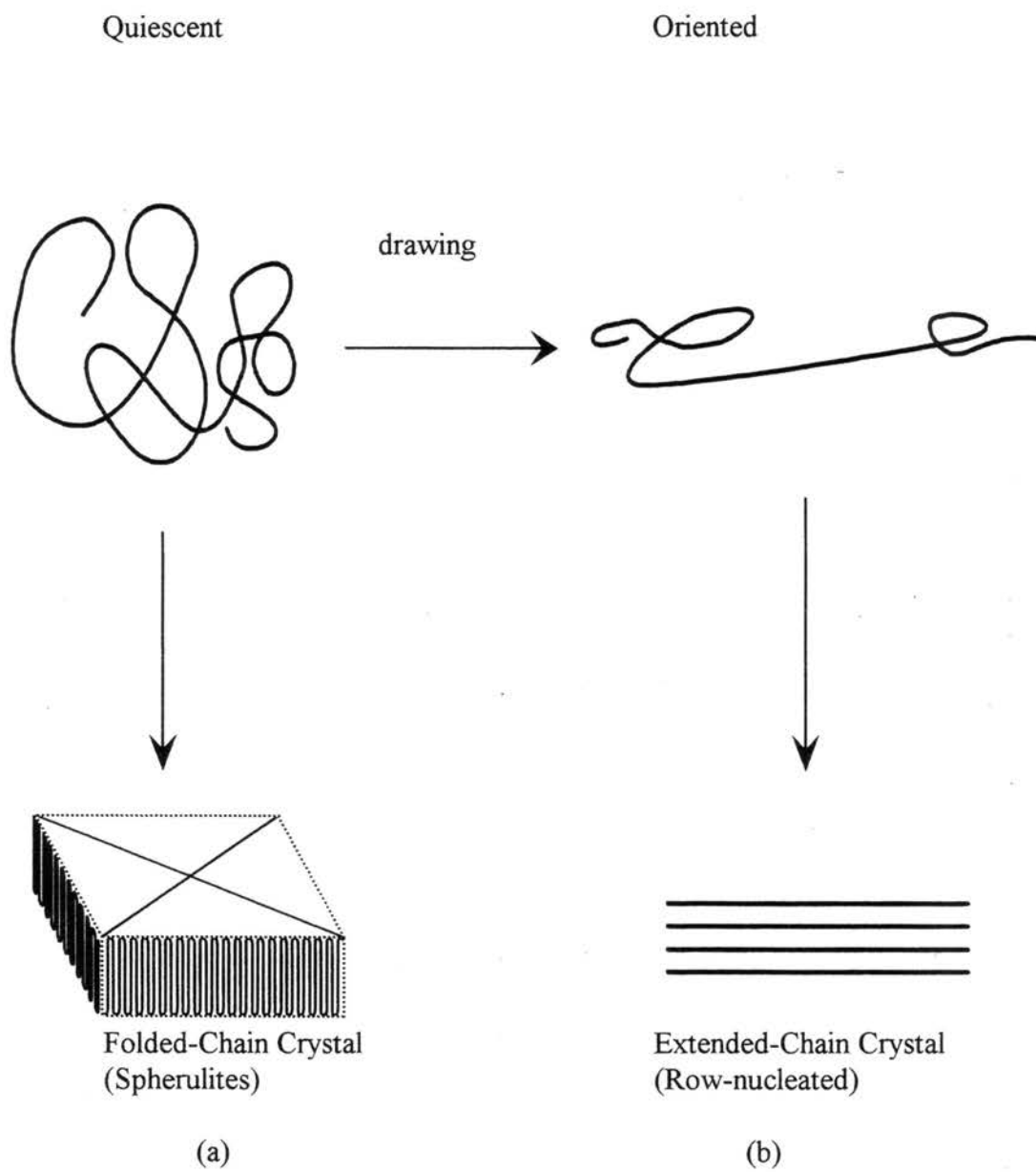
Figure 1. The Crystallization Process (Spevacek, 1989)
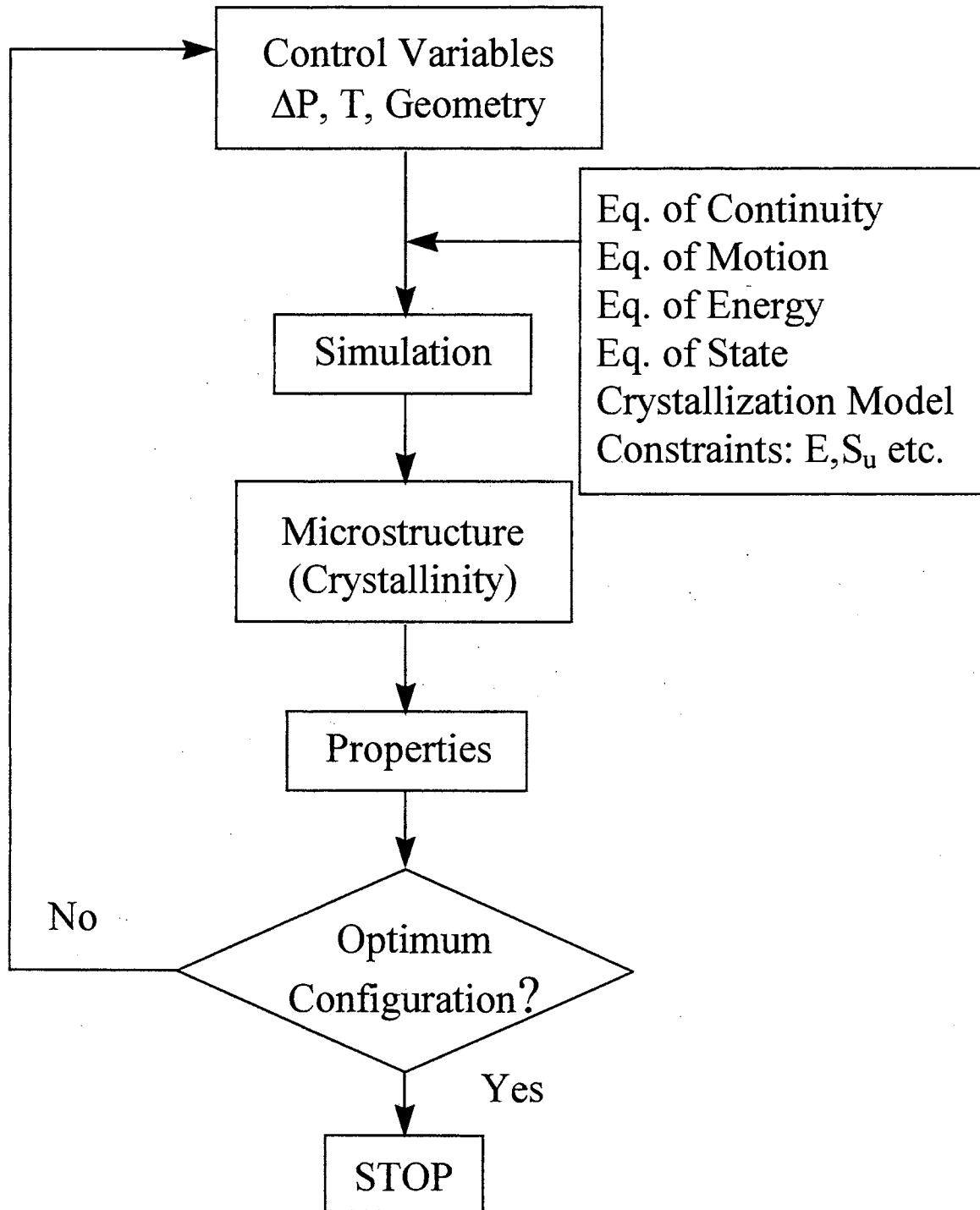
Figure 2. Flow Chart of Material Properties Optimization

Figure 2 shows an algorithm which describes the different sections of the research project and how they are related. The ultimate objective as shown in Figure 2 is to develop an optimization package for polymer processes that can produce an extended chain crystal structure in commonly encountered polymers.

The first step is to develop a model based on polymer kinetic theory that would predict molecular configurations since one of the goals of this thesis is to predict the microstructure by understanding the flow-induced crystallization process. With a better understanding of the crystallization process, the polymer properties can be modified by changing the processing parameters, such as die geometry, pressure, strain rate, strain and temperature. The extent of model development in this effort includes steady state predictions of molecular configurations for different flow fields. A fundamental flow dependent crystallization model was developed that is mathematically tractable, but still incorporates the basic features of more sophisticated models.

Polymer molecules can be simply represented by dumbbells which have two beads joined by a weightless rod. One end of the dumbbell is in the amorphous melt and the other end is in the crystal lattice. The probability of the dumbbell being in a certain orientation can be obtained by kinetic theory. The crystal will form if the bead in the amorphous melt is close enough to the next available lattice site. The number of crystals formed will determined the rate of crystallization. The dynamic modeling of the crystallization process is part of an ongoing research effort in a parallel project and will be eventually combined with the optimization techniques described in this thesis. The next step and the most significant achievement in this thesis is to use the model in conjunction with the equations of continuity and motion to optimize die design by systematic searching

for a specified objective function. This requires the simultaneous solution of the flow field, coupled with the molecular model and an optimization algorithm. General solution routines were readily available for determining the flow field and for this thesis the Fluid Dynamics Analysis Package (FIDAP) was used.

Optimization strategies have been developed for many industrial processes, such as chemical engineering processes, but have only recently been applied to polymer die design. One of the problems involved in die design is that the design variables are defined on the domain and/or boundary. The difficulties in shape optimization arise from the fact that the objective function usually cannot be explicitly expressed in terms of the design variables, especially for field problems.

Several optimization approaches have been conceived and implemented to minimize computational resources (Barone and Caulk, 1982, 1985; Shyy *et al.*, 1988; Braibant and Fleury, 1985; Baysal and Eleshaky, 1992; Braibant and Fleury, 1985; Çabuk and Modi, 1990, 1992). However, the time and effort for developing and solving most polymer processing problems are enormous. The advances made in the use of computer techniques and numerical methods have made the computational problem tractable though a significant effort is still required in developing the program. Nowadays, optimization strategies developed for industrial processes are being used in die design with little regard for computational resources since research in this field is still in its infancy.

In this thesis, the Successive Quadratic Programming by the Han-Powell (SQPHP) technique (Chen and Stadtherr, 1983, 1984) was used to optimize the die geometry for a typical extrusion process. Having obtained the microstructure from the model, the optimization routine will seek the best possible die geometry for specified degrees of

strength or anisotropy in two directions. Thus, the process of flow-induced crystallization can be exploited to improve mechanical properties in one direction without sacrificing too much in the other direction. Thus, this thesis will for the first time, incorporate both flow-induced crystallization and optimization principles into die design.

The organization of the thesis is as follows. Chapter 1 (this chapter) provides a brief introduction to flow-induced crystallization, polymer modeling and optimization and the specific objectives of this work. Chapter 2 describes these principles in more depth with reference to the current state of knowledge. A background of the types of models and optimization methods is also included in Chapter 2. Chapter 3 shows the mathematical derivation of the model and the development of the optimization algorithm along with relevant boundary conditions and optimization parameters. Chapter 4 provides the results obtained from various simulations with some discussion and interpretation. Finally, in Chapter 5, the work in this thesis is summarized, some conclusions are drawn and recommendations are made for future work.

CHAPTER II

BACKGROUND

This chapter provides a description of the fundamental principles involved in polymer kinetic theory, flow-induced crystallization kinetics and the theory of optimization. In the following discussion, emphasis has been given to how kinetic theory is used in flow-induced crystallization models. The optimization theory focuses on nonlinear programming and polymer processing optimization.

Kinetic Theory

Kinetic theory is a branch of statistical mechanics which is the science of determining macroscopic material properties from a microscopic or molecular point of view (Bird *et al.*, 1987b). Unlike continuum mechanics, the local material properties (e.g., density, velocity, and energy) are not continuous functions of space and time. Kinetic theory recognizes forces acting on individual molecules and characterizes the resultant motion of molecules. Equation of state and transport properties of gases and liquids are intimately related to the forces that exist between the molecules. Expressions for the bulk properties in terms of molecular properties and intermolecular forces can be obtained from statistical mechanics (Volkenstein *et al.*, 1963; Flory, 1969; McQuarrie, 1976). These expressions, along with information about intermolecular interactions, may be used to

predict the values of many physical properties for which no experimental data are available. Therefore, a model based on kinetic theory is very versatile and usually has more physical significance.

When statistical mechanics originally emerged in the 19th century, it mainly focused on equilibrium systems and hence was also called statistical thermodynamics (Poisson, 1809). Due to mathematical difficulties, statistical thermodynamics could only deal with ideal monatomic (Philippoff, 1935; Kennard, 1938; Hougen and Watson, 1947), diatomic and polyatomic gases (Wilson, 1959), monatomic crystals (Barnes, 1932; Kittel, 1956), and chemical equilibrium constants (Rittenberg *et al.*, 1934; Gould *et al.*, 1934; Guggenheim, 1941).

In the late 1960's and early 1970's, the introduction of computers and numerical calculations made the application of kinetic theory to the study of simple dense fluids and systems of ionic solutions practical (Rasaiah and Friedman, 1968, 1969; Rasaiah, 1970ab). At the same time, the study of non-equilibrium systems started gaining momentum (Bird *et al.*, 1969; Bird *et al.*, 1971). Kinetic theory has since been successfully used in the development of rheological equations of state (Wedgewood and Bird, 1988; Wiest *et al.*, 1989; Ng and Leal, 1993; Manke and Williams, 1991, 1993; Bird and Wiest, 1995), in Brownian dynamics simulations (van den Brule, 1993a; Öttinger, 1993; Hua and Scheiber, 1996) and in microrheological modeling of heat conduction (van den Brule, 1993b). Other potential applications include the determination of optical, electrical and diffusional properties, and the development of virial and hypervirial theorems (Bird and Wiest, 1995).

One example of the successful application of kinetic theory as mentioned before, is in the development of constitutive equations for dilute polymer solutions (Bird *et al.*,

1987b). The constitutive equation is obtained by construction of the stress tensor which connects rheological behavior and fluid dynamics. The contributions of the stress tensor are from both solvent and the presence of polymer molecules. Usually, the solvent is a low molecular weight substance and a Newtonian equation will be enough to describe the system. The polymer contribution can be from intramolecular forces, intermolecular forces and the bead motion.

Depending on the nature of the macromolecule, the polymer can be modeled as two beads joined by a weightless rigid rod (i.e., a rigid dumbbell model), such as isotactic polypropylene, poly-n-butylisocyanate, proteins in helical forms, DNA in its helix configuration, and tobacco mosaic virus. Rigid dumbbell models account for the orientability of the polymer molecules in flow fields and ignore the molecular stretching and bending motions (Kuhn, 1932; 1933; Kuhn and Kuhn, 1945). The stretching motion of a molecule can be modeled by two beads joined with an extensible spring, i.e., an elastic dumbbell model (Hermans, 1943; Fraenkel, 1952). Bending motions have to be modeled using more than two beads, such as multibead-rod (Kramers, 1944; Kirkwood, 1967) and bead-spring chain (Rouse, 1953; Zimm, 1956) models.

During the forming of the stress tensor, the Configurational Distribution Function (CDF) is needed. The CDF gives the probability of finding the molecular in a certain orientation. For equilibrium systems, the CDF expression can be easily obtained from equilibrium statistical mechanics (Tolman, 1938; Mayer and Mayer, 1940). For a non-equilibrium system, the CDF can be obtained from a force balance among hydrodynamic drag, Brownian, intramolecular, and other forces.

Assumptions for simplifying the mathematical manipulation are necessary during the derivation of the CDF and stress tensor. The most common assumption in kinetic theory is that the velocity distribution is Maxwellian about the mass-average velocity of the solution which is the same as the velocity distribution of a solution at equilibrium (Tolman, 1938; Mayer and Mayer, 1940). One example of a Maxwellian distribution is the Maxwellian velocity distribution for the elastic dumbbell, and is shown below:

$$\Xi_{eq}\left(\dot{\underline{r}}_1, \dot{\underline{r}}_2\right) = \frac{\exp\left\{-\frac{1}{2}\left[m\left(\dot{\underline{r}}_1 - \underline{v}\right)^2 + m\left(\dot{\underline{r}}_2 - \underline{v}\right)^2\right] / kT\right\}}{\int_{-\infty}^{\infty}\int_{-\infty}^{\infty}\exp\left\{-\frac{1}{2}\left[m\left(\dot{\underline{r}}_1 - \underline{v}\right)^2 + m\left(\dot{\underline{r}}_2 - \underline{v}\right)^2\right] / kT\right\}d\dot{\underline{r}}_1 d\dot{\underline{r}}_2} \qquad (2\text{-}1)$$

where:

m = mass of the bead,

$\underline{v}$ = mass-average velocity of the solution,

$\dot{\underline{r}}_1, \dot{\underline{r}}_2$ = velocity of beads 1 and 2, respectively,

k = Boltzmann constant,

T = temperature.

Note should be made that in this study, an underlined quantity is a vector, a doubly underlined quantity is a tensor, and a quantity with an overhead dot is a time derivative. The Maxwellian velocity distribution for an elastic dumbbell can be considered as the product of two normally distributed bead velocities which have the same variance, m / kT, about the mass-average velocity of the solution. The Maxwellian velocity distribution assumption would simplify the expression for the Brownian force term in the CDF and the contribution from the bead motion in the stress tensor. Another assumption for dilute solutions is to neglect the hydrodynamic interaction effect, which is caused by the flow

field disturbance due to the motion of the polymer molecule through the solvent. The

hydrodynamic interaction would affect the velocity distribution and the hydrodynamic drag

term in the CDF.

For the simplest model, i.e., a rigid dumbbell model with a Maxwellian velocity

distribution without external forces and hydrodynamic interaction, Stewart and Sørensen

(1972) obtained a power law expression for simple shear flow.

$$\eta - \eta_s \cong 0.678 nkT\lambda^{2/3}\dot{\gamma}^{-1/3} \qquad (2-2)$$

$$\Psi_1 \cong 1.20 nkT\lambda^{2/3}\dot{\gamma}^{-4/3} \qquad (2-3)$$

where

η = shear viscosity,

η_s = solvent shear viscosity,

n = the number of dumbbells per unit volume,

k = Boltzmann constant,

$\dot{\gamma}$ = shear rate,

Ψ_1 = first normal stress coefficient, $\left(\tau_{xx} - \tau_{yy}\right)/\dot{\gamma}_{yx}^2$,

$$\lambda = \frac{[\eta]_0 \eta_s M}{\tilde{N}kT},$$

$[\eta]_0$ = zero-shear-rate intrinsic viscosity, or $\lim\limits_{\substack{c \to 0 \\ \dot{\gamma} \to 0}} \dfrac{\eta - \eta_s}{c\eta_s}$,

c = mass concentration of the solute,

M = solvent molecular weight,

$\tilde{N}$ = Avogadro's number.

Even with the simplest kinetic theory model, shear thinning phenomena and normal stress effects can be described. Another approach exists which is used to describe the CDF. The "orientation tensor" has been used to describe the probability distribution function of the fiber orientation instead of the whole distribution equation (Advani and Tucker, 1987; Tucker, 1988; Altan, 1990; Henry de Frahan *et al.*, 1992; Chung and Kwon, 1995).

Quiescent Crystallization

Polymer crystallization kinetics under quiescent, isothermal conditions have typically been described by the Avrami theory (1939, 1940, 1941). The Avrami equation has the following form:

$$\frac{\phi_c}{\phi_\infty} = 1 - \exp(-kt^n) \qquad (2\text{-}4)$$

where

ϕ_c = crystal volume fraction at time t,

ϕ_∞ = crystal volume fraction at infinite time,

K = Avrami coefficient,

t = time,

n = Avrami exponent.

The Avrami coefficient and exponent are related to the rate of crystal growth and dimension of crystallization process, respectively. The extension of Avrami theory has been developed for non-isothermal conditions (Nakamura *et al.*, 1972, 1973; Chew *et al.*, 1989) and limited volume (Cardew *et al.*, 1984; Billon *et al.*, 1989; Billon and Haudin, 1989)

The application of the Avrami theory to flow-induced crystallization of polymers from the melt has been questioned (Point and Dosiere, 1989). However, the Avrami approach captures the essential fundamental physics of the early stages of crystallization (Cobbs et al., 1952; Godovski, 1969; Minkova et al., 1992). According to the Avrami model, the value of the Avrami exponent should be an integer between 1 and 4, inclusive.

Flow-Induced Crystallization Models

The properties of semi-crystalline polymers ultimately depend on the structural and morphological features of the system (Blackadder and Lewell, 1970a, 1970b; Barham and Keller, 1985; Chen et al., 1992). These characteristics are controlled by the kinetics and mechanism of crystallization (Holland and Lindenmeyer, 1962; Gutfinger et al., 1975). Unlike the crystallization of monatomic materials, the mechanism of polymer crystallization is more complicated, especially for crystallization processes occurring during flow (Hua and Scheiber, 1996). Most flow-induced nucleation and growth models have been based on the idea that stretching a polymer chain reduced its conformational entropy.

The change in Gibb's free energy, ΔG, for any process can be expressed as

$$\Delta G = \Delta H - T\Delta S \tag{2-5}$$

where

ΔH = the enthalpy change,

T = temperature,

ΔS = entropy change.

For a solidification process or melting, $\Delta G = 0$ which leads to:

$$T_m = \frac{\Delta H_m}{\Delta S_m} \qquad (2\text{-}6)$$

where a subscript m refers to the melting point. The decreasing configurational entropy will eventually elevate the melting point. In consequence of the increased supercoooling, nucleation and growth rates are predicted to increase by many orders of magnitude. However, it has been experimentally proved in many cases that the melting point elevation mechanism has failed (Tree, 1990; McHugh and Spevacek, 1991; McHugh and Yung, 1992; McHugh et al., 1993).

Flow-induced crystallization models can be classified into two main categories. The first one involves introducing the flow effect into the Avrami equation (Ziabicki, 1974; Eder and Janeschitz-Kriegl, 1988; Eder et. al., 1990), the second is based on the thermodynamics approach (Flory, 1947; McHugh, 1975; Bushman and McHugh, 1996).

A modified treatment of the Avrami formation was suggested by Eder and Janeschitz-Kriegl (1988) as follows:

$$-\ln\left[1 - \frac{\phi_c}{\phi_\infty}\right] = \int_0^t MK dz \qquad (2\text{-}7)$$

where

$M = \nu N \Theta_1 e^{-\nu z}$ (nucleation rate),

$K = f_m [G(t-z)\Theta_2]^m$ (growth rate),

G = linear growth rate,

m = dimensionality of growth,

N = total number of potential nucleation sites per unit volume,

f_m = shape factor,

t = present time,

z = past time,

v = the activation frequency,

Θ_i = flow factor.

The activation frequency, v, and linear growth rate, G, are functions of the degree of undercooling and may be affected by the melting point elevation. The modified Avrami model has been successfully used to determine the flow rate dependency in polymer crystal growth from solution studies by McHugh and Spevacek (1991). The modified Avrami models can be considered as semi-empirical models which do not account for the coupling of the rheology and the crystallization in a predictive way.

McHugh (1975) predicted the crystal nucleation rate of polyethylene from xylene solution in terms of the free energy. The free energy was evaluated by means of the elastic dumbbell model. It was demonstrated that an increased nucleation rate was obtained in elongational flow compared to shearing flow.

Bushman and McHugh (1996) developed a crystallization rate model by using Hamiltonian Poisson Brackets (Beris and Edwards, 1994).

$$\frac{d\phi_c}{dt} = \{\phi_c, \mathcal{H}\} + [\phi_c, \mathcal{H}] \qquad (2\text{-}8)$$

where

ϕ_c = crystal volume fraction,

$\mathcal{H}$ = Hamiltonian,

$\{\phi_c, \mathcal{H}\}$ = continuum Poisson bracket,

$[\phi_c, \mathcal{H}]$ = dissipative bracket.

The Hamiltonian, $\mathcal{H}$, is the summation of potential and kinetic energies. Potential energy is the summation of Helmhotz free energy, A, of the deformed molecule and the free energy of the crystallization. The Helmholtz free energy for the extended polymer chain is given as:

$$A = nkT\ln\left\langle \frac{\psi}{\psi_{eq}} \right\rangle \tag{2-9}$$

where

n = number density of molecules,

ψ_{eq} = equilibrium distribution.

The Helmholtz free energy was obtained by the theory of strain-induced crystallization (Gaylord and Lohse, 1976; Gaylord, 1976) and the model of Hookean dumbbell to describe the polymer molecule. The use of "strain"-induced crystallization was based on the assumption that the chain entanglements in flow-induced crystallization play the same role as the chemical crosslinks in strain-induced crystallization and the relaxation time of the molecular entanglement are long compared to the crystallization. However, the model concept is not easy to understand.

Optimization

Optimization techniques provide the tools for a systematic search for the optimum design or set of operating conditions from among all the possible design or operating options. The optimal design criterion is defined by an objective function subject to the

relevant constraints. Typically, objective functions are related to maximum profit or minimum cost: such as minimizing the pressure drop (Çabuk and Modi, 1990, 1992), minimizing process time (Mychajluk *et al.*, 1996), minimizing energy input; and obtaining an extremum in the material geometry or properties: such as maximizing strength (Nonhof, 1996), minimizing the thickness variation (Lee and Soh, 1996; Tucker *et al.*, 1995). The optimization problem can be stated as a general nonlinear programming (NLP) in the following form:

$$\text{Minimize:} \quad f(\underline{x}); \qquad \underline{x} = [x_1, x_2,\ldots, x_n]^T \tag{2-10}$$

$$\text{subject to:} \quad c_i(\underline{x}) = 0, \qquad i = 1, 2,\ldots, m \tag{2-11}$$

$$c_i(\underline{x}) \geq 0, \qquad i = m+1, m+2,\ldots, p \tag{2-12}$$

$$\underline{x}_l \leq \underline{x} \leq \underline{x}_u, \qquad i = 1, 2,\ldots, n \tag{2-13}$$

where:

$\underline{x}$ = design variable vector,

$f(\underline{x})$ = objective function,

$c_i(\underline{x}) = 0$ ($i = 1, 2,\ldots, m$) = equality constraints,

$c_i(\underline{x}) \geq 0$ ($i = m+1, m+2,\ldots, p$) = inequality constraints,

$\underline{x}_l, \underline{x}_u$ = lower and upper limits of variables.

The design variables are assumed to be continuous and not functions of time. An important concept to keep in mind is that maximizing a function can be considered to be the same as minimizing the negative of the function. If the constrains, c_i, do not exist, the problem becomes an unconstrained optimization. For constrained optimization, there are a number of different techniques that are used such as penalty-functions, augmented-Lagrange or multiplier methods.

The following discussion starts with an introduction to the one dimensional Newton methods without constraints which is the simplest optimization problem. This is followed by multi-dimensional Newton methods, and then the methods related to the program (SQPHP) that has been used in this study are discussed: Lagrangian multiplier, generalized reduced gradient, penalty-function methods and successive quadratic programming.

One Dimensional Newton's Method

Newton's method starts at an arbitrary initial point x_0. The function takes a Taylor series expansion at x_k for the k-th iteration. The function is approximated by a quadratic function in which the terms higher than second order are ignored.

$$f(x) \approx f(x_k) + f'(x_k)(x - x_k) + \tfrac{1}{2} f''(x_k)(x - x_k)^2 \qquad (2\text{-}14)$$

The necessary condition for a local minimum requires that $f'(x) = 0$. Thus, Eq. 2-14 is differentiated with respect to x and the first derivative is set equal to zero. Note should be made that the values of k-th iteration are from the previous iteration and are known quantities which should be treated as constants during differentiation. So the Newton method predicts the minimum point value at the k-th iteration as

$$x = x_k - \frac{f'(x_k)}{f''(x_k)} \qquad (2\text{-}15)$$

The current value of x will be used for the next iteration and the iteration will be carried on until the convergence criteria are met. The Newton's method has a quadratic rate of convergence near the solution.

If the first and second derivatives in Newton's method cannot be obtained analytically, the derivatives can be obtained by numerical methods such as finite difference approximations. The truncation error may become important especially for the second derivative and computational resources become important for large numbers of variables, as will be seen in the following section.

Multi-Dimensional Newton's Method

Multi-dimensional optimization is an extension of the one-dimensional case with more than one design variable. The objective function of n design variables, which are represented in vector form, can be evaluated using a quadratic approximation at $\underline{x}^k$. Thus,

$$f(\underline{x}) \approx f(\underline{x}^k) + \underline{\nabla}^T f(\underline{x}^k)\Delta\underline{x}^k + \frac{1}{2}(\Delta\underline{x}^k)^T \underline{\underline{H}}(\underline{x}^k)\Delta\underline{x}^k \qquad (2\text{-}16)$$

where $\Delta\underline{x} = \underline{x}^{k+1} - \underline{x}^k$, and the $\underline{\underline{H}}$ is the Hessian (second derivative matrix) of the objective function. The component ij of $\underline{\underline{H}}$ is defined as:

$$H_{ij} = \frac{\partial^2 f}{\partial x_i \partial x_j} \qquad (2\text{-}17)$$

The quadratic approximation of $f(\underline{x})$ is differentiated with respect to each of the components of $\underline{x}$, and then equated to zero

$$\underline{\nabla}f(\underline{x}) = \underline{\nabla}f(\underline{x}^k) + \underline{\underline{H}}(\underline{x}^k)\Delta\underline{x}^k = 0 \qquad (2\text{-}18)$$

or

$$\underline{x}^{k+1} = \underline{x}^k - \left[\underline{\underline{H}}(\underline{x})^k\right]^{-1}\underline{\nabla}f(\underline{x}^k) \qquad (2\text{-}19)$$

The vector $-\left[\underline{\underline{H}}(\underline{x})^k\right]^{-1}\underline{\nabla}f(\underline{x}^k)$ represents the search direction and is denoted by $\underline{S}$. If $\underline{\underline{H}}(\underline{x})$ is the identity matrix, the search direction is the steepest descent direction. The Hessian matrix is positive definite if the following condition can be met:

$$\underline{x}^T\underline{\underline{H}}\underline{x} > 0, \quad \forall\underline{x}. \tag{2-20}$$

The solution may find a saddle point if the Hessian $H(x)$ is not positive definite.

Evaluation of the second partial derivatives in the Hessian matrix is time consuming and may not be positive definite. Therefore, many methods have been developed to approximate the Hessian matrix by first partial derivatives using the previously approximated Hessian matrix, $\underline{\underline{B}}_k$. Some examples of the Hessian approximate method are the BFGS (Broyden, 1970; Fletcher, 1970; Goldfarb, 1970; Shanno, 1970),

$$\underline{\underline{B}}_{k+1} = \underline{\underline{B}}_k - \frac{\underline{\underline{B}}\underline{d}\underline{d}^T\underline{\underline{B}}}{\underline{d}^T\underline{\underline{B}}\underline{d}} + \frac{\underline{g}\underline{g}^T}{\underline{g}\underline{d}} \tag{2-21}$$

Broyden (1967),

$$\underline{\underline{B}}_{k+1} = \underline{\underline{B}}_k + \frac{\left[\underline{g}-\underline{\underline{B}}\underline{d}\right]\underline{d}^T}{\underline{d}^T\underline{d}} \tag{2-22}$$

and DFP updates (Davidon, 1959; Fletcher and Powell, 1963)

$$\underline{\underline{B}}_{k+1} = \underline{\underline{B}}_k - \frac{\left(\underline{g}-\underline{\underline{B}}_k\underline{d}\right)^T + \underline{d}\underline{g}\underline{g}^T}{\left(\underline{g}^T\underline{d}\right)\left(\underline{g}^T\underline{d}\right)} + \frac{\left(\underline{g}-\underline{\underline{B}}_k\underline{d}\right)\underline{g}^T + \underline{g}\left(\underline{g}-\underline{\underline{B}}_k\underline{d}\right)^T}{\underline{g}^T\underline{d}}. \tag{2-23}$$

where

$\underline{\underline{B}}_{k+1}$ = approximated Hessian matrix for (k+1)th iteration,

$$\underline{d} = \underline{x}_{k+1} - \underline{x}_k, \tag{2-24}$$

$$\underline{g} = \underline{\nabla}f(\underline{x}_{k+1}) - \underline{\nabla}f(\underline{x}_k) \, . \tag{2-25}$$

The approximate Hessian matrix for SQPHP was modified from the BFGS method and

has the following form (Chen and Stadtherr, 1983, 1984):

$$\underline{\underline{B}}_{k+1} = \underline{\underline{B}}_k - \frac{\underline{\underline{B}}_k \underline{d}\underline{d}^T \underline{\underline{B}}_k}{\underline{d}^T \underline{\underline{B}}_k \underline{d}} + \frac{\eta\eta^T}{\underline{d}^T \eta} \tag{2-26}$$

where

$$\underline{\eta} = \theta\underline{g} + (1-\theta)\underline{\underline{B}}_k \underline{d} \tag{2-27}$$

$$\underline{g} = \underline{\nabla}L(\underline{x}_{k+1},\underline{u}) - \underline{\nabla}L(\underline{x}_k,\underline{u}) \tag{2-28}$$

$$\theta = \begin{cases} 1, & \underline{d}^T\underline{g} \geq 0.2\underline{d}^T\underline{\underline{B}}_k\underline{d} \\ \dfrac{0.8\underline{d}^T\underline{\underline{B}}_k\underline{d}}{\underline{d}^T\underline{\underline{B}}_k\underline{d} - \underline{d}^T\underline{g}}, & \underline{d}^T\underline{g} < 0.2\underline{d}^T\underline{\underline{B}}_k\underline{d} \end{cases} \tag{2-29}$$

Usually, a step length λ is introduced, which is multiplied by the search direction to

decelerate or accelerate the search for the stability of convergence.

Lagrangian Multiplier Method

Newton's method only handles problems without constraints and hence may not be

suitable for many practical problems which may have various governing constraints.

Typically, the optimization is subjected to two kinds of constraints: equality constraints

and inequality constraints as shown in Eqs. 2-11 and 2-12.

The inequality constraints can be converted to equality constraints by introducing

the square of slack variables, σ_i^2, then

$$c_i(\underline{x}) - \sigma_i^2 = 0 \ , i = m+1, \, m+2, \ldots, p \tag{2-30}$$

When $\sigma_i^2 = 0$ the constraint is called active or binding; while when $\sigma_i^2 \neq 0$, the constraint is called inactive.

The constraints can be incorporated into the objective function by multiplying by the Lagrange multipliers, w_i. The augmented objective function, called the Lagrangian, is defined as

$$L(\underline{x},\underline{w},\underline{u}) = f(\underline{x}) + \sum_{i=1}^{m} w_i c_i(\underline{x}) + \sum_{i=m+1}^{p} w_i \left[c_i(\underline{x}) - \sigma_i^2 \right]. \qquad (2\text{-}31)$$

The necessary conditions for minimum points are (Dennis, 1959):

$$\frac{\partial L(x)}{\partial x_i} = 0 \qquad \text{for } i = 1,\dots, n \qquad (2\text{-}32)$$

$$\frac{\partial L(\underline{x})}{\partial w_i} = 0 \qquad \text{for } i = 1,\dots, p \qquad (2\text{-}33)$$

$$\frac{\partial L(x)}{\partial \sigma_i} = -2w_i \sigma_i = 0 \quad \text{for } i = m+1,\dots, p \qquad (2\text{-}34)$$

$$w_i \leq 0 \qquad \text{for } i = 1,\dots, p \qquad (2\text{-}35)$$

The dimensionality of the augmented objective function is increased by introducing Lagrange multipliers and slack variables. The Lagrange multiplier also provides information on the sensitivity of the objective function with respect to the constraint constant. The Lagrange multiplier method is not suitable if the necessary equations (Eqs. 2-32 to 2-34) are not linear functions.

Generalized Reduced Gradient Method

The generalized reduced gradient method uses the linear or linearized equality constraint to reduce the number of variables. Suppose the inequality constrains in Eq. 2-

12 do not exist, then m dependent variables, $\underline{x}_D$, can be determined from m equality

constraints and will be eliminated later. The gradient of the objective function is split into

two sub-gradients, one containing (n-m) independent variables and the other containing m

dependent variables, as shown below:

$$\underline{\nabla} f = \begin{bmatrix} \dfrac{\partial f}{\partial \underline{x}_I} \\ \dfrac{\partial f}{\partial \underline{x}_D} \end{bmatrix} \tag{2-36}$$

The total derivatives of the objective function and equality constraints are

$$df(\underline{x}) = \frac{\partial f(\underline{x})}{\partial \underline{x}_I} d\underline{x}_I + \frac{\partial f(\underline{x})}{\partial \underline{x}_D} d\underline{x}_D \tag{2-37}$$

$$dc_i(\underline{x}) = \frac{\partial c_i(\underline{x})}{\partial \underline{x}_I} d\underline{x}_I + \frac{\partial c_i(\underline{x})}{\partial \underline{x}_D} d\underline{x}_D = 0, \quad \text{for i} = 1, \ldots, m \tag{2-38}$$

From the total derivatives of the objective function, the reduced gradient is given as

$$\frac{df(\underline{x})}{d\underline{x}_I} = \frac{\partial f(\underline{x})}{\partial \underline{x}_D} \frac{d\underline{x}_D}{d\underline{x}_I} + \frac{\partial f(\underline{x})}{\partial \underline{x}_I} \tag{2-39}$$

The only unknown term $\dfrac{d\underline{x}_D}{d\underline{x}_I}$ in Eq. 2-39 can be determined by the total derivative of the

equality constraints in Eq. 2-38 and the reduced gradient vector is given as

$$\frac{df(\underline{x})}{d\underline{x}_I} = -\frac{\partial f(\underline{x})}{\partial \underline{x}_D} \left[\frac{\partial c_i(\underline{x})}{\partial \underline{x}_I} \right] \left[\frac{\partial c_i(\underline{x})}{\partial \underline{x}_D} \right]^{-1} + \frac{\partial f(\underline{x})}{\partial \underline{x}_D} \tag{2-40}$$

The advantage of the reduced gradient method is the dimensionality of the reduced

gradient vector, which can be referred to as the search vector, has been reduced to (n-m).

One of the more successful codes for optimization, GRG2 that was developed by Lasdon

and Waren (1978, 1982) at the University of Texas is also available. However, the

nominal optimum point in every iteration cannot be guaranteed in the feasible region; in some cases it is necessary to change the dependent variable to ensure that an optimum point is obtained (Edger and Himmelblau, 1988).

Penalty Function Method

The essential idea of a penalty function method is to transfer the constraints of the optimization problem into a single unconstrained optimization problem. One of the penalty functions, $P(\underline{x}, r)$, for the problem defined in Eqs. 2-10 to 2-12 is

$$P(\underline{x},r) = f(\underline{x}) + \frac{r}{2}\sum_{i=1}^{m} c_i^2(\underline{x}) + \frac{r}{2}\sum_{i=m+1}^{p}\left[\min\left\{0, c_i(\underline{x})\right\}\right]^2 \tag{2-41}$$

where

r = scalar weight.

The unconstrained optimization problem can be solved by any standard technique such as Newton, Quasi-Newton, or Secant method. The penalty function is easy to implement and theoretically related to successive quadratic programming. However, the method has the problems of slow convergence properties, unboundedness from below P (i.e., P can approach negative infinity), ill-conditioning, and numerical instability.

Successive Quadratic Programming

Successive quadratic programming is the name given to the procedure in which quadratic programming is used recursively to minimize an objective function, f, that is approximated locally by a quadratic function. The constraints are approximated by linear functions. The quadratic approximated objective function about $\underline{x}_k$:

$$\frac{1}{2}\underline{d}^T\,\underline{\underline{H}}\underline{d} + \underline{\nabla}^T f\underline{d}$$
(2-42)

subject to linearized equality

$$\underline{\underline{G}}\underline{d} + \underline{c}(\underline{x}_k) \ge 0.$$
(2-43)

where

$\underline{\underline{H}}$ = Hessian matrix

$\underline{d} = \underline{x}_{k+1} - \underline{x}_k$

$\underline{\underline{G}} = \underline{\nabla}c_i(\underline{x}_k)$

A Lagrangian, L, can be constructed based on Eqs. 2-42 and 2-43 (Wilson, 1963):

$$L(\underline{d},\underline{u}_i,\underline{u}_U,\underline{u}_L) = \tfrac{1}{2}\underline{d}^T\,\underline{\underline{H}}\underline{d} + \underline{\nabla}f^T\underline{d} - \underline{u}_i^T(\underline{\underline{G}}\underline{d}+\underline{b})$$
(2-44)

where

u_i = Lagrange multiplier

The minimum point satisfies the well known Kuhn-Tucker conditions:

$$\frac{\partial L(\underline{d},\underline{u}_i)}{\partial\underline{d}} = \underline{\underline{H}}\underline{d} + \underline{\nabla}f - \underline{\underline{G}}\underline{u}_i = 0$$
(2-45)

$$\underline{u}_i^T\left(\underline{\underline{G}}\underline{d} + \underline{b}\right) = 0$$
(2-46)

$$\underline{u}_i \ge 0$$
(2-47)

The set of Eqs. 2-45 and 2-46 are linear and can be easily solved for step $\underline{d}$, and the new

position, $\underline{x}_{k+1}$, can be obtained. For the next iteration, the objective function and

constraints are approximated about $\underline{x}_{k+1}$ and QP is performed again until the convergence

criteria are met.

The successive quadratic programming technique has the same drawbacks as the

Newton's method: 1. Requirement of evaluating the second order derivatives, Hessian

matrix. 2. The Hessian may not be positive definite, in which case the problem may have no solution. 3. The optimization search fails for poor initial guesses. The Hessian matrix problem can be avoided by using the approximate matrix $\underline{B}$ such as Eqs. 2-21 to 2-23 (Han, 1976; Powell, 1978). A poor initial guess can be avoided by introducing a minimum value search along the search direction $\underline{d}$ (Han, 1977).

Criteria for Determining the Optimum Solution

The necessary and/or sufficient conditions provide information at the minimum point. For the problem stated in Eqs. 2-10 to 2-13, the Lagrangian is defined as

$$L(\underline{x},\underline{w},\underline{u}) = f(\underline{x}) + \sum_{i=1}^{m} w_i c_i(\underline{x}) - \sum_{i=m+1}^{p} u_i c_i(\underline{x}) \qquad (2\text{-}48)$$

where

w_i = Lagrange multiplier for equality constraints,

u_i = Lagrange multiplier for inequality constraints.

The sufficient conditions for a local minimum x^* were suggested by Edger and Himmelblau (1988) and have been listed as follows:

(a) $f(\underline{x})$, $c_i(\underline{x})$ are all twice differentiable.

(b) The gradients of the binding constraints and the equality constraints are linear independent.

(c) The Lagrange multipliers exist. (The gradients of the binding constraints and equality constraints are linear independent.)

(d) All of the constraints are satisfied at $\underline{x}^*$.

(e) The Lagrange multipliers u_i^* for the inequality constraints are not negative.

(f) For inequality constraints, $u_i^* c_i(\underline{x}^*) = 0$ (complementary condition: either u_i^* or $c_i(\underline{x}^*)$ equals to zero).

(g) The Lagrangian function is at a stationary point.

(h) The Hessian matrix of L is positive definite for all the active and inactive constraints.

These conditions serve as the basis for the design of some algorithms and as termination criteria for others. If all the sufficient conditions can be met, the point $\underline{x}^*$ is said to be at a local minimum. Or on the other hand, the local minimum can be found based on the sufficient conditions for a given approximated (linear or quadratic) objective function and constraints. In any case, the optimization tools required to optimize polymer processes are available. Before embarking on a discussion of how these tools can be used, it is necessary to define a few polymer processes and the optimization variables associated with them.

Polymer Processing Optimization

There have been few reports of optimization techniques being applied to polymer processing operations. For different processing techniques, the optimization strategy has different objectives. These research efforts can be classified according to the objective of the process: thickness uniformity, thermal uniformity, fiber orientation, cycling time.

Thickness Uniformity

The uniformity in thickness of a sheet in the transverse direction is always a major concern in extrusion processes. In the industry, usually a coat-hanger die has been commonly adopted for delivering the polymer melt from the extruder to form the desired

flat shape. However, the melt will not flow evenly inside the die without installing a buffer which in turn increases the pressure drop. The optimization technique provides a tool to minimize the sheet thickness variation without sacrificing the pressure drop (Smith *et al.*, 1994; Tucker *et al.*, 1995; Chen *et al.*, 1997). Other examples of thickness uniformity can be found in the area of blow molding. The thickness of the blow molded product (such as a milk jar) is usually not uniform. The thickness is highly dependent on the thickness distribution of the parison, which is a hollow preformed polymer before the air is blown into the cavity. The thickness distribution of the parison required to produce a highly uniform final blow molded product can be determined by optimization techniques (Lee and Soh, 1996).

Thermal Uniformity

In injection and compression molding, a non-uniform cavity surface temperature can cause residual stresses in the parts. Residual stress can be alleviated by holding the part in the mold longer. This unfortunately will lower the productivity. By reducing the temperature variation, the residual stress can be attenuated without sacrificing the productivity. By changing the position and power of the heating lines in the mold, a uniform mold surface temperature can be achieved (Barone and Caulk, 1981, 1985).

Fiber Orientation

The fiber orientation in composite polymers is intimately related to the anisotropic strength of the polymer. The material is processed as a suspension of fibers in a polymer melt. As the suspension flows through a die or mold, the polymer deforms and the

deformation changes the orientations of the fibers (Givler *et al.*, 1983; Jackson *et al.*, 1986; Akbar and Altan, 1992). These orientations are subsequently frozen in as the polymer solidifies, and becomes a feature of the finished part. In the tube extruding process, the fibers are oriented in the direction of extrusion, which result in good tube strength in the longitudinal direction and weak strength in the hoop direction for withstanding pressure. By changing the flow or die shape, the hoop-direction orientation can be increased (Ausias *et al.*, 1995, 1996).

Cycling Time

The cycling time is a major factor in injection, compression and resin transfer molding that has to be minimized in order to achieve the maximum productivity. For resin transfer molding, the cycling time includes cure reaction and the flow of resin in the mold (Manoochehri and Parnas, 1996). During molding, the process variables (injection pressures, mold temperature, and initial resin injection temperature) are manipulated to ensure that all of the constraints are satisfied. Within the requirements defined by the constraints on the processing variables, the process is optimized to minimize the cycling time.

In polymer processing optimization, shape optimization techniques are always involved. For shape optimization, some of the design variables are defined on the domain and/or boundary geometry. As the boundary geometry changes during the optimization process, the domain of the model is altered to conform to the new geometry. One example of shape optimization as used in fluid mechanics is in determining the shape of an object of a given volume moving in a viscous fluid at constant speed for a minimum drag

force (Watson, 1971; Pironneau, 1973, 1974; Glowinski and Pironneau, 1975). Shape optimization has been used in aerodynamics to design airfoils having maximum lift force (Baysal and Eleshaky, 1992; Eleshaky and Baysal, 1993), in structural shapes to minimize stress concentration (Zienkiewicz and Campbell, 1973; Francavilla *et al.*, 1975; Dems and Mroz, 1978; Braibant and Fleury, 1985), and in designing metal forming dies to minimize the variation of rate of strain during forging of the workpiece (Han *et al.*, 1993).

For problems without shape optimization, the governing equation is based on the correlation between the objective function and the design variables. The problem can be easily applied to standard optimization techniques. One example is maximizing the welded joint strength by process variables (van Wijk *et al.*, 1996; Nonhof, 1996). Since so many process variables (such as heating time, applied force, and temperature) can affect the joint strength, extensive experiments have been conducted and the correlation between the strength and the process variables is found statistically. Once the correlation has been obtained, the standard optimization can be applied to find the maximum strength for different combination of the process variables.

The difficulties in shape optimization arise from the fact that the objective function usually cannot be explicitly expressed in terms of the design variables, especially for field problems. The governing equations for field problems usually are expressed as a system of partial differential equations which cannot be integrated analytically. Numerical methods are required to solve the governing equations. Since the boundary is one of the design variables, the boundary needs to be modified constantly in the optimization process. Finite difference methods are not very suitable for meshes that are not usually rectangular, unless special techniques are used to map an irregular working geometry to a rectangular

computational domain. Finite element methods are used because of their well known ability to successfully characterize irregular geometries (Dems and Morz, 1978; Shyy *et al.*, 1988).

In the optimization procedure, the derivatives of the objective function and the constraints with respect to the design variables are required. The calculation of the derivatives is the dominant contributor to computational cost. The study of the derivatives is referred to as sensitivity analysis, which has been an active area of optimization study. Therefore, it is desirable to have efficient numerical or analytical methods to determine the sensitivity coefficients and efficient computational methods to solve the resulting equations. A preferable approach is to obtain the sensitivity coefficients analytically from an appropriate set of discretized partial differential equations to eliminate the costly analyses. Examples of the evaluation of sensitivity coefficients include the work by Baysal and Eleshaky (1992), Eleshaky and Baysal (1993), Smith *et al.* (1994), and Tucker *et al.* (1995).

One example of shape optimization by sensitivity analysis was studied by Smith *et al.* (1994) for a polymer sheet extrusion die. The flow field was simulated by using the generalized Hele-Shaw approximation which can be represented as:

$$\nabla \cdot S(P)\nabla P = 0 \tag{2-49}$$

where

P = pressure field,

S = flow conductance.

For a power-law fluid, the flow conductance is a function of the pressure gradient and the half-height of the flow cavity h:

$$S = \frac{h^{2+1/n}}{m^{1/n}(2+1/n)}\|\nabla P\|^{-1+1/n}$$ (2-50)

where

h = half-height of the flow cavity,

m = power-law pre-factor,

n = power law exponent index.

In a Hele-Shaw approximation, the pressure field is solved first and subsequently the velocity field is obtained. Eq. 2-49 implies that the pressure is an implicit function of height which is the design variable. It is assumed that the objective function is determined by a performance measurement G of the process, and G is implicitly dependent on design variable $\underline{x}$ through pressure, P, and explicitly dependent on $\underline{x}$ as shown in following equation.

$$f(\underline{x}) = G(P(\underline{x}),\underline{x})$$ (2-51)

The design sensitivity of F is calculated from

$$\underline{\nabla} f(\underline{x}) = \frac{df}{d\underline{x}} = \frac{\partial G}{\partial P}(P(\underline{x}),\underline{x}) \cdot \frac{dP}{d\underline{x}}(\underline{x}) + \frac{\partial G}{\partial \underline{x}}(P(\underline{x}),\underline{x})$$ (2-52)

The partial derivatives $\frac{\partial G}{\partial P}(P(\underline{x}),\underline{x})$ and $\frac{\partial G}{\partial \underline{x}}(P(\underline{x}),\underline{x})$ are readily available, while $\frac{dP}{d\underline{x}}(\underline{x})$ is implicitly defined by Eq. 2-49. In the formation of the FEM, die half-heights were interpolated in the domain as well as the pressure. The derivative $\frac{dP}{d\underline{x}}(\underline{x})$ can be obtained in the same way as in the standard method of taking derivatives in non-linear FEM.

As can be seen in the example of Smith et $al.$, the formulation of sensitivity analysis is dependent on the problem itself. For different problems, the design sensitivity

vector specific to that problem needs to be determined. Another technique which is analogous to sensitivity analysis is the variational method to obtain the variation of the solution of a direct problem due to boundary variation. Çabuk and Modi (1992) used the variational method to obtain the optimum shape of a planar diffuser.

Another method of generating the sensitivity coefficients is by using a finite difference approximation to repeatedly analyze the flow-field with incremental values of the design variables. This approach though much easier to implement, is potentially computer intensive and hence more expensive especially if the governing equations are difficult to solve.

From the previous discussion, it is evident that there is a need to model flow-induced crystallization for actual polymer processing situations. In the next chapter, the techniques described here will be used to produce an optimization methodology based on a predictive structural model to characterize polymer processes. This effort represents the first time that kinetic theory and successive quadratic programming have been used to exploit flow-induced crystallization in the design and optimization of polymer processing equipment.

CHAPTER III

MATHEMATICAL AND COMPUTATIONAL MODELS

In this chapter, an expression for the probability distribution function for molecular orientation is derived. The distribution function is used to determine the direction and rate of polymer crystallization. The theory of optimization is then described with an emphasis on Successive Quadratic Programming by the Han-Powell (SQPHP) method. Finally, the implementation of the optimization for flow-induced orientation is outlined. A short discussion of spherical coordinates is found in Appendix A which may aid in understanding the remainder of this chapter.

Flow-induced structure formation may include amorphous orientation or the formation of extended chain crystals. The model developed in this chapter is for the general case of simultaneous formation of extended chain crystals and amorphous orientation. In the application of the model (Chapter IV), a simplification can be readily made to represent quiescent crystallization, structure formation in non-crystallizing systems, or orientation at temperatures above the melting point.

Flow-Induced Structure Formation

Flexible polymer molecules consist of very large numbers of carbon atoms bonded in succession with a nearly free rotation about the bonds. Consequently, polymer

35

molecules are very difficult to rigorously model. However, Bird *et al.* (1987b) have shown that polymer molecules can be represented by "bead" models. In a bead model, the mass of the molecule is assumed to be concentrated at discrete points (the beads) which are connected together to approximate the molecule. The specific model is determined by the number of beads and characteristics of the connectors. The simplest example of a bead model is the rigid dumbbell which consists of two beads that are joined by a massless rigid rod.

The configuration of a dumbbell model is determined by specifying the location of the beads by means of position vectors with respect to some fixed coordinate system. Suppose there are two beads in space, beads -1 and +1, as shown in Figure 3. The position of the beads is represented by the vectors $\underline{r}_{-1}$ and $\underline{r}_{+1}$ with respect to an arbitrary origin. The orientation of the rigid connector rod is represented by the connector vector which has a fixed length, L. The connector vector can be represented by $L\underline{u}$ where $\underline{u}$ is a unit vector. That is

$$\underline{r}_{+1} - \underline{r}_{-1} = L\underline{u} \, . \tag{3-1}$$

The length of the dumbbell is fixed. Consequently the motion of the ends of the dumbbell will be on the surface of a sphere. Hence, spherical coordinates are the most suitable coordinate system for the problem at hand.

Lu +1

-1

$\underline{r}_{+1}$

$\underline{r}_{-1}$

O
Arbitrary Origin
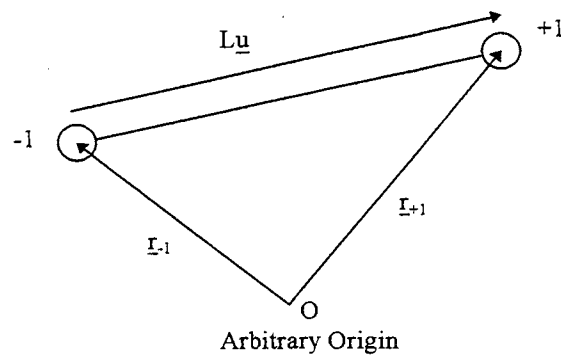
Figure 3. Rigid Dumbbell Model

The assumptions of the model are listed below:

1. The polymer molecule is modeled as a rigid dumbbell.

2. The system is at isothermal conditions.

3. The inertial force in the equation of motion is neglected due to the bead's small mass and sluggish movement.

4. The flow field is homogeneous and the fluid is incompressible.

5. There is no hydrodynamic bead interaction, i.e., the velocity perturbation term is neglected.

6. The friction tensor is isotropic in the hydrodynamic force term.

7. Equilibration in momentum space is assumed for the velocity distribution in the Brownian motion term, i.e., the velocity distribution is Maxwellian about the mass-average velocity of the melt at the center of mass of the dumbbell.

8. Intermolecular forces are neglected.

9. The rate of polymer crystal growth is proportional to the probability of finding the molecule in the orientation direction.

The Equation of Motion for the Beads of the Dumbbell

The forces experienced by the beads are (1) the hydrodynamic drag force, (2) the force due to Brownian motion, and (3) the external force as shown in Figure 4. An intramolecular force is not included because there is no "spring" in a *rigid* rod dumbbell. The inertial force can be neglected because bead movement is assumed to be very sluggish and also because the mass of the bead is very small.

Hydrodynamic Drag Force. The hydrodynamic drag force is the force due to the difference between the velocity of the bead and the surrounding fluid. Thus, the drag force can be represented as (Bird *et al.*, 1987b):

$$\underline{F}_v^{(h)} = -\underline{\underline{\zeta}} \cdot \left[[\![\underline{\dot{r}}_v]\!] - (\underline{v}_v + \underline{v}'_v) \right] \qquad (3\text{-}2)$$

where

$\underline{\underline{\zeta}}$ = friction tensor,

$[\![\underline{\dot{r}}_v]\!]$ = velocity-space averaged bead velocity,

$\underline{v}_v$ = velocity of the surrounding fluid at bead v,

$\underline{v}'_v$ = perturbation velocity of the flow field.

The subscript v identifies the bead and may take on values of $+1$ and -1. In most cases, the friction tensor $\underline{\underline{\zeta}}$ is isotropic (i.e., $\underline{\underline{\zeta}} = \underline{\underline{\delta}}\zeta$, where the scalar ζ is called the friction coefficient and $\underline{\underline{\delta}}$ is the unit tensor). The velocity-space averaged bead velocity for the rigid dumbbell is defined as:

$$[\![\underline{\dot{r}}_v]\!] = \iint \underline{\dot{r}}_v \Xi \, d\dot{r}_{+1} d\dot{r}_{-1} \ . \qquad (3\text{-}3)$$
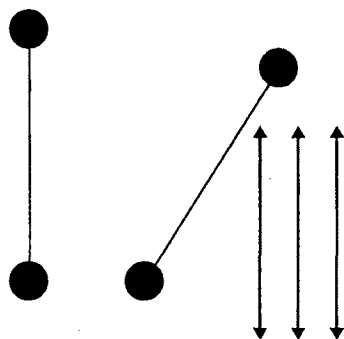
(a) Hydrodynamic Drag Force
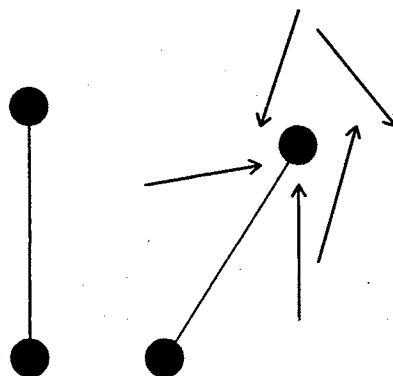
(b) Brownian Force
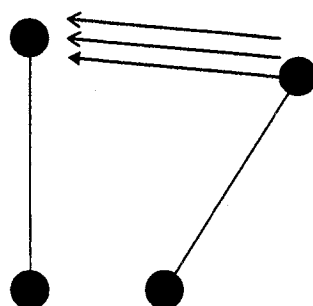
(c) Intermolecular Force

Figure 4. Forces Acting on Dumbbell

where:

Ξ = velocity distribution function

$\dot{r}_{+1}$, $\dot{r}_{-1}$ = bead velocity

Examination of Eq. 3-3 shows that determination of a numerical value for $[\![\dot{r}_\nu]\!]$ requires a

priori knowledge of the distribution function. However, determination of the distribution

function is the goal of this derivation. Hence, $[\![\dot{r}_\nu]\!]$ is a variable.

The fluid velocity at position $\underline{r}$ can be defined as

$$\underline{v}_\nu = \underline{v}_0 + [\underline{\underline{\kappa}} \cdot \underline{r}_\nu],\tag{3-4}$$

where $\underline{\underline{\kappa}}$ is the transpose of the velocity gradient tensor and the subscript $\nu = +1, -1$:

$$\underline{\underline{\kappa}} = (\underline{\nabla}\underline{v})^\dagger \text{ and}\tag{3-5}$$

$\underline{v}_0$ is a vector independent of position.

The trace of $\underline{\underline{\kappa}}$ must be zero (i.e., $\kappa_{11} + \kappa_{22} + \kappa_{33} = 0$) if the fluid is incompressible. The

perturbation velocity $\underline{v}'_\nu$ of the flow field at bead ν results from the motion of the other

bead and is referred to as hydrodynamic interaction. The hydrodynamic interaction is

assumed to be insignificant for reasons of simplicity.

Using Eqs. 3-2 and 3-4, the difference between the hydrodynamic forces acting on

the two beads is given by

$$\underline{F}_{+1}^{(h)} - \underline{F}_{-1}^{(h)} = -\zeta\left[[\![\dot{\underline{r}}_{+1}]\!] - \underline{v}_0 - \left(\underline{\underline{\kappa}} \cdot \underline{r}_{+1}\right)\right] + \zeta\left[[\![\dot{\underline{r}}_{-1}]\!] - \underline{v}_0 - \left(\underline{\underline{\kappa}} \cdot \underline{r}_{-1}\right)\right]\tag{3-6}$$

Assuming that the bead -1 is in the crystal, and the bead +1 is part of a polymer chain that

is in the amorphous melt, it is evident that the total mass of the crystal is much greater

than (even at the nucleation stage) that of the polymer chain in the melt. Hence, it can be

said that the crystal is moving with the fluid with velocity $\underline{v}_0$, and experiences no drag or

Brownian forces. Since the placement of the origin is arbitrary, it can be placed at the

crystal, bead -1. Then, the position vectors are:

$$\llbracket \dot{r}_{+1} \rrbracket = \underline{v}_0 + L\left(\underline{\underline{\kappa}} \cdot \underline{u} \right)$$
$$\llbracket \dot{r}_{-1} \rrbracket = \underline{v}_0$$

$$(3\text{-}7)$$

Substituting Eq. 3-7 into Eq. 3-6, the following equation can be obtained

$$\underline{F}_{+1}^{(h)} - \underline{F}_{-1}^{(h)} = -\zeta L\left[\llbracket \dot{u} \rrbracket - \left(\underline{\underline{\kappa}} \cdot \underline{u} \right) \right]$$

$$(3\text{-}8)$$

<u>Brownian Force.</u> The Brownian force is due to the thermal fluctuations in the liquid

which causes the beads to be jostled about in an irregular manner. The effect of the

hydrodynamic force is to distort the probability distribution function in space, while the

effect of the Brownian force is to make the probability distribution function evenly

distributed.

A simple form for the average velocity term in the force due to Brownian motion is

obtained by using the Maxwell velocity as defined in Eq. 2-1. This is tantamount to using

the classical "equilibration in momentum space" assumption, since the bead momentum

was defined as the product of the bead mass and the Maxwell velocity distribution

function which is in "equilibrium." The details of the derivation of this equation are

available in Appendix B following the work of Bird $et\ al.$ (1987b)

$$\underline{F}_{+1}^{(b)} = -\frac{kT}{L}\left(\frac{\partial}{\partial \underline{u}} \ln \psi \right)$$

$$(3\text{-}9)$$

where ψ = configurational probability distribution function,

T = absolute temperature,

k = Boltzmann constant.

The configurational probability distribution function $\psi(\theta, \phi)$ is defined so that the probability of a dumbbell oriented between the angles θ and $(\theta + d\theta)$, ϕ and $(\phi + d\phi)$ is given by $\psi(\theta, \phi)\sin\theta d\theta d\phi$. Note that $(\sin\theta d\theta d\phi)$ is a differential increment of area on the "surface" of the unit sphere.

External Force. Examples of external forces are gravitational and electrical force. Gravitational and electrical forces are important in high speed centrifugal fields and electrical charged (ionic) polymers, respectively. The intermolecular force can be represented by the negative of the gradient of the intermolecular potential, Γ

$$F_{+1}^{(\Gamma)} = -\frac{1}{L}\frac{\partial}{\partial \underline{u}}\Gamma.$$ (3-10)

The intermolecular force acting on bead -1 is not present, because the bead is already in the crystal. One commonly used potential is the Lennard-Jones potential which is shown in Figure 5 and is defined as:

$$\Gamma = 4E\left[\left(\frac{\delta}{r_{sep}}\right)^{12} - \left(\frac{\delta}{r_{sep}}\right)^{6}\right]$$ (3-11)

where:

E = maximum depth of the potential well,

r_{sep} = separation distance from the bead in the crystal,

σ = distance at which potential is zero.
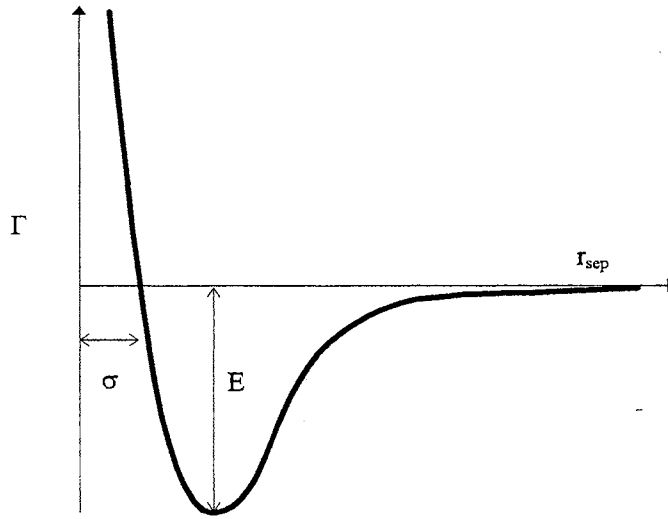
Figure 5. Lennard-Jones Potential

The differences between forces acting on the two beads are added together and the

θ- and ϕ-components are projected out by multiplying the summation of forces by

$\left(\underline{\underline{\delta}} - \underline{uu}\right)$:

$$\left(\underline{\underline{\delta}} - \underline{uu}\right) \cdot \left[\left(F_{+1}^{(h)} - F_{-1}^{(h)}\right) + \left(F_{+1}^{(b)} - F_{-1}^{(b)}\right) + \left(F_{+1}^{(\Gamma)} - F_{-1}^{(\Gamma)}\right)\right] = 0 \qquad (3\text{-}12)$$

When the force expressions from Eqs. 3-8 to 3-10 are substituted into Eq. 3-12 the result

is:

$$\left(\underline{\underline{\delta}} - \underline{uu}\right) \cdot \left(-\varsigma L\left(\llbracket \dot{u} \rrbracket - \underline{\underline{\kappa}} \cdot \underline{u}\right) - \frac{kT}{L}\frac{\partial}{\partial \underline{u}}\ln \psi - \frac{1}{L}\frac{\partial \Gamma}{\partial \underline{u}}\right) = 0 \qquad (3\text{-}13)$$

The momentum-space averaged rate of change of the orientation vector $\llbracket \dot{u} \rrbracket$ can be

obtained from a rearrangement of Eq. 3-13. Thus, the result is:

$$\llbracket \dot{u} \rrbracket = \left[\underline{\underline{\kappa}} \cdot \underline{u} - \underline{\underline{\kappa}}:\underline{uuu}\right] - \frac{1}{12\lambda}\frac{\partial}{\partial \underline{u}}\ln \psi - \frac{1}{12kT\lambda}\frac{\partial \Gamma}{\partial \underline{u}} \qquad (3\text{-}14)$$

where $\lambda = \varsigma L^2/12kT$ is the time constant for the rigid dumbbell.

Equation of Continuity for the Distribution Function

For the rigid dumbbell model, the bead on the end of the rod can only be found on the surface of the hemisphere with radius L as shown in Figure 6. Only a hemisphere was considered instead of a unit sphere because the other hemisphere was occupied by the crystal. The rate of change of probability for finding a bead on the surface element A is

$$\frac{\partial}{\partial t} \psi(\theta, \phi, t) \Delta\theta \sin\theta \Delta\phi \qquad (3\text{-}15)$$

Notice that the "$\sin\theta$" in Eq. 3-15 is the scale factor for the azimuthal (i.e., in the ϕ direction) unit vector, $\underline{t}$, in the spherical coordinate system. The rate at which beads enter the surface element A is

$$(\llbracket\dot\theta\rrbracket\psi)|_\theta \sin\theta\Delta\phi - (\llbracket\dot\theta\rrbracket\psi)|_{\theta+\Delta\theta} \sin\theta\Delta\phi$$
$$+(\llbracket\dot\phi\rrbracket\psi)|_\phi \Delta\theta - (\llbracket\dot\phi\rrbracket\psi)|_{\phi+\Delta\phi} \Delta\theta \qquad (3\text{-}16)$$

where

$$\llbracket\dot\theta\rrbracket = \llbracket\frac{d\theta}{dt}\rrbracket = \text{average time rate of change of the coordinate } \theta$$

$$\llbracket\dot\phi\rrbracket = \llbracket\frac{d\phi}{dt}\rrbracket = \text{average time rate of change of the coordinate } \phi$$

Equating Eqs. 3-15 and 3-16 and dividing by $\Delta\theta\sin\theta\Delta\phi$; when $\Delta\theta$ and $\Delta\phi$ are allowed to approach zero, the following expression can be obtained.

$$\frac{\partial\psi}{\partial t} = -\left(\frac{1}{\sin\theta}\frac{\partial\llbracket\dot\theta\rrbracket\sin\theta\psi}{\partial\theta} + \frac{1}{\sin\theta}\frac{\partial\llbracket\dot\phi\rrbracket\psi}{\partial\phi}\right) \qquad (3\text{-}17)$$

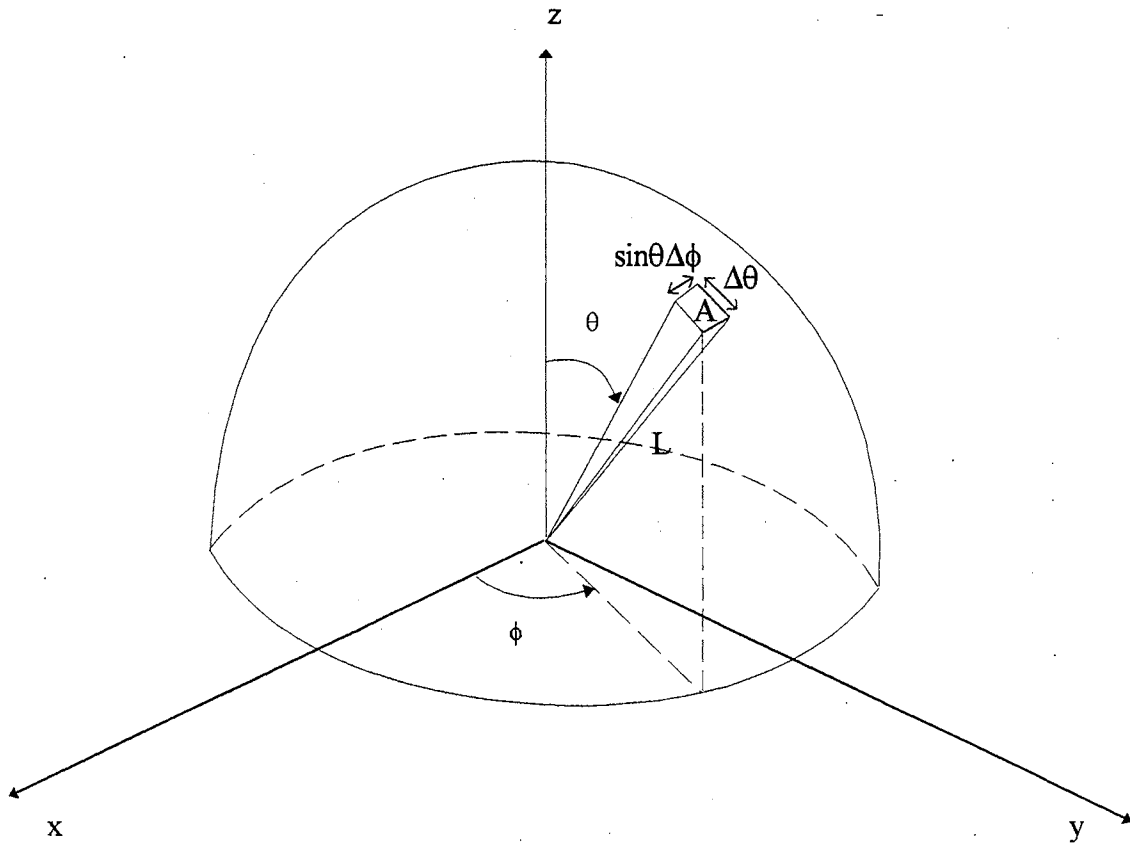Eq. 3-17 can be represented in term of the average unit vector $\llbracket u\rrbracket$ as:

Figure 6. Surface Element $\sin\theta\Delta\theta\Delta\phi$ on Hemisphere

$$\frac{\partial \psi}{\partial t} = -\left(\frac{\partial}{\partial \underline{u}} \cdot [[\dot{\underline{u}}]]\psi\right) \tag{3-18}$$

The main idea of an equation of continuity for the configurational probability distribution function is that dumbbells leaving one orientation must end up in another, and is analogous to the equation of continuity in continuum fluid mechanics.

Substitution of the expression for $[[\dot{\underline{u}}]]$ from Eq. 3-14 into the equation of continuity gives the diffusion equation:

$$\frac{\partial}{\partial t}\psi = \underbrace{\frac{1}{12\lambda}\left(\frac{\partial}{\partial \underline{u}} \cdot \frac{\partial}{\partial \underline{u}}\psi\right)}_{Brownian} - \underbrace{\frac{\partial}{\partial \underline{u}} \cdot [\underline{\underline{\kappa}} \cdot \underline{u} - \underline{\underline{\kappa}} : \underline{uuu}]\psi}_{Hydrodynamic} + \underbrace{\frac{1}{12kT\lambda}\frac{\partial}{\partial \underline{u}} \cdot \left(\frac{\partial \Gamma}{\partial \underline{u}}\psi\right)}_{Intermolecular} \tag{3-19}$$

Eq. 3-19 is the general diffusion equation for the rigid dumbbell model. Any external force is assumed to be relatively small compared to the hydrodynamic force. The assumption is especially true in polyolefins in which only short range weak van der Waals forces are present. Therefore, no external forces are included in the present derivation. For more detailed work about unsteady-state modeling in the presence of an intermolecular force resulting from a Lennard-Jones potential, refer to Mendes' work (1997). In order to make the equation useful, the flow field must be defined and converted to spherical coordinates to obtain the probability distribution function.

The effect of the flow field enters into the diffusion equation through the tensor $\underline{\underline{\kappa}}$. For a general, two-dimensional, homogeneous velocity field, the rate of strain tensor is the same at all points in the flow field. The velocity is linear and defined in the following equations.

$$u_x = ax + by + c$$
$$u_y = dx + ey + f$$

(3-20)

where a, b, c, d, e and f are coefficients related to the type of flow under consideration. The transpose of the velocity gradient tensor in the rectangular coordinate system becomes

$$\underline{\underline{\kappa}} = \begin{vmatrix} a & b & 0 \\ d & e & 0 \\ 0 & 0 & 0 \end{vmatrix}$$

(3-21)

The tensor $\underline{\kappa}$, as well as the other terms in the diffusion equation (i.e., Eq. 3-19) must be represented by spherical coordinates, i.e., the polar angles θ and ϕ.

The velocity components in spherical coordinates u_θ and u_ϕ are defined as the partial derivatives of the θ and ϕ coordinates with respect to time. The velocity in the θ direction, u_θ can be related to Cartesian coordinates by the chain rule:

$$u_\theta \equiv \frac{\partial \theta}{\partial t} = \frac{\partial \theta}{\partial x}\frac{\partial x}{\partial t} + \frac{\partial \theta}{\partial y}\frac{\partial y}{\partial t} + \frac{\partial \theta}{\partial z}\frac{\partial z}{\partial t}$$

(3-22)

The derivatives with respect to Cartesian coordinates can be obtained from the definition of the spherical coordinate system which is defined in Appendix A. Then, the θ directional velocity can be obtained as:

$$u_\theta = \cos\theta\cos\phi u_x + \cos\theta\sin\phi u_y - \sin\theta u_z$$

(3-23)

The Cartesian velocities in Eq. 3-23 are defined in Eq. 3-19. When the Cartesian coordinates are converted to spherical coordinates:

$$u_\theta = r\sin\theta\cos\theta\left[a\cos^2\phi + (b+d)\sin\phi\cos\phi + e\sin^2\phi\right]$$
$$+ c\cos\theta\cos\phi + f\cos\theta\sin\phi$$

(3-24)

By the same approach, u_ϕ can also be obtained:

$$u_\phi = -\sin\phi u_x + \cos\phi u_y \tag{3-25}$$

$$u_\phi = r\sin\theta\left[(e-a)\sin\phi\cos\phi - b\sin^2\phi + d\cos^2\phi\right] - c\sin\phi + f\cos\phi \tag{3-26}$$

Similarly, the transpose of the velocity gradient tensor can be expressed in spherical coordinates as:

$$\underline{\underline{\kappa}} = \begin{vmatrix} \dfrac{\partial u_r}{\partial r} & \dfrac{1}{r}\dfrac{\partial u_r}{\partial\theta} - \dfrac{u_\theta}{r} & \dfrac{1}{r\sin\theta}\dfrac{\partial u_r}{\partial\phi} - \dfrac{u_\varphi}{r} \\[2ex] \dfrac{\partial u_\theta}{\partial r} & \dfrac{1}{r}\dfrac{\partial u_\theta}{\partial\theta} + \dfrac{u_r}{r} & \dfrac{1}{r\sin\theta}\dfrac{\partial u_\theta}{\partial\phi} - \dfrac{u_\varphi}{r}\cot\theta \\[2ex] \dfrac{\partial u_\phi}{\partial r} & \dfrac{1}{r}\dfrac{\partial u_\phi}{\partial\theta} & \dfrac{1}{r\sin\theta}\dfrac{\partial u_\phi}{\partial\phi} + \dfrac{u_r}{r} + \dfrac{u_\theta}{r}\cot\theta \end{vmatrix} \tag{3-27}$$

Only two components are required in the derivation, as can be seen from the following expression which is the only term containing the $\underline{\underline{\kappa}}$ tensor in Eq. 3-19:

$$[\underline{\underline{\kappa}}\cdot\underline{u} - \underline{\underline{\kappa}}:\underline{uuu}]\psi = \left(\underline{s}\kappa_{21}\psi + \underline{t}\kappa_{31}\psi\right) \tag{3-28}$$

Again, $\underline{s}$ and $\underline{t}$ are the unit vectors in the θ and ϕ direction respectively.

The two components κ_{21} and κ_{31} of the transpose of the velocity gradient are

$$\kappa_{21} = \frac{\partial u_\theta}{\partial r} = \sin\theta\cos\theta\left[a\cos^2\phi + (b+d)\sin\phi\cos\phi + e\sin^2\phi\right]$$

$$\kappa_{31} = \frac{\partial u_\phi}{\partial r} = \sin\theta\left[(e-a)\sin\phi\cos\phi - b\sin^2\phi + d\cos^2\phi\right] \tag{3-29}$$

Upon substitution, the second term on the right hand side of Eq. 3-19 becomes:

$$\frac{\partial}{\partial\underline{u}}\cdot[\underline{\underline{\kappa}}\cdot\underline{u} - \underline{\underline{\kappa}}:\underline{uuu}]\psi = \left(\underline{s}\frac{\partial}{\partial\theta} + \underline{t}\frac{1}{\sin\theta}\frac{\partial}{\partial\phi}\right)\cdot\left(\underline{s}\kappa_{21}\psi + \underline{t}\kappa_{31}\psi\right). \tag{3-30}$$

Taking the dot product on the right hand side of Eq. 3-28 which becomes

$$\frac{\partial}{\partial \underline{u}} \cdot [\underline{\underline{\kappa}} \cdot \underline{u} - \underline{\underline{\kappa}} \colon \underline{uuu}]\psi = \frac{\partial}{\partial \theta}\left(\kappa_{21}\psi\right) + \frac{\cos\theta}{\sin\theta}\kappa_{21}\psi + \frac{1}{\sin\theta}\frac{\partial}{\partial\phi}\left(\kappa_{31}\psi\right) \qquad (3\text{-}31)$$

Substituting the components of $\underline{\underline{\kappa}}$ (i.e., Eq. 3-29) into Eq. 3-31 and performing the differentiation with respect to θ and ϕ

$$\frac{\partial}{\partial \underline{u}} \cdot [\underline{\underline{\kappa}} \cdot \underline{u} - \underline{\underline{\kappa}} \colon \underline{uuu}]\psi = \left[a\cos^2\phi + (b+d)\sin\phi\cos\phi + e\sin^2\phi\right]$$
$$\left[\left(2\cos^2\theta - \sin^2\theta\right)\psi + \sin\theta\cos\theta\frac{\partial\psi}{\partial\theta}\right]$$
$$+\left[(e-a)\left(\cos^2\phi - \sin^2\phi\right) - (2b+2d)\sin\phi\cos\phi\right]\psi \qquad (3\text{-}32)$$
$$+\left[(e-a)\sin\phi\cos\phi - b\sin^2\phi + d\cos^2\phi\right]\frac{\partial\psi}{\partial\phi}$$

The first term on the right hand side of the Eq. 3-19 can be obtained by performing

a standard dot product operation of the vector $\dfrac{\partial}{\partial \underline{u}} = \underline{s}\dfrac{\partial}{\partial\theta} + \underline{t}\dfrac{1}{\sin\theta}\dfrac{\partial}{\partial\phi}$ with itself. That

gives:

$$\frac{\partial}{\partial \underline{u}} \cdot \frac{\partial}{\partial \underline{u}}\psi = \frac{\partial^2\psi}{\partial\theta^2} + \frac{\cos\theta}{\sin\theta}\frac{\partial\psi}{\partial\theta} + \frac{1}{\sin^2\theta}\frac{\partial^2\psi}{\partial\phi^2} \qquad (3\text{-}33)$$

A more detailed derivation can be found in Appendix A.

The probability distribution function, ψ, for molecular configurations can be

obtained by substituting Eqs. 3-32 and 3-33 into Eq. 3-19, and assuming that the

molecular configurations are in steady state. After some rearrangement, the diffusion

equation (i.e., Eq 3-19) yields:

$$A\frac{\partial^2\psi}{\partial\theta^2} + B\frac{\partial^2\psi}{\partial\phi^2} + C\frac{\partial\psi}{\partial\theta} + D\frac{\partial\psi}{\partial\phi} + E\psi = 0 \qquad (3\text{-}34)$$

where:

$$A = \frac{1}{12\lambda} \tag{3-35a}$$

$$B = \frac{1}{12\lambda \sin^2 \theta} \tag{3-35b}$$

$$C = \frac{\cos \theta}{12\lambda \sin \theta} - \sin \theta \cos \theta \{ a + [(e-a)\sin \phi + (b+d)\cos \phi]\sin \phi \} \tag{3-35c}$$

$$D = [(a-e)\cos \phi + (b+d)\sin \phi]\sin \phi - d \tag{3-35d}$$

$$E = -\{ a + [(e-a)\sin \phi + (b+d)\cos \phi]\sin \phi \}\left(\frac{1+3\cos 2\theta}{2} \right) \tag{3-35e}$$
$$+ (a-e)\cos 2\phi + (b+d)\sin 2\phi$$

Since the bottom hemisphere (in Figure 6) has been occupied by the crystal, a no-flux boundary condition, or $\partial\psi/\partial\theta = 0$, applied is at the equator. In the computational domain boundary, the probability at $\phi = 0$ is the same as the probability at $\phi = \pi$. Another point needs to be specified to determine the solution in conjunction with the above two boundary conditions. Physically the north pole is a point, but mathematically the point is represented by a line of $\theta = 0$ with arbitrary ϕ. The value of the point at the north pole will be assigned a finite number first, and the probability distribution function will be solved in the whole domain. Then the probability distribution function ψ would be determined by the normalization condition:

$$\int_0^{2\pi} \int_0^{\pi/2} \psi \sin \theta d\theta d\phi = 1. \tag{3-36}$$

Boundary conditions then are

At $\theta = 0$, ψ = finite constant

At $\theta = \pi/2$, $\partial\psi/\partial\theta = 0$

$$\psi|_{\phi=0} = \psi|_{\phi=\pi}$$

Eq. 3-34 is an elliptic partial differential equation with variable coefficients. This equation has to be solved numerically in most cases. A few exceptions do exist, two of which are described below.

Analytical Solutions for Diffusion Equation

Two analytical solutions are available for the diffusion equation. These are for steady planar elongational and simple shearing flows.

Steady Planar Elongational Flow. A steady planar elongational flow is given by the velocity field

$$u_x = \dot{\varepsilon}x; \ u_y = -\dot{\varepsilon}y; \ u_z = 0 \tag{3-38}$$

in which the elongation rate $\dot{\varepsilon}$ is not a function of time. The coefficients in Eq. 3-20 become $a = \dot{\varepsilon}, e = -\dot{\varepsilon}$ and $b = c = d = f = 0$.

$$\Lambda\psi - (12\lambda\dot{\varepsilon})\Omega_e\psi = 0 \tag{3-39}$$

where Λ and Ω_e are linear operators:

$$\Lambda\psi \equiv \left[\frac{1}{\sin\theta}\frac{\partial}{\partial\theta}\left(\sin\theta\frac{\partial\psi}{\partial\theta} \right) + \frac{1}{\sin^2\theta}\frac{\partial^2\psi}{\partial\theta^2} \right], \tag{3-40}$$

$$\Omega_e\psi = \left[\frac{(\cos^2\phi - \sin^2\phi)}{\sin\theta}\frac{\partial}{\partial\theta}\left(\sin^2\theta\cos\theta\psi \right) - 2\frac{\partial}{\partial\phi}\left(\sin\phi\cos\phi\psi \right) \right] \tag{3-41}$$

The probability distribution for steady planar elongational flow has the form:

$$\psi(\theta,\phi) = \frac{\exp(6\lambda\dot{\varepsilon}\sin^2\theta\cos2\phi)}{J} \tag{3-42}$$

where J is the normalization constant

$$J = \int_0^{2\pi} \int_0^{\pi/2} \exp(6\lambda\dot{\varepsilon}\sin^2\theta\cos 2\phi)\sin\theta\, d\theta\, d\phi \qquad (3\text{-}43)$$

Steady Simple Shearing Flow. The velocity field of a steady simple shearing flow is given by

$$u_x = \dot{\gamma}y; \quad u_y = 0; \quad u_z = 0 \qquad (3\text{-}44)$$

in which the shear rate $\dot{\gamma}$ is not a function of time. The coefficients in Eq. 3-20 become $b = \dot{\gamma}$ and $a = c = d = e = f = 0$. Eq. 3-34 then becomes

$$\Lambda\psi - (12\lambda\dot{\gamma})\Omega_s\psi = 0 \qquad (3\text{-}45)$$

where Λ is the same operator defined in Eq. 3-40 and Ω_s are linear operator for shearing flow:

$$\Omega_s\psi \equiv \left[\frac{\sin\phi\cos\phi}{\sin\theta}\frac{\partial}{\partial\theta}(\sin^2\theta\cos\theta\psi) - \frac{\partial}{\partial\phi}(\sin^2\phi\psi)\right]. \qquad (3\text{-}46)$$

The probability distribution for steady simple shearing flow can be obtained using the perturbation method (Bird *et al.*, 1971). The solution has the form:

$$\psi(\theta,\phi) = \frac{1}{2\pi}\left[1 + (12\lambda\dot{\gamma})\phi_1 + (12\lambda\dot{\gamma})^2\phi_2 + \cdots\right] \qquad (3\text{-}47)$$

where $\phi_1 = \frac{1}{12}P_2^2 s_2$ $\qquad (3\text{-}48)$

$$\phi_2 = -\tfrac{1}{84}P_2^0 c_0 + \tfrac{1}{72}P_2^2 c_2 + \tfrac{1}{280}P_4^0 c_0 - \tfrac{1}{6720}P_4^4 c_4 \qquad (3\text{-}49)$$

$$\phi_3 = -\tfrac{19}{7560}P_2^2 s_2 - \tfrac{1}{18480}P_4^2 s_2 + \tfrac{1}{221760}P_6^2 s_2 + \tfrac{1}{25200}P_4^4 s_4 - \tfrac{1}{15966720}P_6^6 s_6 \qquad (3\text{-}50)$$

$$\begin{aligned}
\phi_4 = &-\tfrac{1}{10395}P_2^0 c_0 - \tfrac{23}{45360}P_2^2 c_2 - \tfrac{727}{720720}P_4^0 c_0 - \tfrac{3}{616000}P_4^2 c_2 \\
&+ \tfrac{7517}{864864000}P_4^4 c_4 - \tfrac{1}{110880}P_6^0 c_0 + \tfrac{71}{139708800}P_6^2 c_2 + \tfrac{1}{39916800}P_6^4 c_4 \\
&- \tfrac{71}{3353011200}P_6^6 c_6 + \tfrac{1}{823680}P_8^0 c_0 - \tfrac{1}{1037836800}P_8^4 c_4 + \tfrac{1}{99632332800}P_8^8 c_8
\end{aligned} \qquad (3\text{-}51)$$

$P_n^m s_m$, and $P_n^m c_m$ are spherical harmonics and

$$s_m = \sin m\phi \tag{3-52}$$

$$c_m = \cos m\phi \tag{3-53}$$

The P_n^m are defined as:

$$P_n^m(x) = (1-x^2)^{|m|/2} \frac{d^{|m|}}{dx^{|m|}} P_n(x). \tag{3-54}$$

where P_n are the Legendre polynomials which are defined as:

$$P_n(x) = \frac{(-1)^n}{2^n n!} \frac{d^n}{dx^n}(1-x^2)^n \tag{3-55}$$

For spherical harmonics $x = \cos\theta$. The properties of spherical harmonics are described in more detail by Hirschfelder, Curtiss and Bird (1964). As seen in Eqs. 3-48 to 3-51, the numbers of terms increases dramatically as the desired precision increases. The perturbation method is only good for $\lambda\dot{\gamma}$ less than or equal to 1.0 (Stewart and Sørensen, 1972).

The effect of the flow field on the probability distribution function is determined by the introduction of the Weissenberg number (*We*)

$$We = \lambda\kappa \tag{3-56}$$

where λ is the characteristic time, and κ is a characteristic strain rate in the flow. The characteristic time λ is defined as follows for the rigid dumbbell.

$$\lambda = \zeta L^2 / 12kT \tag{3-57}$$

The characteristic strain rate, κ, is defined as

$$\kappa = \sqrt{II/2}. \tag{3-58}$$

where

$$II = tr(\underline{\underline{\dot{\gamma}}} : \underline{\underline{\dot{\gamma}}}) = \text{second invariant,}$$

$$\underline{\underline{\dot{\gamma}}} = (\underline{\nabla v})^\dagger + (\underline{\nabla v}) = \text{rate of strain tensor.}$$

In shearing flow, the characteristic strain rate is the shear rate while in elongational flow, the characteristic strain rate is twice the elongation rate.

A scalar description of the orientation state predicted by the probability distribution function can be found by determining the orientation parameter. The orientation parameter represents the degree of the molecular orientation with respect to the x-axis and is defined as:

$$O_x = \frac{1}{2}\left(3\langle \sin^2\theta\cos^2\phi\rangle - 1\right) \tag{3-59}$$

where:

$$\langle \sin^2\theta\cos^2\phi\rangle = \int_0^{2\pi}\int_0^{\pi/2} \psi(\theta,\phi)\sin^2\theta\cos^2\phi\sin\theta d\theta d\phi \tag{3-60}$$

The expression in the angle brackets is the square of the projection of the orientation vector onto the x-axis. The corresponding quantities for the y- and z-directional orientation parameters are $\langle \sin^2\theta\sin^2\phi\rangle$ and $\langle \cos^2\theta\rangle$, respectively. The expression $\langle \cos^2\theta\rangle$ has been used in the well known Hermans orientation parameter (Hermans, 1946) to characterize axisymmetry with respect to the z-axis. The values of the orientation parameter become 1, 0, and -1/2 for molecules perfectly aligned in x-direction, totally random, and perpendicular to the x-axis, respectively.

Polymer crystal growth is highly dependent on the molecular orientation. The polymer crystal forms when certain orientations of the polymer molecule fall into the

lattice site. Assuming that the molecules which are oriented close to the lattice site are near enough, the polymer crystal will form, while molecules far away from the lattice site are still considered to be in the amorphous state. The idea can be visualized by considering the existence of an infinitely deep square well potential near the lattice site as shown in Figure 7. The distance from the lattice site to the bead in amorphous state is represented by the distance l, while l_0 represents the well width. Since the well depth is infinite, once the molecule falls into the lattice site it will never be able to bounce back to the amorphous region. The probability of finding a molecule in the lattice site ψ_c can be obtained as

$$\psi_c = \int_0^{2\pi} \int_0^{\pi/2} \psi_\phi \, \psi \sin\theta \, d\theta \, d\phi \qquad (3\text{-}61)$$

where

ψ_ϕ = probability of the molecule falling into the lattice site
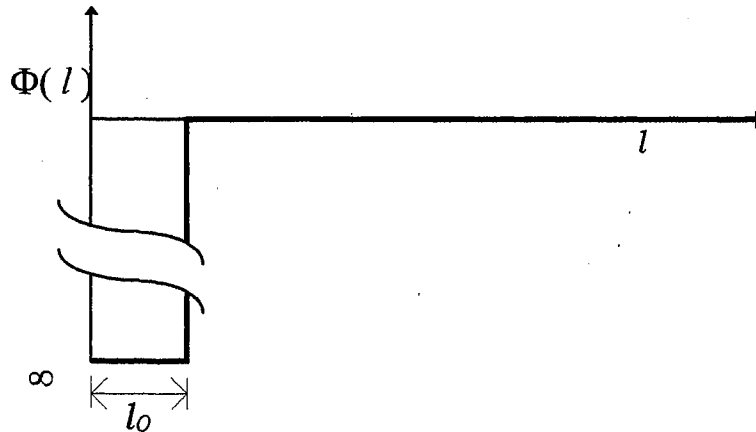

Figure 7. Square Well Potential

The value of ψ_ϕ depends on the nature of the potential considered. In this case, i.e., for a square-well potential, the probability of the molecule falling into the lattice site is given by

$$\begin{aligned} \psi_\phi &= 1 \quad \forall \quad l \le l_0 \\ \psi_\phi &= 0 \quad \forall \quad l > l_0 \end{aligned} \tag{3-62}$$

For simple elongational flow, and arranging the spherical coordinate system such that the north pole points in the direction of flow, the molecule orientation is

$$\psi(\theta) = \frac{1}{J} \exp\left(\frac{9}{2}\lambda \dot{\varepsilon} \cos^2 \theta\right) \tag{3-63}$$

where

$\dot{\varepsilon}$ = elongational rate,

J = normalization constant which is $\displaystyle\int_0^{2\pi}\int_0^{\pi/2} \exp\left(\frac{9}{2}\lambda \dot{\varepsilon}\cos^2\theta\right)\sin\theta\, d\theta\, d\phi$.

Then, the probability of finding a molecule in the lattice site which is at the north pole of the spherical coordinate system is

$$\begin{aligned} \psi_c &= \int_0^{2\pi}\int_0^{\pi/2} \psi_\phi \psi \sin\theta\, d\theta\, d\phi \\ &= \frac{1}{J}\int_0^{2\pi}\int_0^{\theta_0} \exp\left(\frac{9}{2}\lambda\dot{\varepsilon}\cos^2\theta\right)\sin\theta\, d\theta\, d\phi \end{aligned} \tag{3-64}$$

where

θ_0 = the angle corresponding to the distance l_0.

Eq. 3-64 suggests that ψ_c is a function of the elongational rate and potential width. Assuming that the rate of polymer crystal growth is proportional to ψ_c and the effect of the potential width can be absorbed into the proportionality constant, then the rate of polymer crystal growth is proportional to ψ. Hence, the probability of molecular

orientation is proportional to the amount of the polymer formed in the direction of orientation and is indicative of the relative strength of the material in a given direction. The molecular orientation can be projected onto the x and y axes and will provide a measure of the material strength in the x- and y-direction. Thus the relative x- and y-directional strength is

$$S_x = \int_0^{2\pi} \int_0^{\pi/2} \left| \sin^2 \theta \cos \phi \psi \right| d\theta d\phi \qquad (3\text{-}65)$$

$$S_y = \int_0^{2\pi} \int_0^{\pi/2} \left| \sin^2 \theta \sin \phi \psi \right| d\theta d\phi \qquad (3\text{-}66)$$

The objective function of optimization is based on the S_x and S_y.

SQPHP Method

In this section, the optimization program used in this study is outlined (Chen and Stadtherr, 1983). SQPHP combines four successfully implemented optimization algorithms as mentioned in Chapter II: successive quadratic programming, Lagrangian multiplier method, generalized reduced gradient method and penalty method. The basic ideas of the SQPHP are briefly described in the following paragraph.

As in successive quadratic programming, the objective function is approximated by a quadratic function, and the constraints are linearized. The approximate Hessian matrix, $\underline{\underline{B}}$, is obtained by the modified BFGS method to ensure a positive definite matrix. The upper and lower limits of the variables are treated as additional inequality constraints. The constraints as well as the upper and lower limits were multiplied by Lagrange multipliers and incorporated with the objective function to form a Lagrangian. By the same technique used in the generalized gradient method, the linear equality constraints can be eliminated

by Gaussian elimination. The reduced quadratic programming was performed to obtained the search direction $\underline{S}$. A line search procedure was conducted to make sure that the objective function is not only reduced, but also satisfies the constraints along the search direction. The line search procedure determines the step length, which can be used to avoid the problem of having a bad starting point, $\underline{x}_0$. The schematic flow chart of the SQPHP code is shown in Figure 8. A description of each step is given below:

(1) The iteration number k is set to zero. The optimization begins with a starting point, $\underline{x}_0$, in the space of the variables. The approximate Hessian matrix, $\underline{\underline{B}}_0$, of the Lagrangian, $L(\underline{x}, \underline{w}, \underline{u})$, and the vector of the penalty parameters, $\underline{r}$, are set to the identity matrix and the zero vector, respectively.

(2) The functions, constraints, and their first derivatives are computed at $\underline{x}_0$.

(3) A Quadratic Programming step (QP) is performed to obtain the search direction, $\underline{S}_k$, and the Lagrange multipliers, $\underline{u}_k$, for k-th iteration.

(4) The penalty parameters are updated as $\underline{r}_k = \max.\{|\underline{u}_k|, \ 0.5(\underline{r}_k+|\underline{u}_k|)\}$.

(5) If the convergence criterion, CONV, is small or equals a user-specified acceptable tolerance, ACC, the program stops, otherwise it proceeds to update the penalty parameters.

(6) A line search is performed to determine the step-length parameter, t_k. Failure checks and evaluation of functions and derivatives at trial points are also performed during this step.

(7) Let $x_{k+1} = x_k + t_k \underline{S}_k$ for the next iteration.

(8) $\underline{\nabla}L(\underline{x}_{k+1}, \underline{u}_k)$ is computed at x_{k+1} and $\underline{\underline{B}}_{k+1}$ is updated. The approximate Hessian matrix is computed using the previous Hessian and the gradient of the Lagrangian function

$$k = 0$$
$$\underline{r} = \underline{0}$$
$$\underline{\underline{B}}_0 = \underline{\underline{I}}$$

(1)

Compute
$f(\underline{x}_0)$, $\underline{\nabla}f(\underline{x}_0)$, $\underline{c}_i(\underline{x}_0)$, $\underline{\nabla}c(\underline{x}_0)$

(2)

Set
$k = k + 1$

(9)

Perform QP
$\underline{S}_k$, $\underline{u}_k$

(3)

Update
$\underline{r}$

(4)

Compute
$\underline{\nabla}L(\underline{x}_{k+1}, \underline{u}_k)$, $\underline{\underline{B}}_{k+1}$

(8)

CONV $\leq$ ACC

(5)

Yes

Stop

No

Calculate
$\underline{x}_{k+1} = \underline{x}_k + t_k\underline{S}_k$
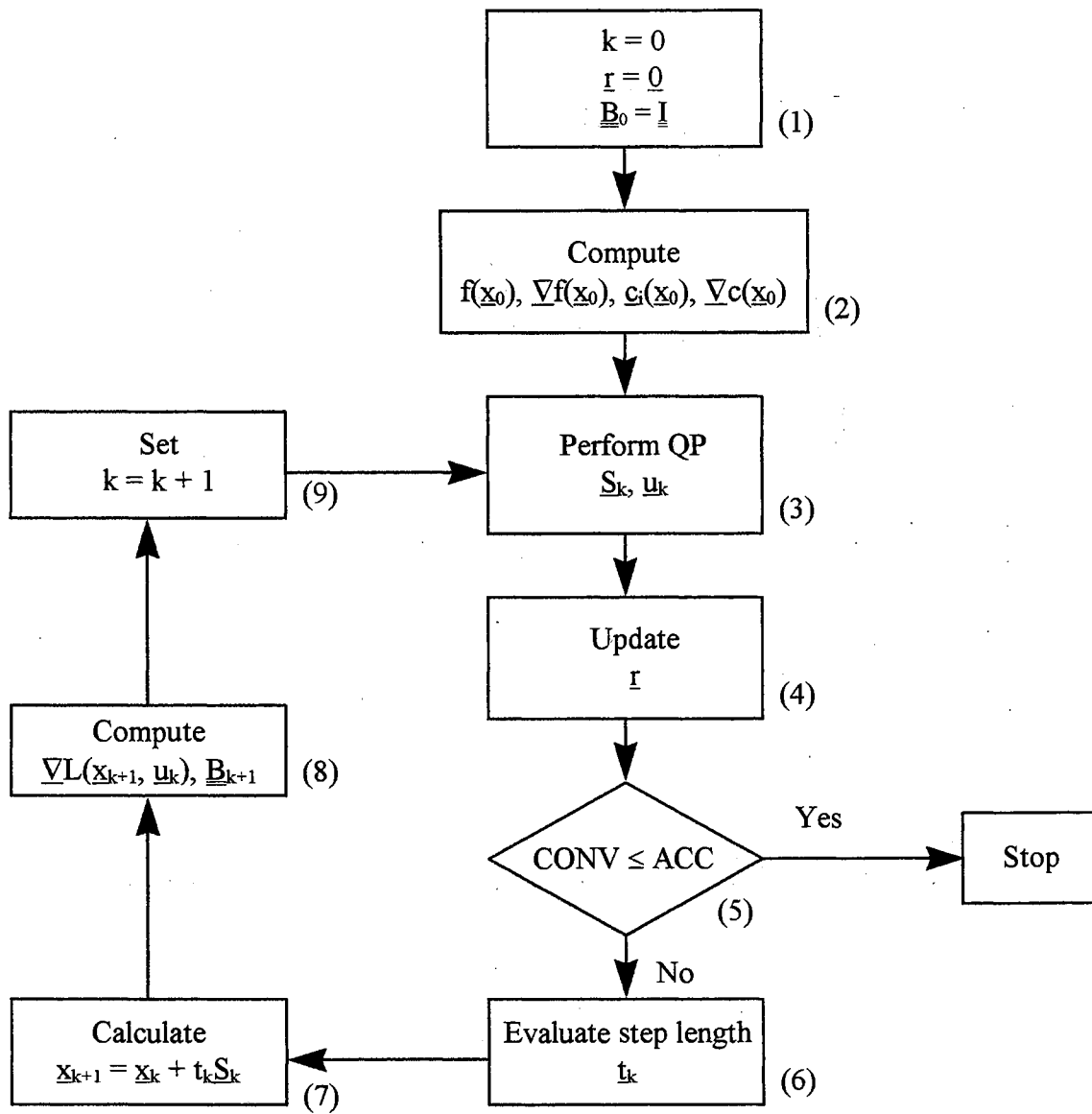
(7)

Evaluate step length
t_k

(6)

Figure 8. Flow Chart of SQPHP

(9) Set $k = k + 1$ and return to step (3).

CHAPTER IV

RESULTS AND DISCUSSION

In this chapter, the behavior of the probability distribution function will first be described. The results obtained from the numerical simulation are compared with the analytical solution for elongational flow and are also compared with the results obtained by using the perturbation method at low Weissenberg number (*We*) in shearing flow. Next, the interface between FIDAP and the optimization routine will be described using a test case. Finally, a die geometry optimization, subject to anisotropy and strength constraints, will be presented.

Probability Distribution Function Prediction

The probability distribution function (PDF) was obtained as described in Chapter III. The following discussion is divided into different sections according to the different flow fields under consideration: elongational, simple shear or general flows.

Planar Elongational Flow

Steady planar elongational flow was examined first because an analytical solution was available for this flow. The planar elongational flow field is described by

$$u_x = \dot{\varepsilon}x; \; u_y = -\dot{\varepsilon}y; \; u_z = 0 \tag{4-1}$$

where

x, y = Cartesian coordinates

$\dot{\varepsilon}$ = elongation rate.

The elongation direction for this flow field is in the x-direction.

The flow field is illustrated in Figure 9, with the hemisphere representing the possible positions of the dumbbell ends. The hemisphere is analogous to the north hemisphere of earth. If the earth's axis of rotation is taken to be the z-axis, the point where the hemisphere intersects the z-axis is called the north pole, while the circle line where the hemisphere intersects with the x-y plane is called the equator. The arrows indicate the direction and the magnitude of the flow velocity.

The distribution function, ψ, is plotted for various values of *We* in Figure 10. The probability distribution function on a 3-D spherical surface is shown in the θ and ϕ domain. The point at the north pole corresponds to the line $\theta = 0°$, while the $\theta = 90°$ line represents the equator. The positive and negative x-axis corresponds to $\phi = 0°$ and $\phi = 180°$, respectively. Only $0 \le \phi \le 180°$ was shown in the figure instead of $0 \le \phi \le 360°$, because $\psi|_{\phi} = \psi|_{\phi+180°}$.

The crystallization direction depends on the molecular orientation. The polymer orientation will be preferred (high distribution function) or excluded (low distribution function) in certain directions due to the hydrodynamic force under flow conditions. For quiescent conditions ($\dot{\gamma} = 0 \ s^{-1}$, *We* = 0), the distribution function is a constant with a value of $\frac{1}{2\pi}$. Therefore, the polymer will crystallize at the same rate in all directions.
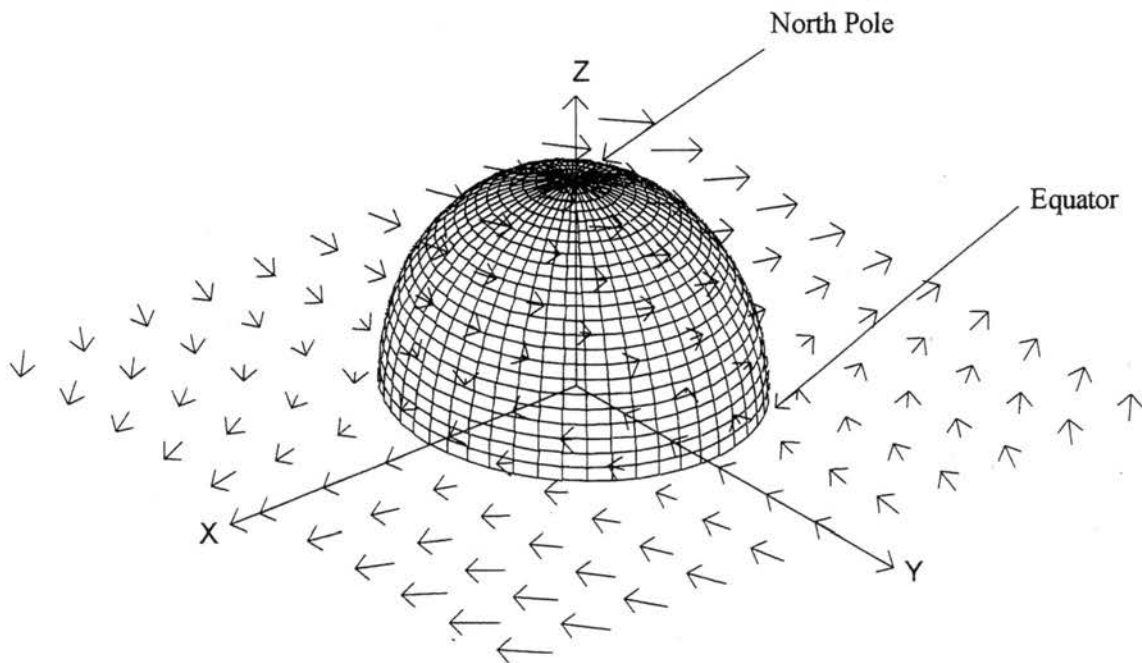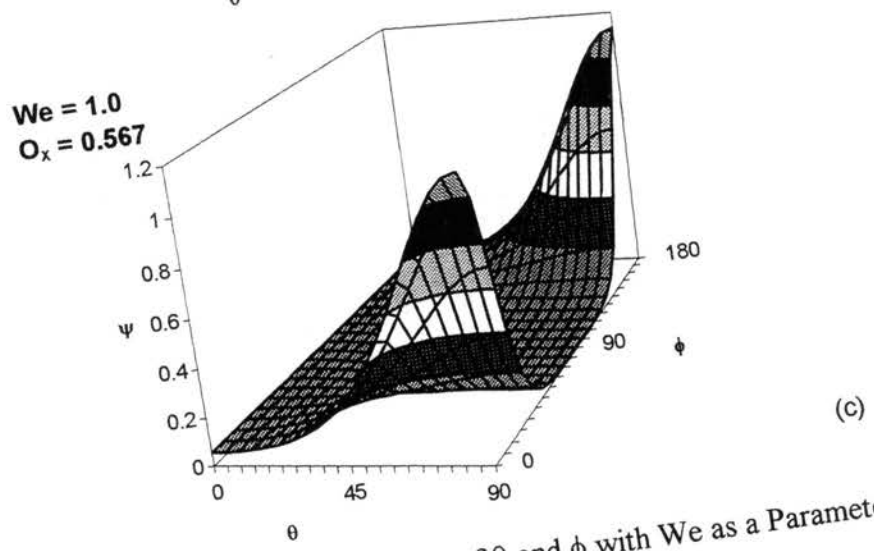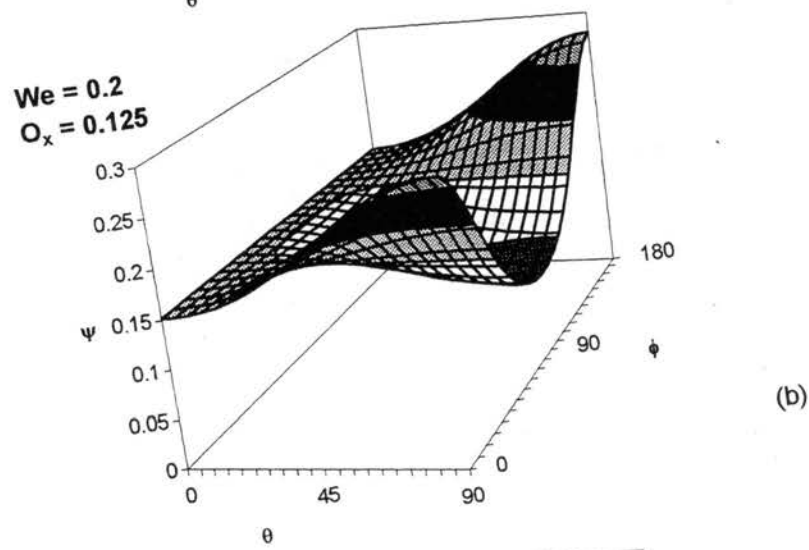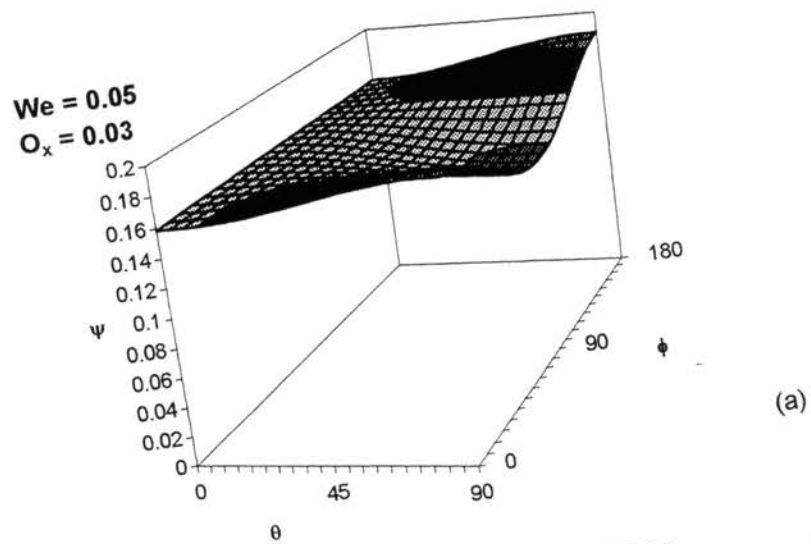
Figure 9. Planar Elongational Flow Pattern

We = 0.05
$O_x = 0.03$

(a)

We = 0.2
$O_x = 0.125$

(b)

We = 1.0
$O_x = 0.567$

(c)

Figure 10. Ψ as a Function of θ and ϕ with We as a Parameter

The two peaks on each graph of Figure 10 represent the preferred orientation in the elongational directions. For a small elongation rate, i.e., We = 0.05 (Figure 10a), the profile is flat compared to Figures 10b and 10c where the Weissenberg numbers are 0.2 and 1.0 respectively., and the orientation parameter, O_x, is close to zero which indicates that the molecular orientation is totally random. As the elongation rate increases, the peak becomes higher, and the value of the orientation parameter increases. The higher peak represents a large number of polymer molecules oriented in the peak direction which is to say that the molecules will preferentially grow as an extended chain crystal in that direction.

Figure 10 also shows a large variation near the equator because the velocity gradient occurs in the x-y plane. According to the equation of continuity, the increased probability of orientation at the equator results in a reduced probability at the north pole as shown in Figure 10.

When the numerical results were compared with the analytical solution (Eq. 3-39), a percentage error was determined according to the following equation.

$$\% \text{ error} = \frac{\text{numerical solution} - \text{analytical solution}}{\text{analytical solution}} \times 100\% . \qquad (4\text{-}2)$$

The mesh size affects the accuracy of the solution at high *We*, especially in elongational flow. Figure 11 shows the percentage error for different mesh sizes for *We* = 1.0. By inspecting Eq. 3-39, the solution is seen to be an exponential function and has a maximum value at $\theta = 90°$ and $\phi = 0°$, and a minimum value along $\phi = 40°$ and $135°$. Figure 11 shows that the numerical solution has a positive deviation from the analytical solution near $\theta = 90°$ and $\phi = 0°$, which corresponds to the flow direction and the
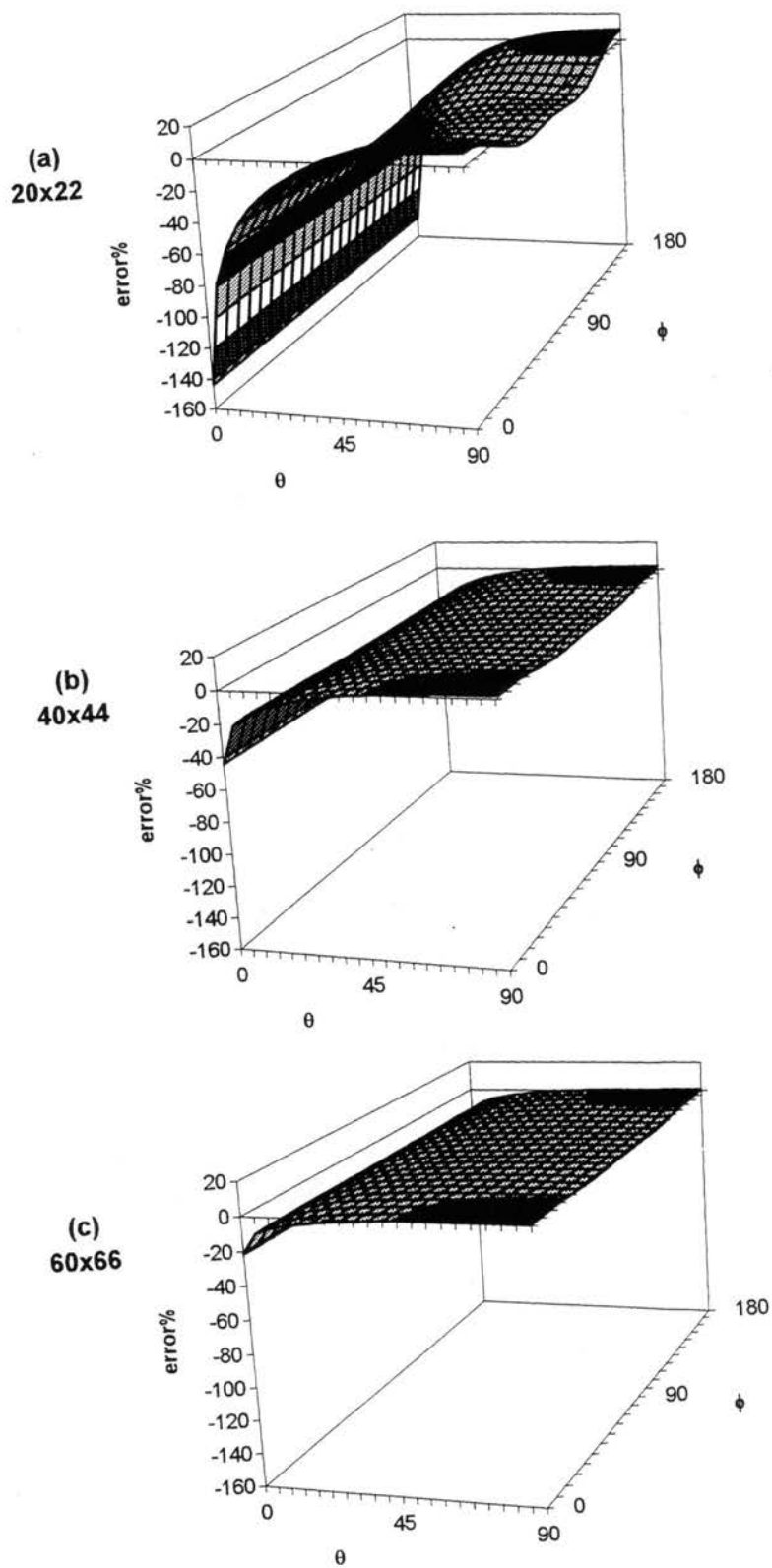
Figure 11. Effect of Mesh Size

maximum PDF value. Also, Figure 11 shows a negative deviation from the analytical solution near the north pole. The percentage errors at the maximum value of PDF are within 8, 2 and 1% for 20×22, 40×44, and 60×66 mesh size, respectively. The maximum errors near the north pole ($\theta = 0°$) correspond to the minimum value of the analytical solution and since the magnitude of the value at this point is very small compared to the rest of the domain, the error introduced is not important. Notice that the area near the north pole always looks bigger on the map compared to that on the globe (sphere). So the actual negative areas on the hemisphere in Figure 11 are relatively smaller than the positive area. A 40×44 mesh size was used in the optimization calculations.

The solutions obtained in Figure 12 are based on a 60×66 mesh. The percentage errors in the region of interest (i.e., near $\theta = 90°$ and $\phi = 0°$) are about 0.08% and 0.92% for We = 0.2 and 1.0, respectively. The region near the north pole has a larger error; however, since the region has relatively small values of ψ, hence the overall error is not significant as explained in the previous paragraph. Thus, the numerical method could predict probability distributions in the region of interest with at least 99% accuracy.

Steady Simple Shear Flow

Steady simple shear flow was examined because a perturbation method solution and experiment results of polymer orientation were available. The simple shear flow field as illustrated in Figure 13, is described by

$$u_x = \dot{\gamma}y; \; u_y = 0; \; u_z = 0 \tag{4-3}$$
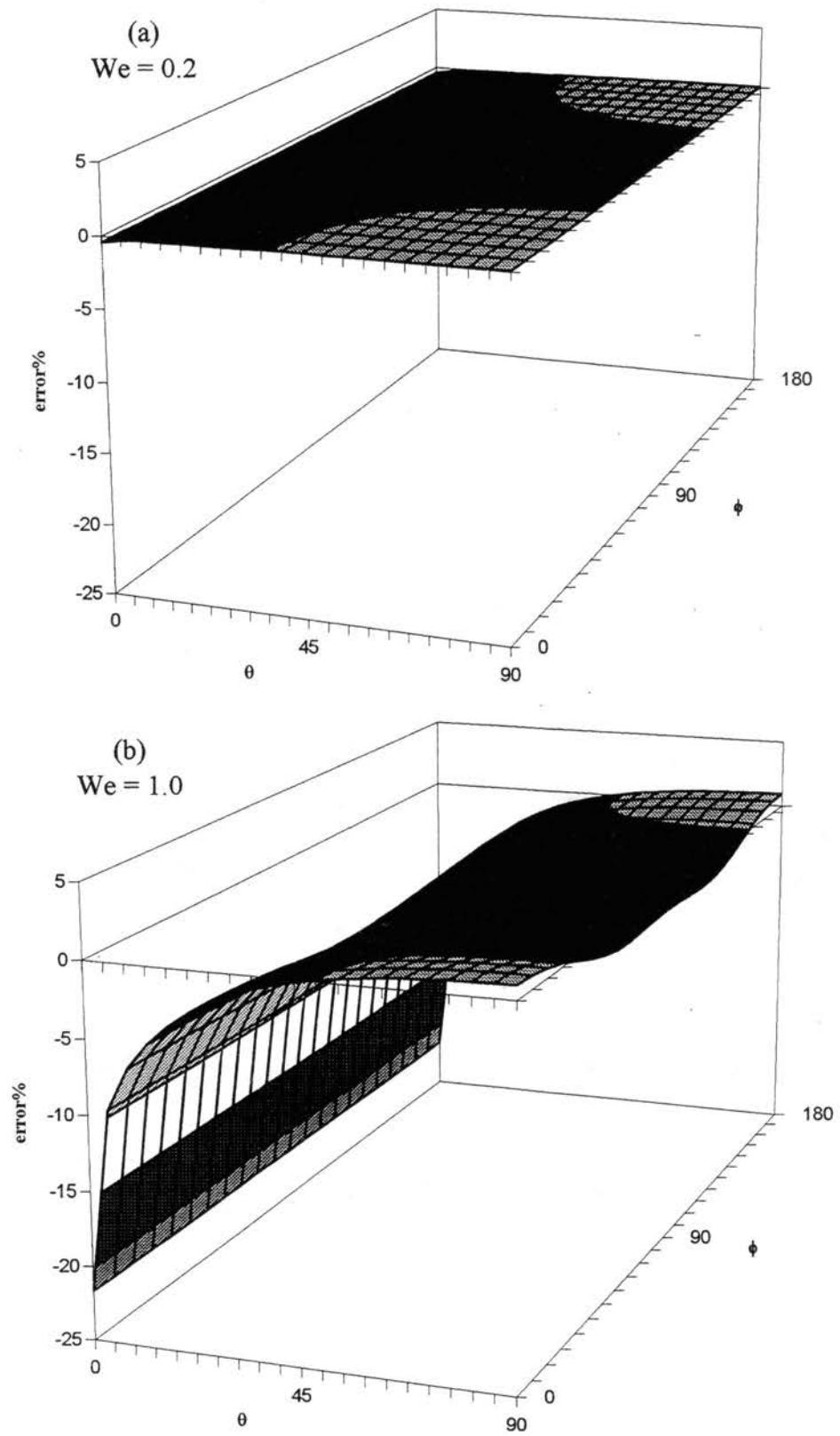
Figure 12. Percentage Error for Numerical Solution in Planar Elongational Flow
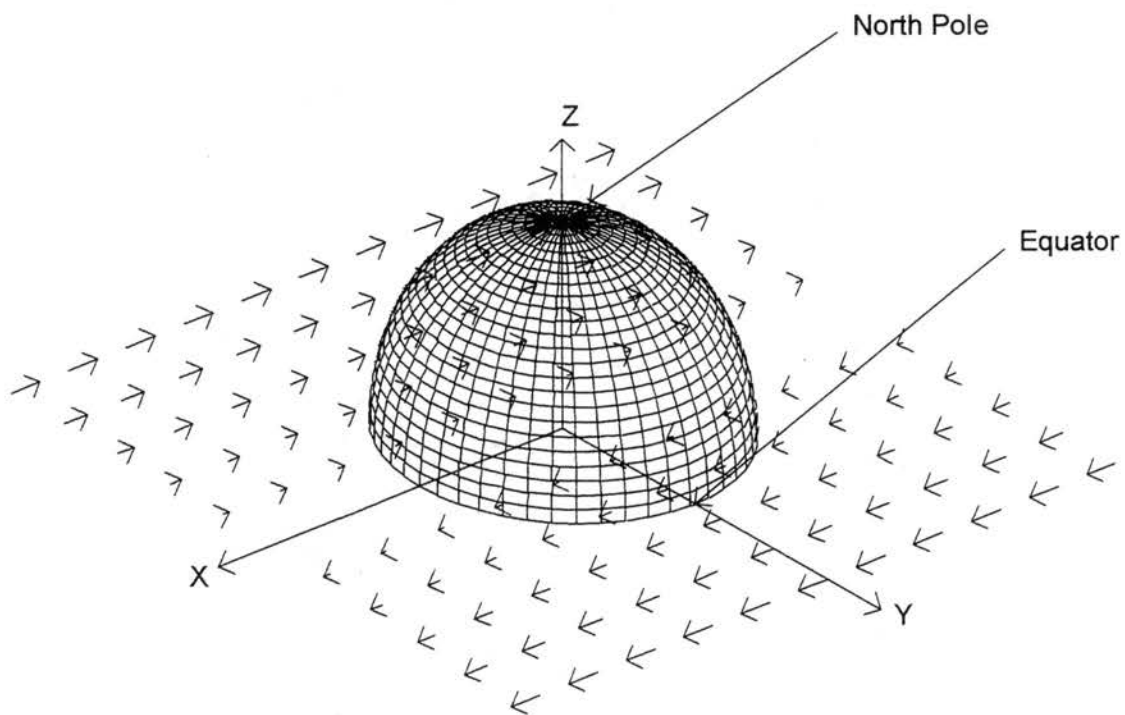
Figure 13. Simple Shear Flow Pattern

where

u_x, u_y, u_z = x-, y- and z-component of velocity

$\dot{\gamma}$ = shear rate

y = coordinate.

The distribution function, ψ, is plotted for various values of *We* from small to large shear rates in Figure 14. As in elongation flow, the profile is relatively flat for small shear rates, while the height of the peak increases with increasing shear rate.

The peak of the PDF (usually at the equator, $\theta = 90°$) moves toward the shearing direction (i.e., $\phi = 0°$) as the shearing rate increasing. Shearing flow can be thought of as elongational flow with the coordinate system rotated 45°. The peak is close to $\phi = 45°$ for small shearing rates as showed in Figure 14a, and shifts to 20° for *We* = 1.0 as seen in Figure 14c.

The value of ϕ, corresponding to the maximum in the distribution function is plotted as a function of *We* in Figure 15. Note that discrete values of the angle are used (i.e., the graph is not continuous) because a finite number of mesh points were used to calculate the probability distribution function. However, the trend shows a monotonic decrease in the maximum PDF angle with increasing *We*.

The reason for the position of the peaks shifting with increasing shear rate is because shearing flow is a rotational flow. If a dumbbell is placed in a shearing flow field, it will rotate in a pattern similar to a Jeffery orbit (Jeffery, 1922). A Jeffrey orbit describes the locus of the end of a fiber rotating about the z-axis of a frame of reference which

We = 0.01
O_x = 0.0001

We = 0.1
O_x = 0.013

We = 1.0
O_x = 0.281
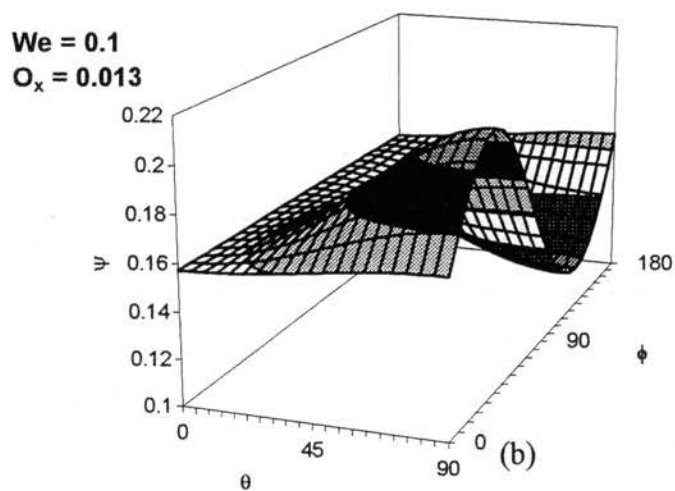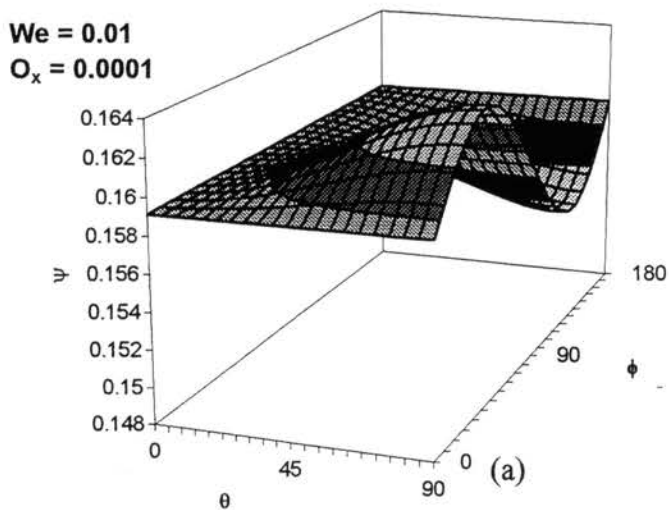
Figure 14. Ψ as a Function of θ and ϕ with We as a Parameter
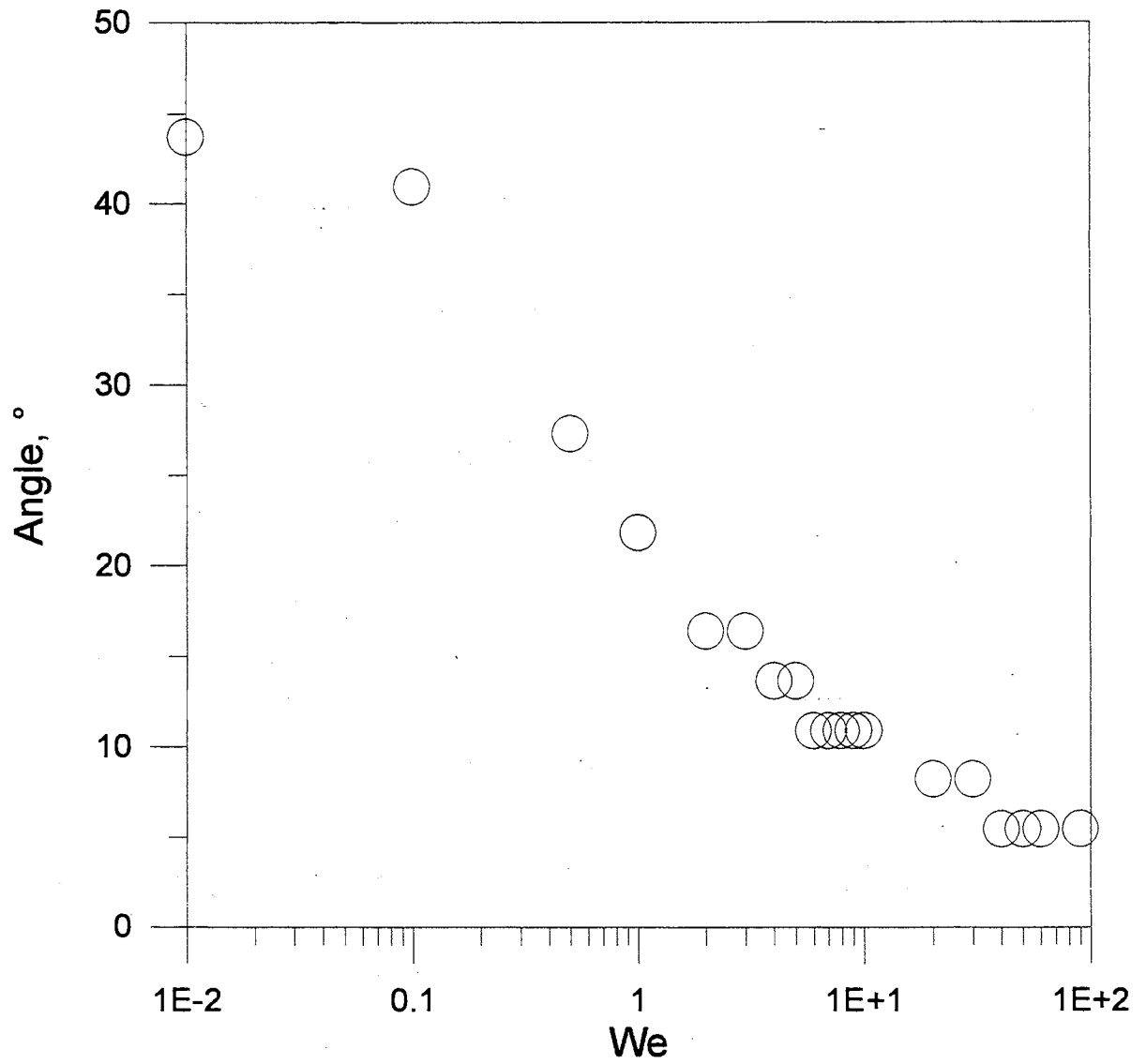
Figure 15. Maximum in the Distribution Function as a Function of *We*

moves with the fluid and the origin of which is at the center of mass of the fiber. The fiber

rotates rapidly in the vicinity of $\phi = 90°$ and very slowly near $\phi = 0°$. In contrast, a

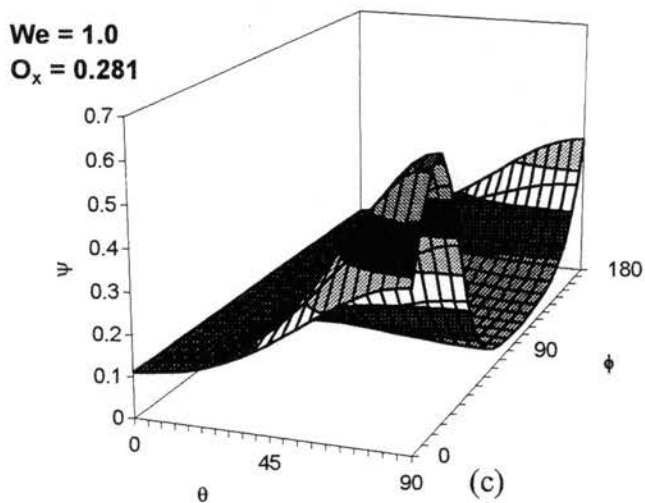dumbbell in an elongational flow will tend to be aligned in the direction of flow, and hence

the height of the peak greater than in shearing flow. A comparison of Figure 14c and 10c

for $We = 1.0$ shows that the height of the probability contour in elongational flow is much

greater than that in shearing flow. This explains why extended chain crystals are more

readily formed in elongational flow than shearing flow.

The numerical solution was found to be in good agreement with the solution

obtained from the perturbation method for low We. The percentage errors shown in

Figure 16 are no more than 0.002% and 0.25% for We values of 0.01 and 0.1,

respectively. The solution for steady shearing flow is a series expansion in terms of

spherical harmonics as shown in Eq. 3-47. The perturbation method can only describe

conditions close to the quiescent condition. This seems reasonable since by analogy, a

Taylor series can only describe a function near the point of expansion. A truncation error

analysis has been conducted for truncating terms after 5th term in Eq. 3-47, and the results

indicate that the truncation error is relatively important for small values of θ. For small

We (such as $We = 0.01$), the truncation error phases out very quickly, and the error is

mainly contributed from the size of the mesh. For $We = 0.1$, the truncation error becomes

relatively important for small value of θ. However, the maximum percentage error is still

only 0.25% and hence, the model can be considered to be reasonably correct in its

prediction.

A similar form of Eq. 3-45 using a coefficient of 6 instead of 12 was used to

describe the rigid dumbbell probability distribution in dilute polymer solutions (Bird and
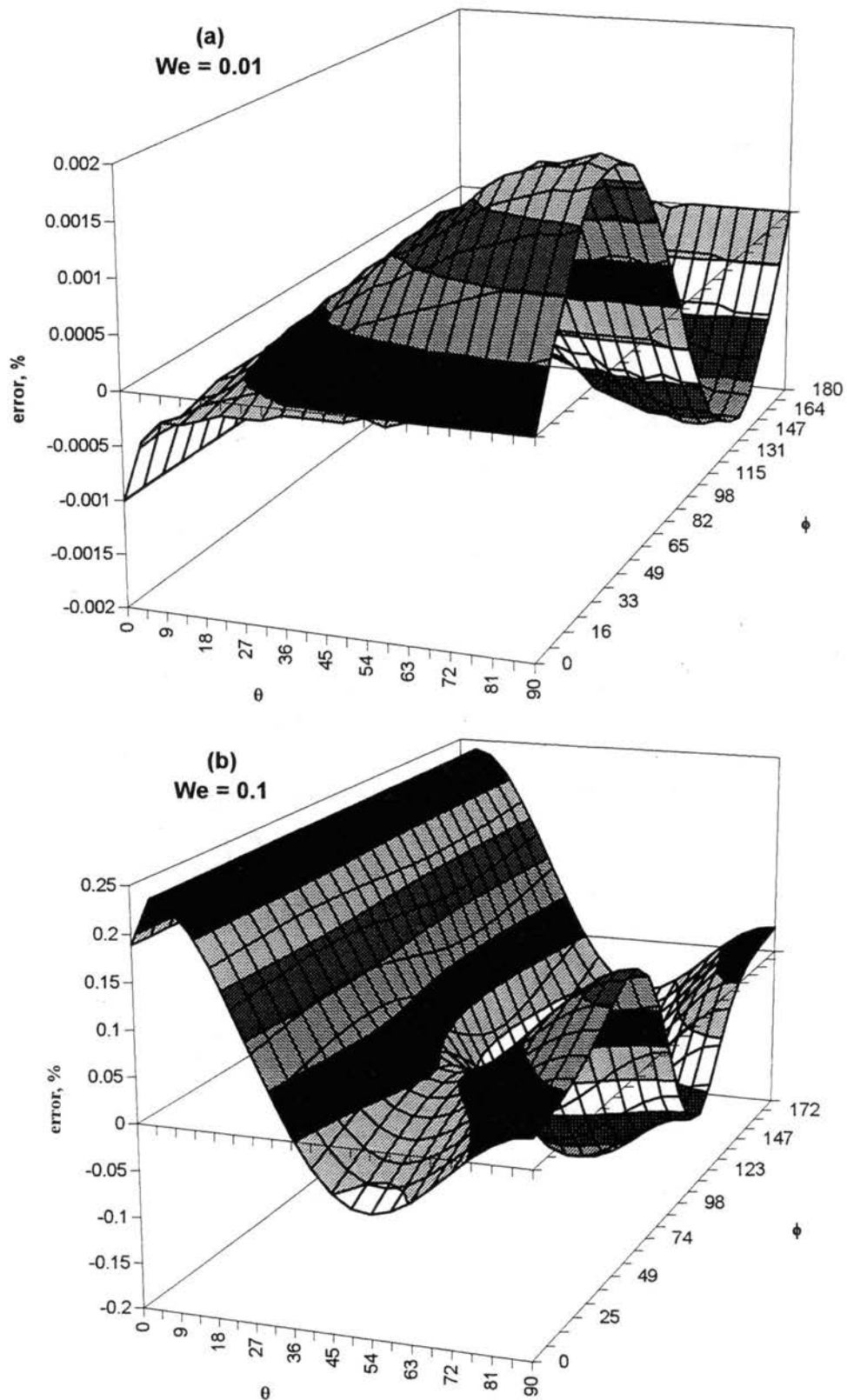
Figure 16. Percentage Error for Numerical Solution of Shearing Flow at Different *We*

Warner, 1971). The numerical solution did not compare favorably with the perturbation method solution for *We* greater than one. Nonetheless, the solution thus obtained was qualitatively consistent with the expected behavior.

The model was also compared with experimental results. Hongladarom *et al.* (1996) used X-rays to measure the orientation of hydroxypropyl cellulose (HPC) in water undergoing shear flow. HPC has a rigid backbone and is classified as a liquid crystalline polymer (LCP). Consequently, at zero shear rates some degree of order was observed. The comparison between the model and the experimental data is shown in Figure 17. Below a critical value of shear rate $\dot{\gamma}$ the flow had very little effect. One interpretation for this is that below a critical shear rate, thermal agitation dominates. Both experiment and model showed an increase in orientation with increasing shear rate above the critical value. The model does not account for the pre-existing molecular order in LCP. One way of modeling the pre-existing molecular order is by including the hindrance to the motion of the polymer chain by the adjacent polymer. However, the rigid-rod model still shows the right qualitative trend for the molecular orientation.

General Flow

Since no constraints were imposed on the flow tensor $\underline{\kappa}$ in the development of the diffusion equation, the most significant feature of the model is its capability to solve general flow problems without the assumption of a symmetric $\underline{\kappa}$. The probability distribution function for $We = 0.1$ with different flow fields is shown in Figure 18. The flow fields for different graphs are defined in Table II. The flow field in each case can be considered to be the summation of appropriately weighted shearing and elongational
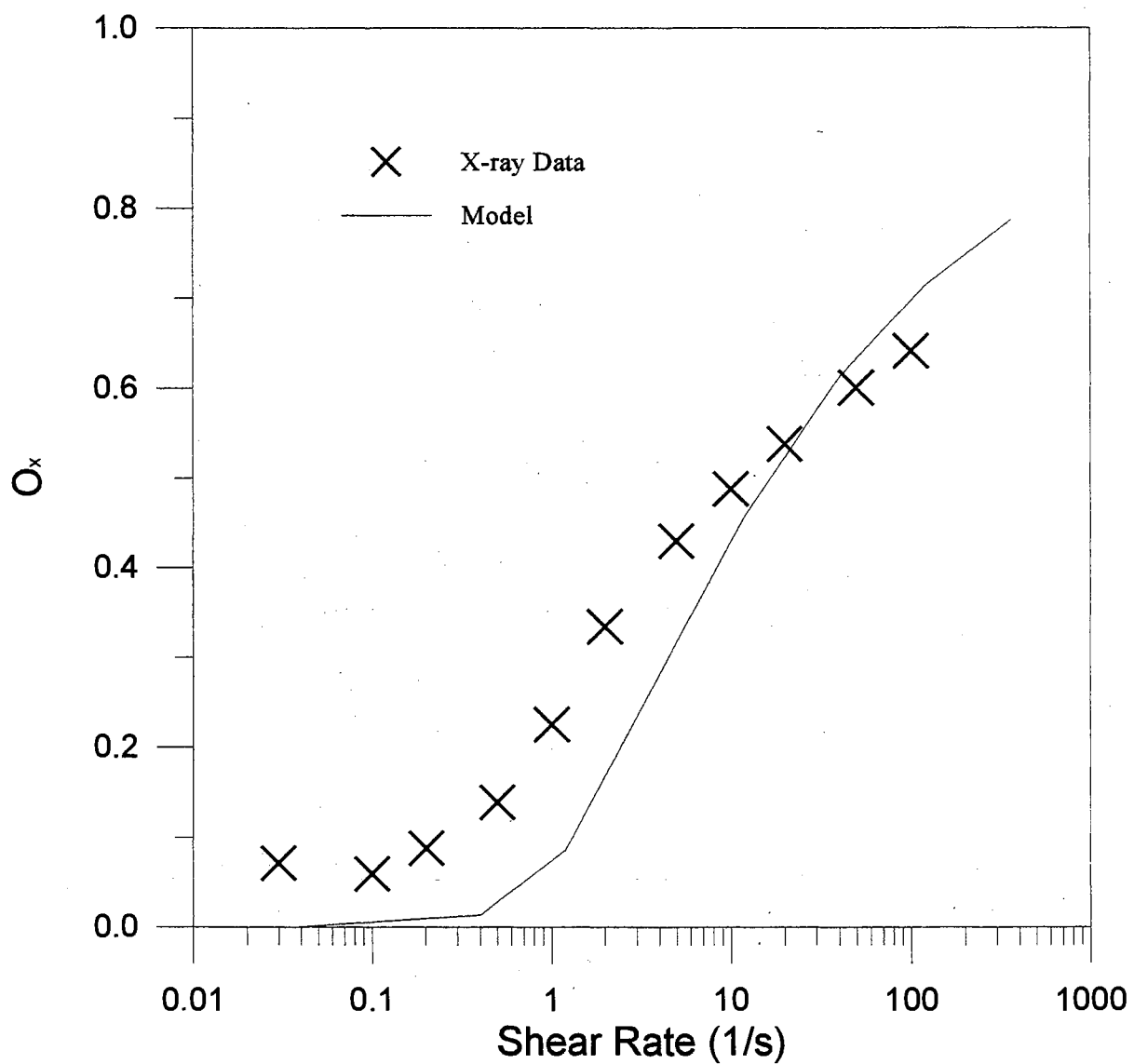
Figure 17. Comparison of the Molecular Orientation of HPC in Steady Shear to the Model Prediction
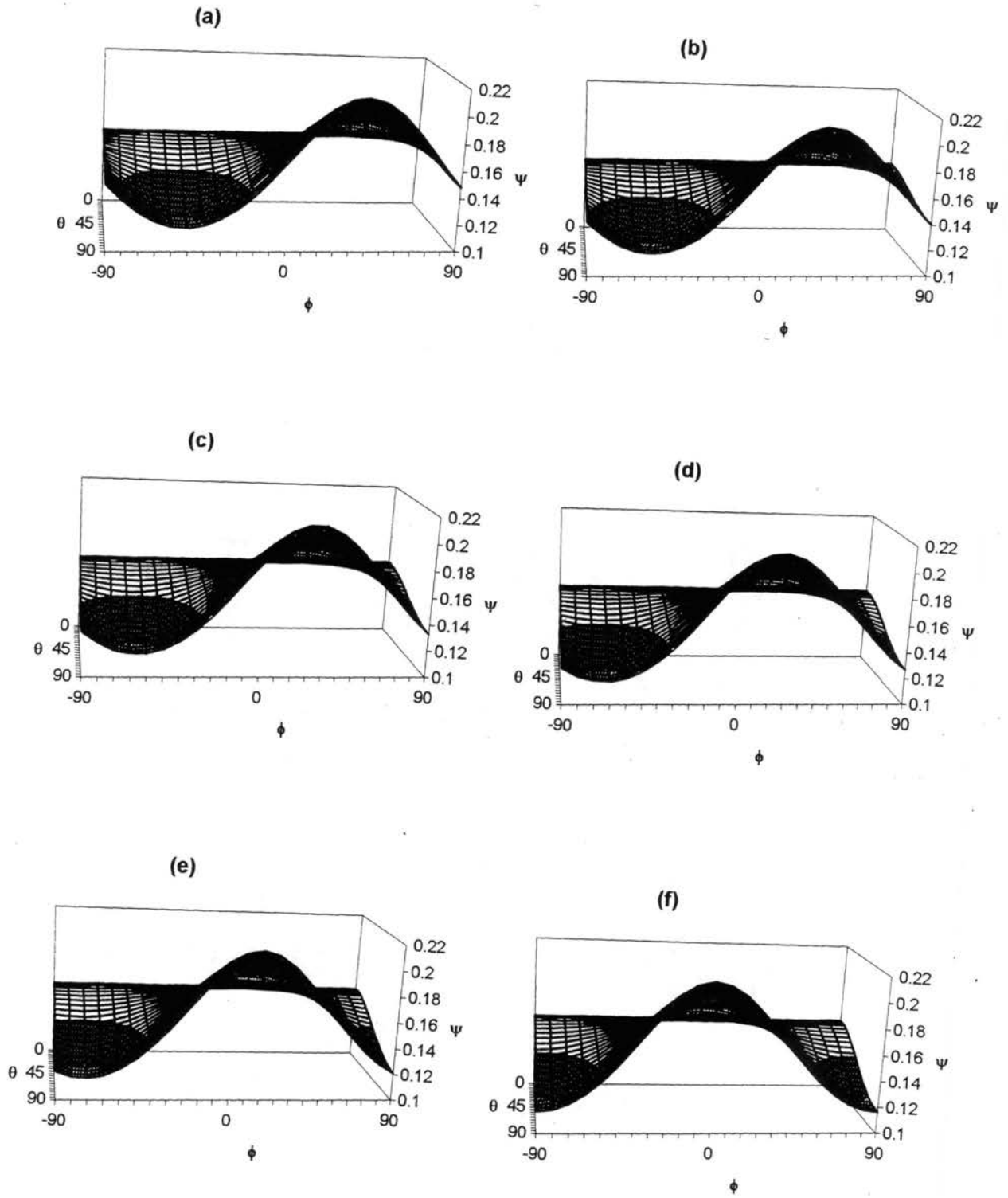
Figure 18. ψ in General Flow

flows. Note that the gradient tensors are not symmetric except in the elongational flow

case (f). Figure 18 shows the maximum probability angle shifting from ϕ approximately

equal to 41° for pure shearing flow (a) to ϕ equal to 0° for elongational flow (f). The

magnitude of the peaks does not change significantly (0.5%) for different velocity

gradients, but the height of the peaks should change for higher We, e.g., Figures 10c and

14c for $We = 1.0$, as mentioned before. The orientation parameters change substantially

from 0.0131 in shearing flow to 0.0616 in elongational flow for the same We.

TABLE II

THE VELOCITY GRADIENT TENSOR FOR DIFFERENT FLOW FIELDS

	(a)	(b)	(c)	(d)	(e)	(f)
$\underline{\underline{\kappa}}$	$\begin{vmatrix} 0 & 1 & 0 \\ 0 & 0 & 0 \\ 0 & 0 & 0 \end{vmatrix}$	$\begin{vmatrix} 0.1 & \sqrt{24}/5 & 0 \\ 0 & -0.1 & 0 \\ 0 & 0 & 0 \end{vmatrix}$	$\begin{vmatrix} 0.2 & \sqrt{21}/5 & 0 \\ 0 & -0.2 & 0 \\ 0 & 0 & 0 \end{vmatrix}$	$\begin{vmatrix} 0.3 & 0.8 & 0 \\ 0 & -0.3 & 0 \\ 0 & 0 & 0 \end{vmatrix}$	$\begin{vmatrix} 0.4 & 0.6 & 0 \\ 0 & -0.4 & 0 \\ 0 & 0 & 0 \end{vmatrix}$	$\begin{vmatrix} 0.5 & 0 & 0 \\ 0 & -0.5 & 0 \\ 0 & 0 & 0 \end{vmatrix}$
O_x	0.0131	0.0242	0.0345	0.0442	0.0532	0.0616

Implementation of Optimization

The primary goal of this work was to optimize polymer processes. The SQPHP

was used to find optimum points for the die configuration. In the process of optimization,

the velocity field is required to evaluate the probability distribution function. Since

analytical solutions are generally not available, some numerical method such as the Finite

Element Method (FEM) must be used. The commercial software package FIDAP, which

is based on FEM, was used to solve many aspects of the flow problem. FIDAP obviated

the need to develop a code to solve the fluid flow problem and to generate the necessary

mesh for FEM. Since FIDAP is based on FEM, complicated geometries with complicated

boundary conditions could be simulated. The only disadvantage in using FIDAP is that

the source code for the program was not available. The non-availability of the source

code was not a significant drawback because of the inherent flexibility and relatively user-

friendly interface and extensive documentation provided by the FIDAP vendor.

In FEM, the entire flow domain is divided into a finite number of elements. In this

study, a 9-node quadrilateral element was used as shown in Figure 19a. The FEM

technique results in values of the velocity field at the nodes. The velocity field inside the

element was found by interpolation with a quadratic equation.
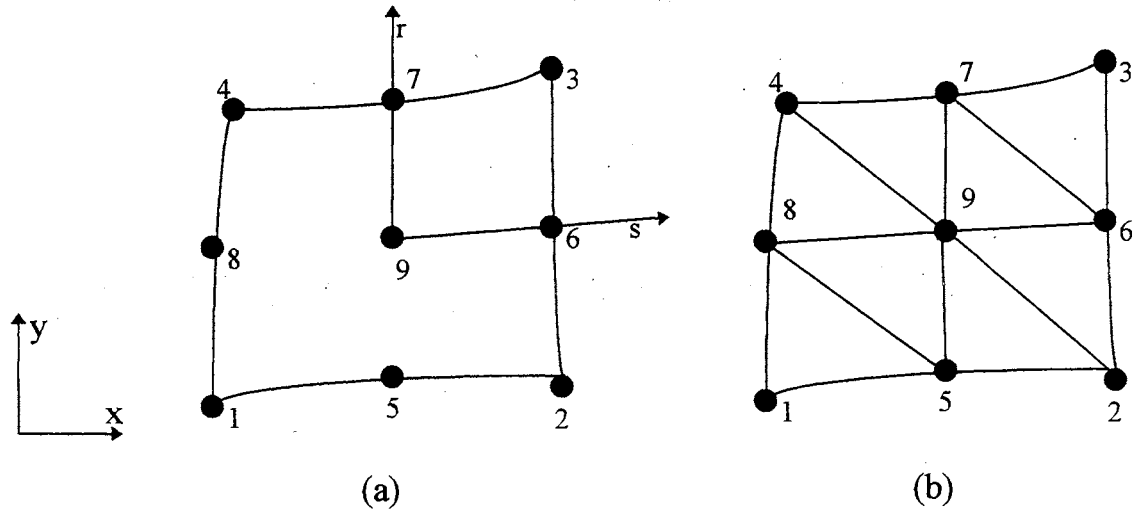
Figure 19. Definition of Natural Coordinates

In order to obtain the velocity components, the finite element needs to be further divided into 8 triangle sub-element as shown in Figure 19b and the velocity coefficients (i.e., a, b, c, d, e, and f in Eq. 3-20) in the sub-elements can be obtained by the velocities on the 3 corners of the triangle element.

A molecular configuration that reached steady state instantaneously was assumed. So instead of tracing out the change in the flow field along the trajectory of the fluid inside the flow domain, only the molecular configuration at the exit is required for analysis.

Since the source code of FIDAP was not available, the necessary parameters for optimization were stored in files to pass between programs. The curve to be optimized was defined by points which were stored in the file geo. The probability distribution function was evaluated after FIDAP finished the velocity calculations. The program rdbase.f, provided by FIDAP, was modified to read the results database and to evaluate the objective function. The value of objective function was saved to a file called obj for further optimization using SQPHP.

As mentioned in Chapter III, the SQPHP algorithm requires the first derivative of the objective function and constraints to evaluate the Hessian matrix. There is no explicit expression for the relation between the geometry and objective function. Hence, the first derivative is obtained numerically by forward differences.

Optimization

The optimization algorithm, SQPHP, was first tested with 13 standard nonlinear constrained problems in the literature (Himmelblau, 1972; Betts, 1978; Dayde, 1989). The main purpose of testing the SQPHP code was to check for correctness rather than

efficiency. Some standard test problems were available in the literature, and the tested problems are listed in Appendix B with the solutions from the literature and the SQPHP program. The SQPHP solutions (i.e., the minimum point obtained and the corresponding objective function) agreed with the solution provided in the literature except for problems 4, 11, and 12 as shown below.

Problem 4 (Dayde, 1989)

Minimize: $f(\underline{x}) = 100(x_2 - x_1^2)^2 + (1 - x_1)^2 + 100(x_3 - x_2^2)^2 + (1 - x_2)^2$ (4-4)

Subject to: $9x_1 + 6x_2 + x_3 - 100 = 0$ (4-4a)

$10x_1 + 20x_2 + x_3 - 100 \geq 0$ (4-4b)

$40 - x_1 - 2x_2 - 4x_3 \geq 0$ (4-4c)

$x_i \geq 0, \quad i = 1, 2, 3$ (4-4d)

$\underline{x}_o = [1, 1, 1]^T$

$f(\underline{x}_o) = 0$

$\underline{x}^* = [6.67, 6.67, 0]^T$

$f(\underline{x}^*) = 3.3 \times 10^5$

SQPHP results, same as High (1991)

$\underline{x}^* = [6.5983, 5.8663, 5.4173]$

$f(\underline{x}^*) = 2.26 \times 10^5$

Problem 11 (Himmelbalu, 1972; Betts, 1978; Dayde, 1989)

Minimize: $f(\underline{x}) = -0.5(x_1x_4 - x_2x_3 + x_3x_9 - x_5x_9 + x_5x_8 - x_6x_7)$ (4-5)

Subject to: $1 - x_3^2 - x_4^2 \geq 0$ (4-5a)

$1 - x_9^2 \geq 0$ (4-5b)

$1 - x_5^2 - x_6^2 \geq 0$ (4-5c)

$1 - x_1^2 - (x_2 - x_9)^2 \geq 0$ (4-5d)

$1 - (x_1 - x_5)^2 - (x_2 - x_6)^2 \geq 0$ (4-5f)

$1 - (x_1 - x_7)^2 - (x_2 - x_8)^2 \geq 0$ (4-5g)

$1 - (x_3 - x_5)^2 - (x_4 - x_6)^2 \geq 0$ (4-5h)

$1 - (x_3 - x_7)^2 - (x_4 - x_8)^2 \geq 0$ (4-5i)

$1 - x_7^2 - (x_8 - x_9)^2 \geq 0$ (4-5j)

$x_1x_4 - x_2x_3 \geq 0$ (4-5k)

$x_3x_9 \geq 0$ (4-5l)

$-x_5x_9 \geq 0$ (4-5m)

$x_5x_8 - x_6x_7 \geq 0$ (4-5n)

$x_9 \geq 0$ (4-5o)

$x_i = 1, \quad i = 1,\ldots, 9$

$f(\underline{x}_o) = 0$

$\underline{x}^* = [0.9971, -0.0758, 0.5530, 0.8331, 0.9981, -0.0623, 0.5642, 0.8256,$
$\qquad 0.0000024]^T$ (Himmelblau, 1972)

$\underline{x}^* = [0.91878, 0.39476, 0.11752, 0.99307, 0.91878, 0.39476, 0.11752, 0.99307,$
$\qquad -0.60445 \times 10^{-14}]^T$ (Betts, 1978; Dayde, 1989)

$f(\underline{x}^*) = -0.8660$

SQPHP results

$\underline{x}^* = [0.86602, 0.5, 0, 1.0, 0.86602, 0.5, 0, 1, 0]^T$

$f(\underline{x}^*) = -0.86602$

Problem 12 (Himmelblau, 1972; Betts, 1978)

Minimize: $f(x) = -75.196 + 3.8112\, x_1 - 0.12694 x_1^2 + 2.0567 \times 10^{-3} x_1^3$
$\qquad - 1.0345 \times 10^{-5} x_1^4 + 6.8306 x_2 - 0.030234 x_1 x_2 + 1.28134 \times 10^{-3} x_2 x_1^2$
$\qquad - 3.5256 \times 10^{-5} x_2 x_1^3 + 2.266 \times 10^{-7} x_2 x_1^4 - 0.25645 x_2^2 + 3.4604 \times 10^{-3} x_2^3$
$\qquad - 1.3514 \times 10^{-5} x_2^4 + 28.106/(x_2 + 1) + 5.2375 \times 10^{-6} x_1^2 x_2^2 \qquad \text{(4-6)}$
$\qquad + 6.3 \times 10^{-8} x_1^3 x_2^2 - 7 \times 10^{-10} x_1^3 x_2^3 - 3.4054 \times 10^{-4} x_1 x_2^2$
$\qquad + 1.6638 \times 10^{-6} x_1 x_2^3 + 2.8673 \exp(0.0005 x_1 x_2)$

Subject to: $0 \le x_1 \le 75$ $\qquad\qquad\qquad\qquad\qquad\qquad\qquad$ (4-6a)

$\qquad\qquad 0 \le x_2 \le 65$ $\qquad\qquad\qquad\qquad\qquad\qquad\qquad$ (4-6b)

$\qquad\qquad x_1 x_2 - 700 \ge 0$ $\qquad\qquad\qquad\qquad\qquad\qquad\qquad$ (4-6c)

$\qquad\qquad x_2 - 5(x_1/25)^2 \ge 0$ $\qquad\qquad\qquad\qquad\qquad\qquad$ (4-6d)

$\qquad\qquad (x_2 - 50)^2 - 5(x_1 - 55) \ge 0$ $\qquad\qquad\qquad\qquad\qquad$ (4-6f)

$\qquad\qquad \underline{x}_o = [90, 10]^T$

$\qquad\qquad f(\underline{x}_o) = 82.828$

$\underline{x}^* = [75, 65]^T$

$f(\underline{x}^*) = -58.903$

SQPHP results

$\underline{x}^* = [46.2, 50.63]^T$

$f(\underline{x}^*) = -6.58$

For problems 4 and 11, the minimum points obtained were different than the literature values. However, SQPHP reached solutions that had smaller values of the objective function than those reported in the literature. Hence the SQPHP code has the ability to search for and determine the minimum point with greater accuracy than the techniques reported in the literature. In problem 12, the value of the objective function provided in the literature cannot be obtained even by substituting the minimum value determined in the

same work. A possible explanation is that the problem or solution in the literature (Betts, 1978) may have a typographical error. In conclusion, from the results of the test cases considered, SQPHP is observed to be more than adequate to meet the requirements of the shape optimization.

Verification Case - Diffuser Shape Optimization

In order to verify the technique, a die optimization problem was found with a known solution. The problem involves the maximization of the pressure rise in a diffuser. The flow field in the diffuser was assumed to be 2-dimensional incompressible, laminar flow governed by the steady-state Navier-Stokes equation. The configuration of the plane diffuser shown in Figure 20. The entrance height was W_1 and length L. Only the upper half of the diffuser was modeled, because of symmetry.
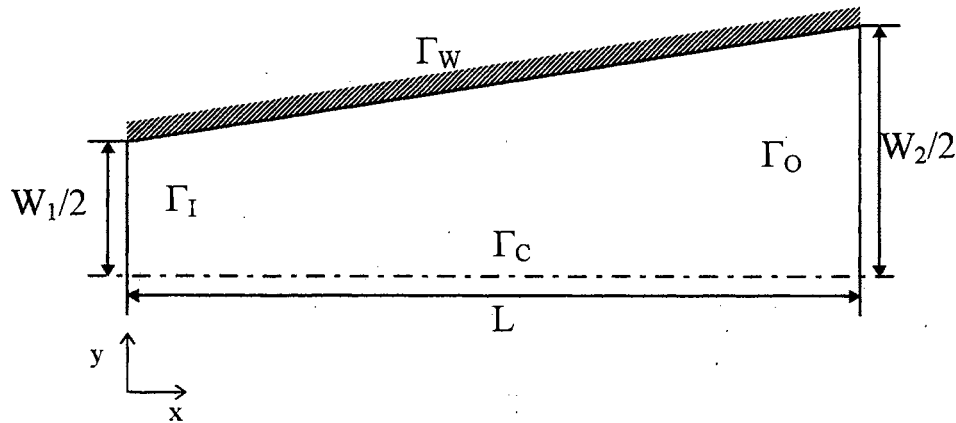
Figure 20. Schematic Diagram of a Plane Diffuser

A no-slip condition was imposed on the die wall, Γ_w. A parabolic velocity profile (i.e., slit flow) was imposed at the entrance, Γ_I. There was no y-component of velocity on the center line, Γ_c. Thus, we have the following

$$\frac{u_x}{V_{avg}} = \frac{3}{2}\left[1 - \left(\frac{y}{W_1/2}\right)^2\right] \quad \text{on } \Gamma_I$$

$$u_x = u_y = 0 \qquad \text{on } \Gamma_w \qquad\qquad (4\text{-}7)$$

$$u_y = 0 \qquad \text{on } \Gamma_c$$

When the fluid passed through the diffuser the velocity decreases and the kinetic energy is converted to a static pressure rise. In terms of energy, the kinetic energy has been transferred to work due to flow. The maximum pressure rise can be reached by minimizing the friction lose on the wall of the diffuser. The velocity weighted pressure was chosen as the objective function to account for the pressure variation along the inlet and outlet regimes of the diffuser.

$$f(\underline{x}) = -\left(\int_{\Gamma_I} p\underline{u} \cdot \underline{n} ds + \int_{\Gamma_o} p\underline{u} \cdot \underline{n} ds\right) \qquad\qquad (4\text{-}8)$$

It should be noted that the objective function was multiplied by -1 for convenience. This operation is justified since maximization of the positive objective function is the same as minimization of the negative objective function, which was required by the SQPHP code.

The shape of the diffuser can be defined by drawing a spline between points on the wall. The shape of the diffuser can be assumed to be a straight line. Since the inlet width is specified, maximum pressure can be achieved by varying the height of the exit. For a parabolic shape diffuser, two design variables are required viz. the heights at the middle and at the exit of diffuser. The desired shape of the diffuser can be defined by using higher degrees of the spline line.

The Reynolds number for diffuser is defined as follows.

$$Re = \frac{W_1 V_{avg} \rho}{\mu} \qquad (4\text{-}9)$$

where

ρ = density

μ = viscosity

The diffuser was modeled for Re = 200 with the following parameters:

V_{avg} = 4. cm/sec

W_1 = 1. cm

L = 3. cm

ρ = 1. g/cm^3

μ = 0.02 g/cm·sec

A 9-node quadrilateral element was used for the velocity variables, while the pressure was discretized using the bilinear approximation. The size of the mesh was 31 × 15 elements. One of the typical concerns for models using the FEM is mesh distortion. For the worst case considered, the mesh still remained regular as shown in Figure 21. The shapes for different number of design variables are plotted in Figure 22, along with the results obtained for a similar optimization by Çabuk and Modi (1992). The comparison between this work and Çabuk and Modi's work can not be exact, because the boundary conditions were different. Çabuk and Modi specified three additional boundary conditions, as shown in the following equations:

Y

X
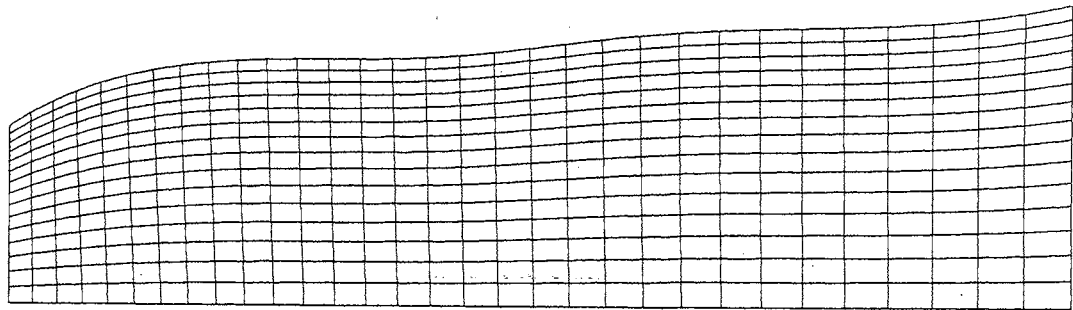
Figure 21. Diffuser Mesh
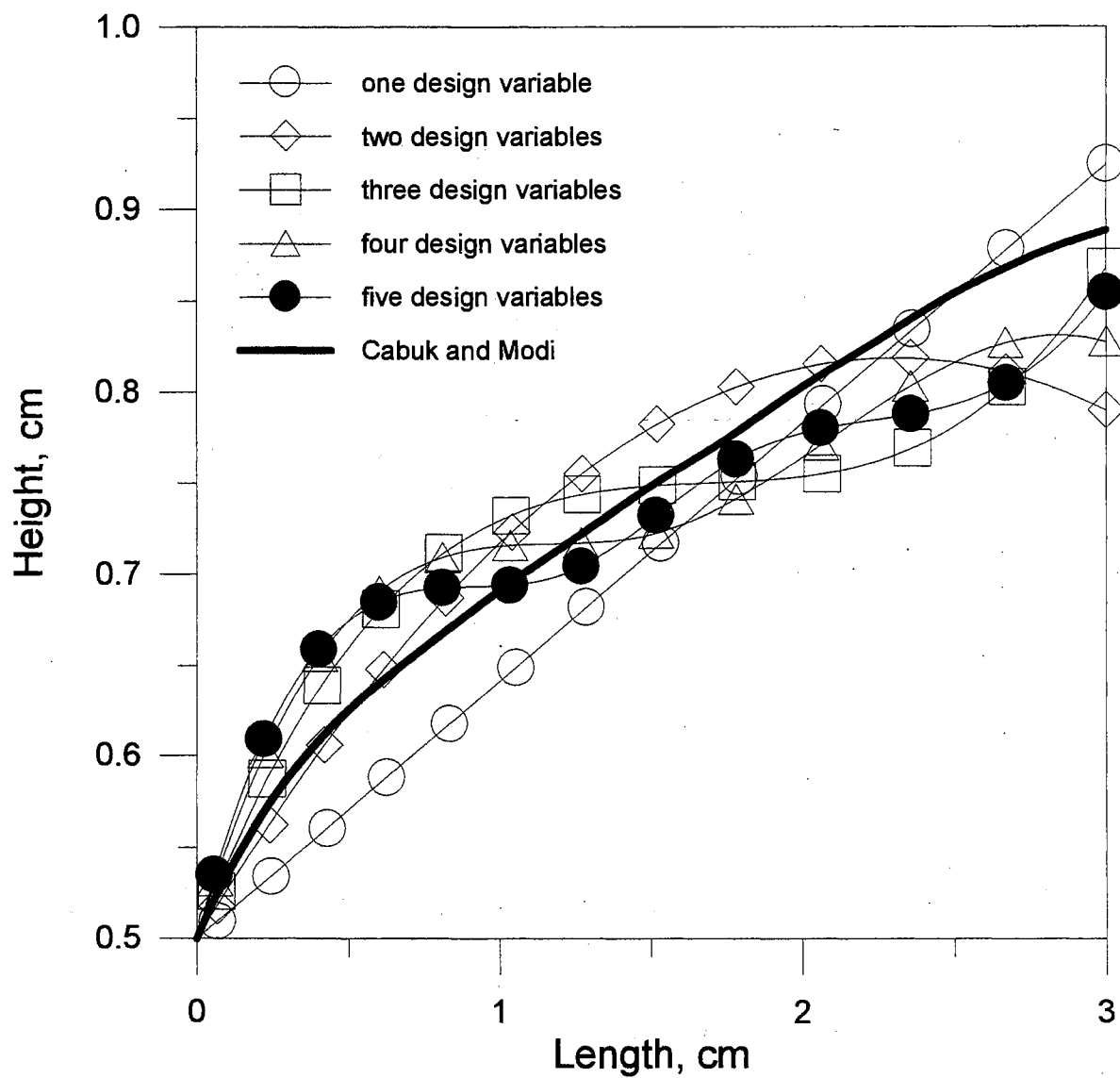
Figure 22. Diffuser Shape for Different Number of Design Variables

$$\frac{\partial u_y}{\partial n} = 0 \qquad \text{on } \Gamma_I$$

$$\frac{\partial u_x}{\partial n} = \frac{\partial u_y}{\partial n} = 0 \quad \text{on } \Gamma_O \qquad\qquad (4\text{-}10)$$

$$\frac{\partial u_y}{\partial n} = 0 \qquad \text{on } \Gamma_C$$

When the boundary condition is specified as the outer normal derivative on the boundary, it is referred to as a Neumann-type boundary condition. The Neumann-type velocity boundary conditions cannot be specified by FIDAP. However, the diffuser shapes in Figure 22 are at least qualitatively similar to those of Çabuk and Modi. The corresponding objective functions are shown in Table III.

TABLE III.

THE EFFECT OF DESIGN VARIABLES TO OPTIMIMUM OBJECTIVE FUNCTION

Number of Design Variable	One	Two	Three	Four	Five
$f(\underline{x}^*)$	-5.656	-6.201	-6.357	-6.395	-6.413

The pressure rise based on the shape obtained by Çabuk and Modi has a value of 5.656 which is approximately the value for the straight shaped diffuser in Figure 22. A higher pressure rise can be achieved by using a higher spline order. The objective function is plotted as a function of the number of iterations in Figure 23. The objective function dropped rapidly in the first couple of iterations and slowly plateaus out which indicated that the optimum shape did indeed converge to the minimum point. The figure also showed that lower objective functions can be achieved by using more design variables.
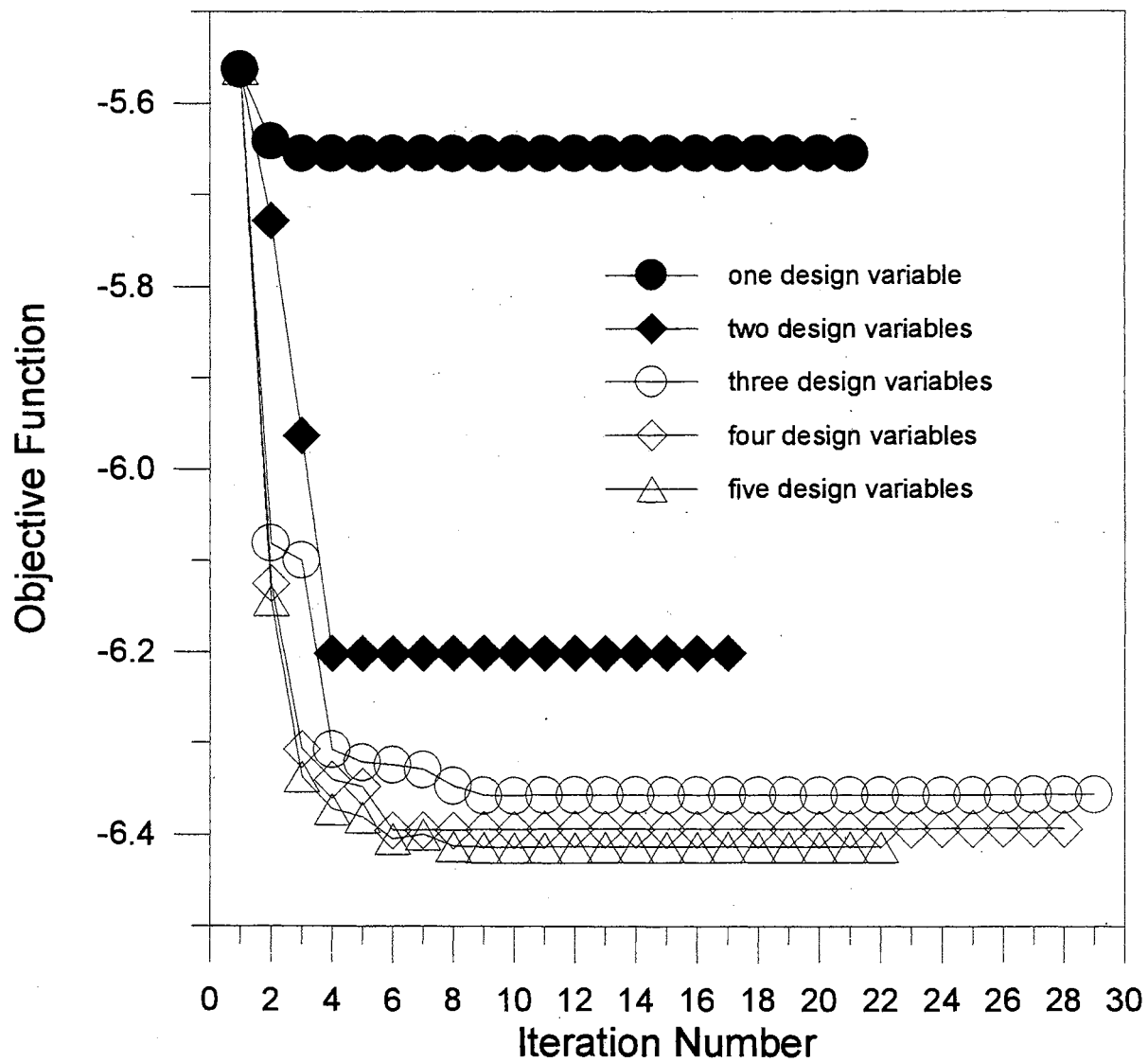
Figure 23. Objective Function for Different Number of Design Variables

Verification Case - Slit Flow

Before introducing the model to the optimization algorithm, a well characterized slit flow which is defined as fluid flow between two parallel plates as shown in Figure 24, was first used to demonstrate the effect of the flow field on the x-direction strength. The flow field can be described by the following equation:
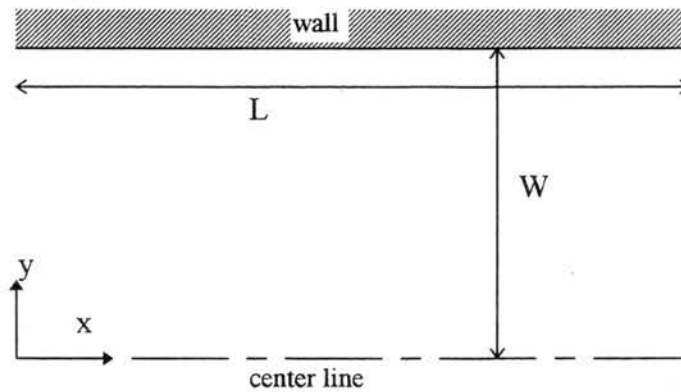
Figure 24. Slit Die

$$u_x = \frac{W^2}{2\mu}\frac{dP}{dx}\left[1-\left(\frac{y}{W}\right)^2\right] \qquad (4\text{-}11)$$

where W is the half width of the slit, and $\underline{\underline{\kappa}}$ is given by

$$\underline{\underline{\kappa}} = -\frac{W^2}{\mu}\frac{dP}{dx}\begin{vmatrix} 0 & y & 0 \\ 0 & 0 & 0 \\ 0 & 0 & 0 \end{vmatrix} \qquad (4\text{-}12)$$

Eq. 4-12 suggests that the shear rate is zero at the center and linearly increases to a maximum on the wall. The flow field was solved by FIDAP with the following boundary conditions.

$$\left. \begin{array}{ll} \sigma_x = C & \text{on } \Gamma_{\text{I}} \\ u_x = u_y = 0 & \text{on } \Gamma_{\text{w}} \\ u_x = 0 & \text{on } \Gamma_{\text{c}} \end{array} \right\}$$ (4-13)

where

σ_x = x component of total normal stress, $\underline{\sigma}$

The total normal stress vector, $\underline{\sigma}$, was defined as

$$\underline{\sigma} = \left(-p\underline{\underline{\delta}} + \mu\underline{\dot{\gamma}} \right) \cdot \underline{n}$$ (4-14)

where

$\underline{\underline{\delta}}$ = unit tensor

$\underline{n}$ = outward normal unit vector

For slit slow, the x-direction normal stress equals pressure, while for other cases the x-direction normal stress is not the same as pressure. However, in a rough sense the pressure drop was still used to characterize the stress. The following parameters were used for the slit flow calculations.

$\sigma_x = 2 \times 10^6$ dyne/cm^2

W = 1. cm

L = 3. cm

$\rho = 0.9$ g/cm^3

$\mu = 7.083 \times 10^4$ g/cm·sec

The x-direction strength, as shown in Figure 25, increases from the center where the shear rate is zero, to a maximum at the wall where the shear rate is highest.
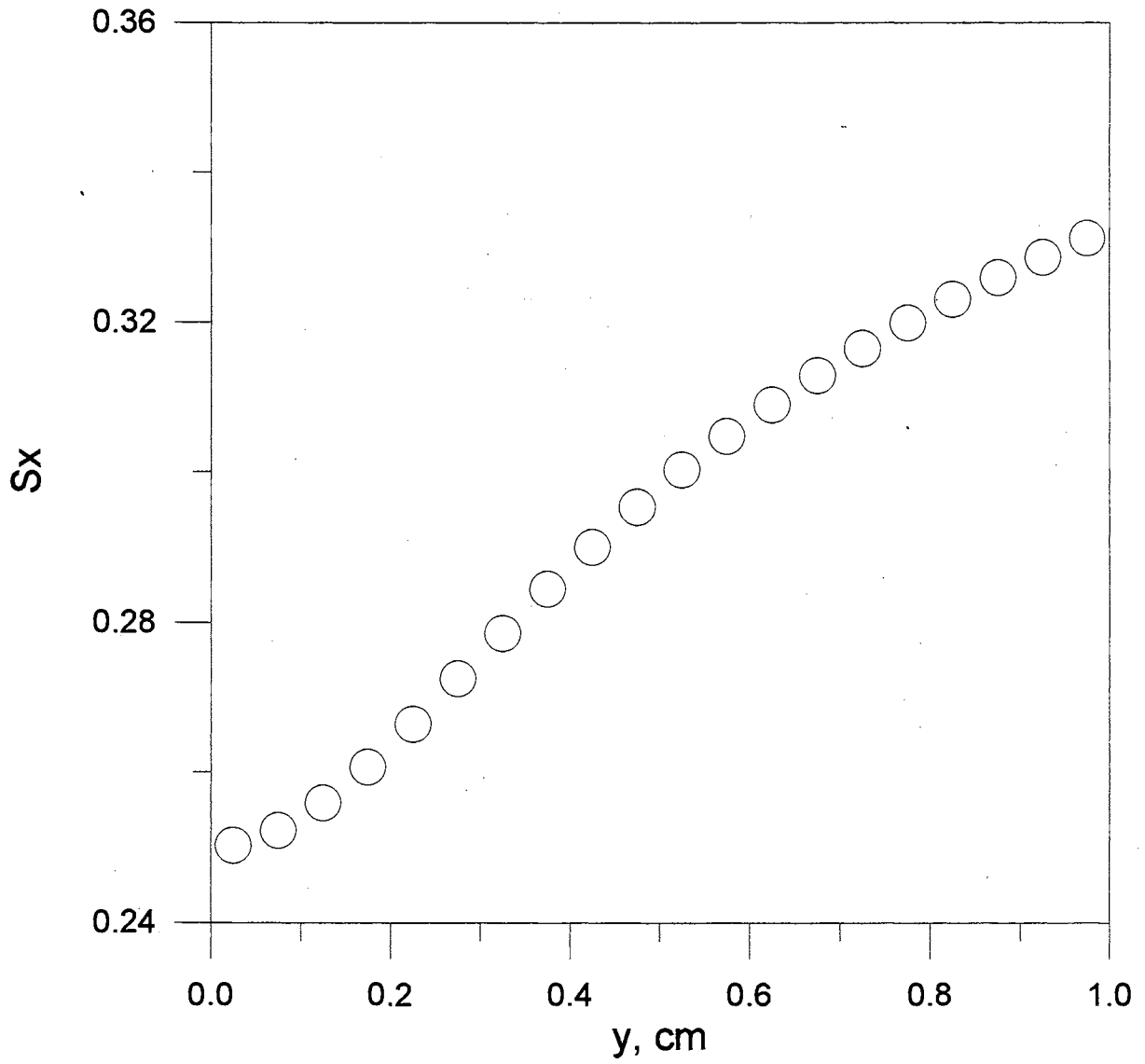
Figure 25. x-Direction Strength Along Width

Minimizing x-Direction Strength Variation

The goal of the optimization is to design an extruder die which can produce a material with the minimum variation of x-directional strength. Hence, the objective function $f(\underline{x})$ was defined as the standard deviation of the x-direction strength along the die exit.

$$f(\underline{x}) = \sqrt{\frac{\sum_i \left(w_i S_{xi} - \overline{S}_x\right)^2}{n}} \qquad (4\text{-}15)$$

where

$\overline{S}_x$ = average of relative x-direction strength,

w_i = weighting factor,

n = number of sub-elements across the exit.

The weighting factors depend on the mesh spacing. For non-uniform mesh spacing, the weighting factors are not all the same, i.e., for larger spacing the weighting factors are greater than those for smaller spacing. In this case, however, a uniform mesh spacing was used and hence the weighting factors were identically equal to one.

The shape of the die was defined by a 3 point spline which had the x-coordinates of 0, 1.5, and 3 cm as shown in Figure 26. The optimization was performed by varying the height of two points, $x = 0$ and $x = 1.5$, while the point on the exit was kept fixed ($x = 3$. cm, $y = 1$ cm). The material properties were the same as those for the slit flow calculation. The total normal stress was specified as 2×10^5 dyne/cm^2 at the die inlet. Also, the initial shape of the die was a straight converging channel. Since instantaneous

attainment of the equilibrium molecular configurations was assumed, it is sufficient to

consider molecular configurations at the die exit only.
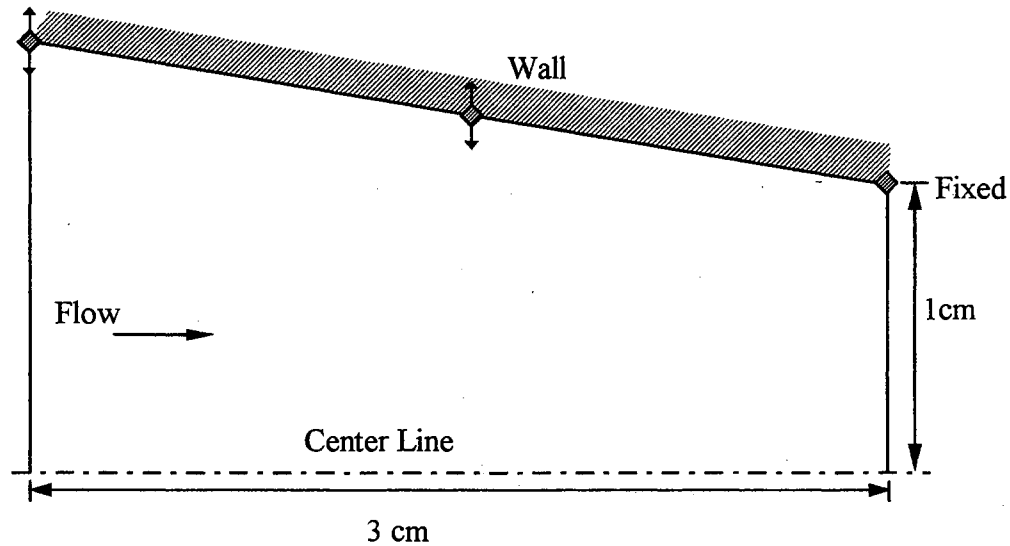
Figure 26. Configuration for Die Geometry Optimization

The x-direction strength change during the optimization is shown in Figure 27, and

the corresponding shape is shown in Figure 28. In the converging channel, the center

portion is dominated by extensional flow while near the wall, shearing flow is the

dominant flow field. As discussed in the section on Probability Distribution Function

Prediction earlier in this chapter, extensional flow is more effective than shearing flow in

aligning molecules in the flow direction. Also since the x-direction strength is assumed to

be proportional to the orientation, there is, therefore, a variation in the x-direction strength

along the y direction as shown in Figure 26. If the angle of convergence is increased, the

effect of extensional flow at the center correspondingly increases. Hence, the molecules

are more aligned than before and the corresponding variation in the x-direction strength
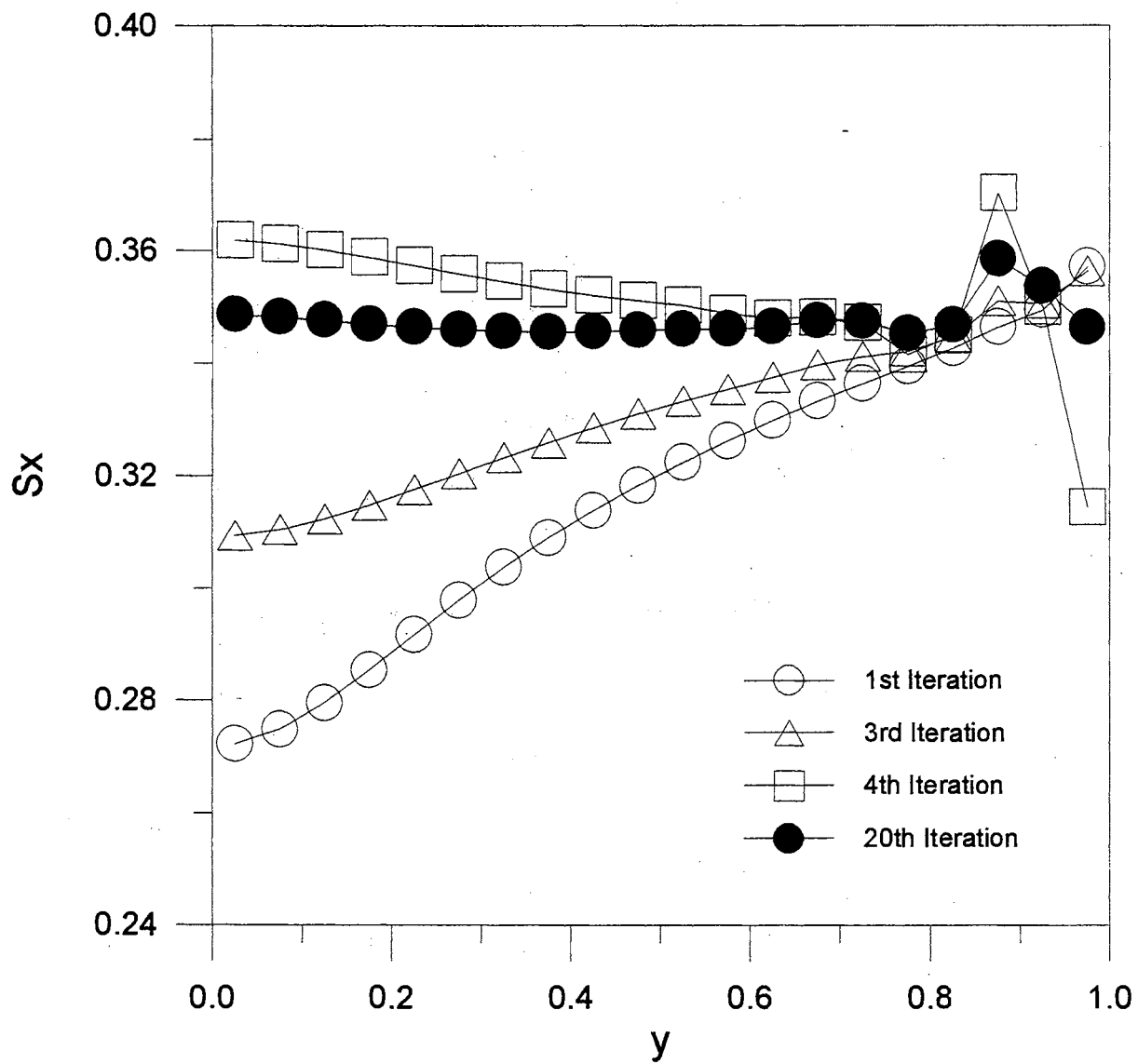
Figure 27. x-Direction Strength at Successive Iteration
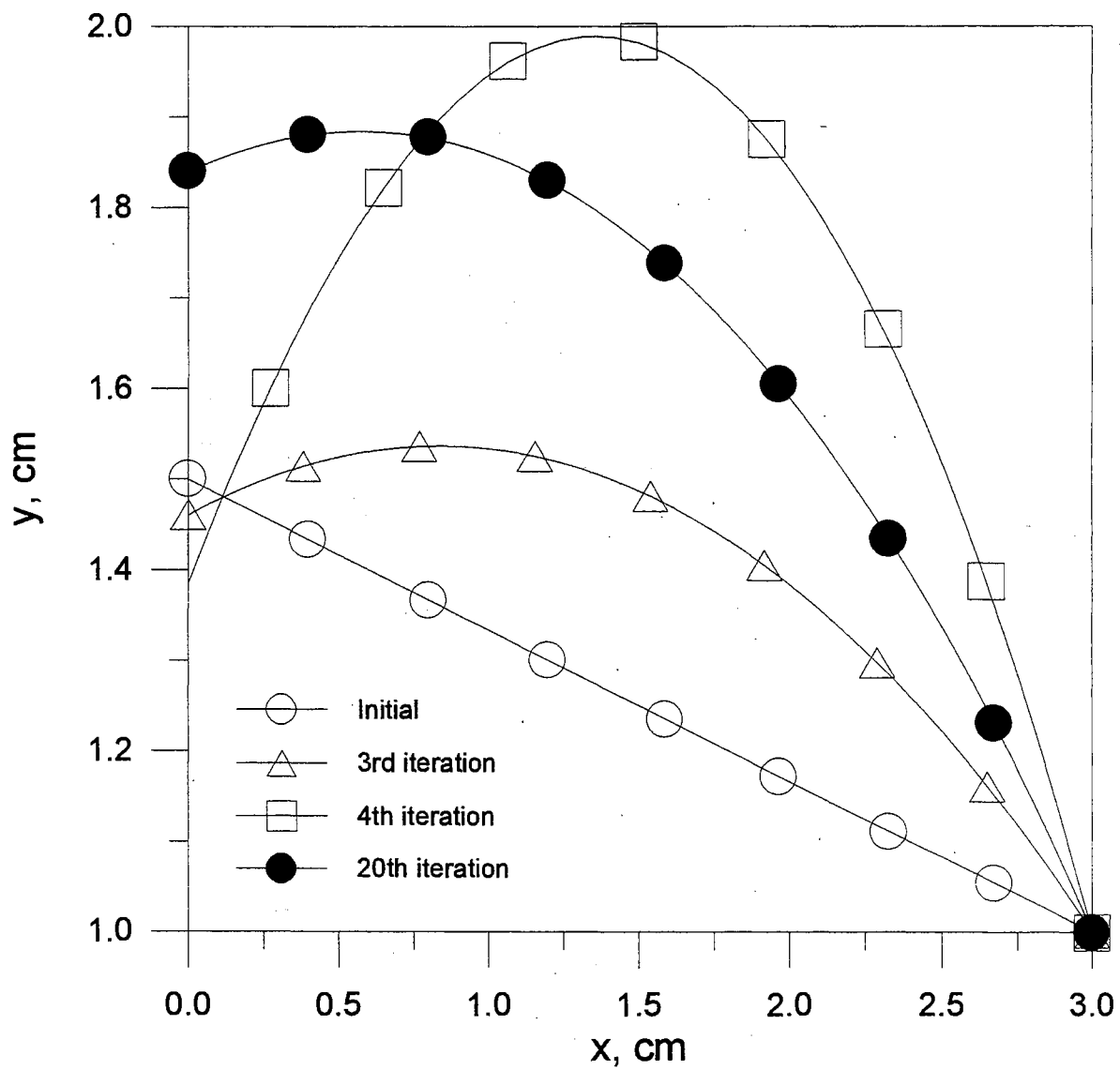
Figure 28. Die Shape at Successive Iteration

along the y direction in Figure 27 is less than that for the original converging channel. Sometimes there is a chance that the x-direction strength at the center is higher than other regions as shown in the 4th iteration of Figure 27. In this situation however, the resultant increase in entrance width will increase the flow rate through the die and also the shear rate near the wall. The optimized die has a fairly uniform x-direction strength along the die. Figure 28 shows that the shape of the die required to maintain the specified pressure drop changes dramatically within the first four iterations and finally converges after 20 iterations to an optimum shape.

The effect of varying the pressure differences was also studied, and the resultant shapes obtained are shown in Figure 29. Figure 29 shows that as the pressure drop increases, the angle of convergence decreases and the shape of the die tends to be more parabolic in nature. The corresponding objective function is plotted as a function of the number of iterations required for convergence in Figure 30. In all cases, it is observed that the program was successful in reaching the minimum value of the objective function.

98
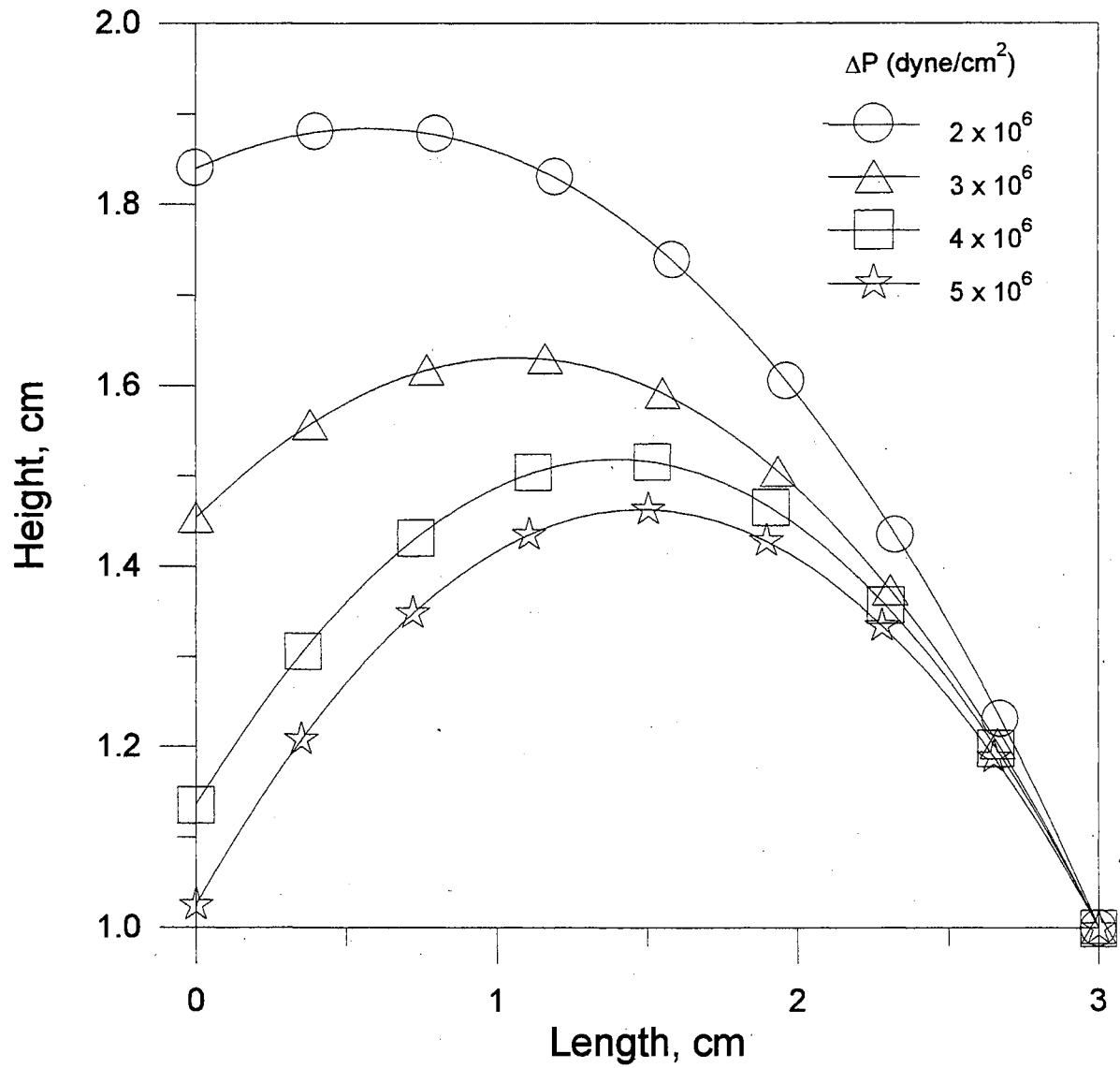
Figure 29. Optimized Die Shape for Different Pressure Drops
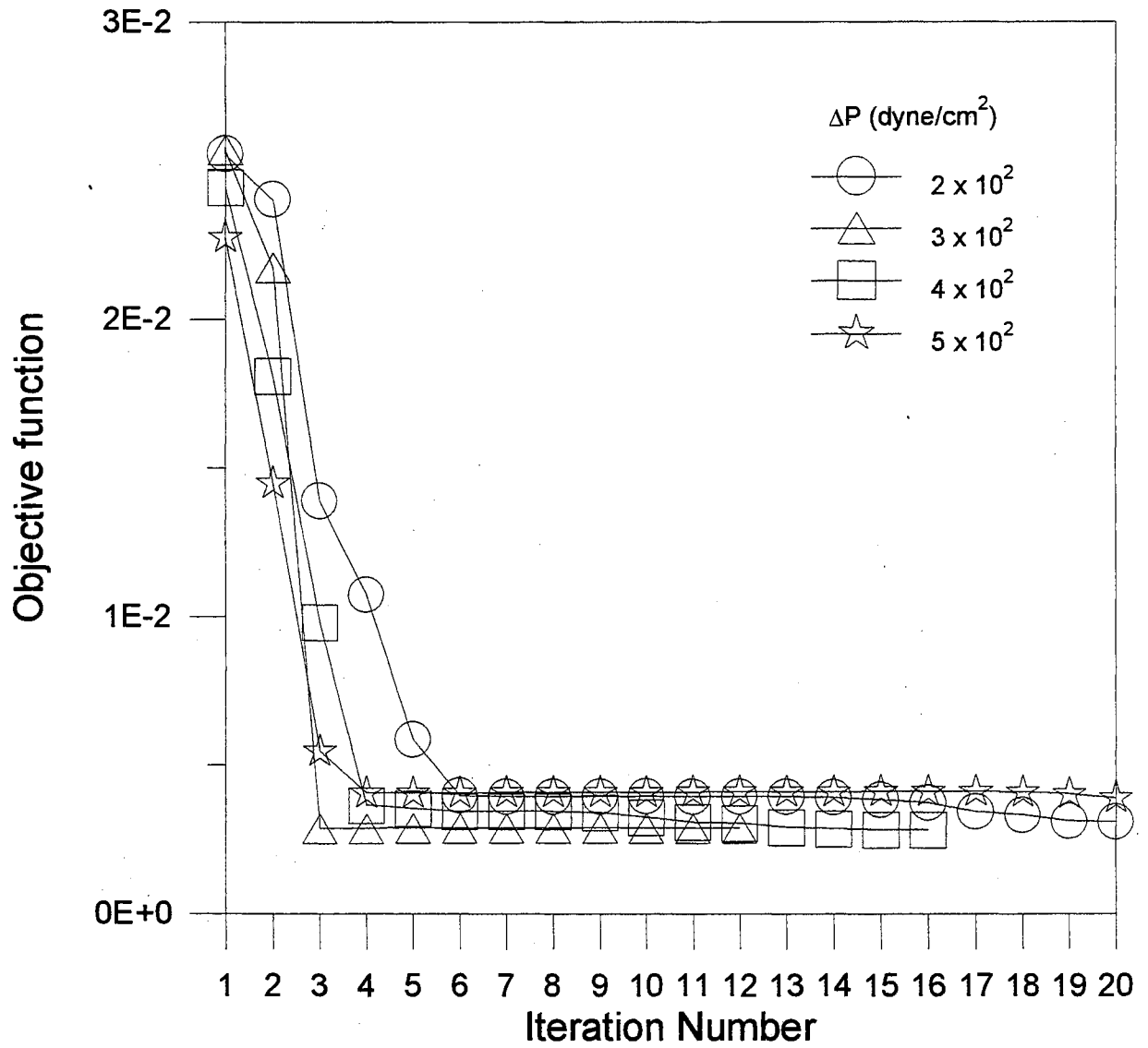
Figure 30. Objective Function Value for Die Optimization

CHAPTER V

SUMMARY, CONCLUSIONS AND RECOMMENDATIONS

Summary and Conclusions

This work was successful in achieving both of its main objectives viz. the development of an elementary kinetic model which qualitatively describes molecular orientation and the design of a die geometry optimization technique which incorporates the molecular model and which can account for anisotropic effects in the mechanical properties of the polymer during the formation of extended chain crystals. The main conclusions are summarized below.

1. A molecular model based on polymer kinetic theory was developed for predicting the steady state configuration of polymer molecules in a flow field. This model was sufficiently general that it could handle a variety of flow conditions. Some of the flow fields that were tested were planar elongational flow, simple shearing flow and mixed heterogeneous flow. In all cases, the overall molecular configurations predicted by the model were at least qualitatively in agreement with expected results.

2. The Weissenberg number (We) was used as the rheological parameter for characterization of the process and different values were used to correlate the behavior of the model for various flow fields. Published results and analytical solutions (wherever available) were used to verify model predictions and in all cases were seen

100

to be in reasonable agreement with the model. The maximum in the probability distribution function or the most preferred orientation for various flow fields was plotted and was seen to be consistent with expected preferences for different flow fields.

3. The model predictions were also compared with results from x-ray diffraction experiments using an orientation parameter as the basis of comparison. The results were in very good agreement.

4. A die optimization technique was developed which combined elements of the model and the Successive Quadratic Programming by the Han-Powell optimization algorithm. This was the first time that flow-induced crystallization concepts were combined with optimization principles in a die design process.

5. The die design optimization technique was tested for a planar diffuser and slit flow and the results obtained were qualitatively consistent with published results.

6. The optimization technique was used to generate an optimum die geometry for a given degree of anisotropy. This was a three-step process that involved determination of the flow field using FIDAP, prediction of molecular configurations using the model, and using these results in the optimization algorithm to minimize the objective function and determine the best possible geometry for the given conditions.

Recommendations

Although the work described in this thesis represents a significant development in the area of polymer processing, die design using FIC principles still remains essentially uncharted territory and hence, there is room for improvement and refinement in the

techniques used in modeling polymer orientation and optimization of die design. The following recommendations are made for future research:

1. The unsteady-state kinetic model needs to be developed to account for the different flow field experienced by the molecules from entrance to exit of the die. The model in this thesis assumes steady-state and would only work for systems which have a very quick response or for small changes of flow field in the trajectory of the fluid in the domain under consideration. For systems with low response the molecular orientation would be much slower due to the flow field change.

2. The model should include the effect of restricted motion of the polymer chain segments in the presence of the other molecules in the neighborhood. The effect of restricted motion cannot be achieved by introducing the general phase-space kinetic theory.

3. Potential functions and effects of other forces including intermolecular and intramolecular forces can be included to account for interactions that may exist in polymer solutions and melts. Also, the effect of hydrodynamic interaction using suitable hydrodynamic interaction tensors is a possible area of investigation.

4. The computational resources required for obtaining probability distribution function of molecular orientation need to be reduced. By introducing the orientation tensor to approximate the probability distribution, a substantial reduction in system resources can be expected.

5. A freely jointed bead-rod chain configuration can be used to represent the polymer molecules. This will more accurately capture the nature and the physics of the polymer orientation process.

6. The computational resources required can be substantially reduced by performing a

   sensitivity analysis to determine the first derivative in the optimization algorithm

   instead of using finite difference method.

BIBLIOGRAPHY

Advani, S. G.; Tucker, C. L. III The Use of Tensors to Describe and Predict Fiber Orientation in Short Fiber Composites. *Journal of Rheology* **1987**, *31*(8), 751-784.

Akbar, S.; Altan, M. C. On the Solution of Fiber Orientation in Two-Dimensional Homogeneous Flow. *Polym. Eng. Sci.* **1992**, *32*(12), 810-822.

Alamo, R. G.; Mandelkern, L. Crystallization Kinetics of Random Ethylene Copolymers. *Macromol.* **1991**, *24*(24), 6480-6493.

Alfonso, G. C.; Pedemonte, E.; Ponzetti, L. Mechanism of Densification and Crystal Perfection of Poly(ethylene terephthalate). *Polymer* **1979**, *20*, 104-112.

Alfonso, G. C.; Verdona, M. P.; Wasiak, A. Crystallization Kinetics of Oriented Poly(ethylene terephthalate) from the Glassy State. *Polymer* **1978**, *19*, 711-716.

Altan, M. C.; Subbiah, S.; Guceri, S. I.; Pipes, R. B. Numerical Prediction of Three-Dimensional Fiber Orientation in Hele-Shaw Flows. *Polym. Eng. Sci.* **1990**, *30*(14), 848-859.

Amram, B.; Bokobza, L.; Monnerie, L.; Queslel, J. P. Fouier-transfor Infra-red Dichroism Study of Molecular Orientation in High Cis-1,4-Polybutadiene. *Polymer* **1988**, *29*, 1155-1160.

Ausias G.; Jarrin, J; Vincent, M. Optimization of the Tube-Extrusion Die for Short-Fiber-Filled Polymers. *Comp. Sci. & Tech.* **1996**, *56*(7), 719-724.

Ausias G.; Jarrin, J; Vincent, M. Optimization of the Extrusion Process For Glass-Fiber-Reinforced Tubes. *J. Thermoplastic Composite Materials* **1995**, *8*(4), 435-448.

Avrami, M. Granulation, Phase Change, and Microstructure Kinetics of Phase Change. III. *Journal of Chemical Physics* **1941**, *9*, 177-184.

Avrami, M. Kinetics of Phase Change II Transformation-Time Relations for Random Distribution of Nuclei. *Journal of Chemical Physics* **1940**, *8*, 212-224.

Avrami, M. Kinetics of Phase Change. I General Theory. *Journal of Chemical Physics* **1939**, *7*, 1103-1112.

Baker, W. E.; Rudin, A.; Schreiber, H. P.; El-Kindi, M. The Effect of Processing on Rheological and Molecular Characteristics of a Low Density Polyethylene. **1993**, *33*(7), 377-382.

Barham, P. J., Hill, M. J., Keller, A. Gelation and the Production of Surface Grown Polyethylene Fibres. *Colloid and Polymer Science* **1980**, *258*(8), 899-908.

Barham, P. J., Keller, A. Review High-Strength Polyethylene Fibres from Solution and Gel Spinning. *Journal of Materials Science* **1985**, *20*, 2281-2302.

Barnes, R. B., Z. *Physik.*, **1932**, *75*, 723.

Barone, M. R.; Caulk, D. A. Optimal Arrangement of Holes in a Two-dimensional Heat Conductor by a Special Boundary Integral Method. **1982**, *18*, 675-685.

Barone, M. R.; Caulk, D. A. Optimal Thermal Design of Injection Molds for Filled Thermosets. **1985**, *25*(10), 608-617.

Bartczak, Z.; Cohen, R. E.; Argon, A. S. Evolution of the Crystalline Texture of High-Density Polyethylene during Uniaxial Compression. *Macromol.* **1992**, *25*(18), 4692-4704.

Bayer, R. K.; Zachmann, H. G. Properties of Elongational Flow Injection-Molded Polyethylene. Part 1: Influence of Mold Geometry. *Polymer Engineering and Science* **1989**, *29*(3), 186-192.

Baysal, O.; Eleshaky, M. E. Aerodynamic Design Optimization Using Sensitivity Analysis and Computational Fluid Dynamics. *AIAA Journal* **1992**, *30*(3), 718-725.

Beris, A. N.; Edwards, B. J. Thermodynamics of Flowing Systems with Internal Microstructure. London: Oxford University Press, 1994.

Billon, N.; Escleine, J. M.; Haudin, J. M. Isothermal Crystallization Kinetics in a Limited Volume. A Geometrical Approach Based on Evans' Theory. *Colloid & Polymer Science* **1989**, *267*, 668-680.

Billon, N.; Haudin, J. M. Overall Crystallization Kinetics of Thin Polymer Films. General Theoretical Approach. I. Volume Nucleation. *Colloid & Polymer Science* **1989**, *267*, 1064-1076.

Bird, R. B.; Johnson, M. W., Jr.; Curtiss, C. F. Potential Flows of Dilute Polymer Solutions by Kramers' Method. *The Journal of Chemical Physics* **1969**, *51*(7), 3023-3026.

Bird, R. B.; Warner, H. R., Jr.; Evans, D. C. Kinetic Theory and Rheology of Dumbbell Suspensions with Brownian Motion. *Adv. in Polym. Sci.* **1971**, *8*, 1-90.

Bird, R. B.; Armstrong, R. C.; Hassager O. *Dynamics of Polymeric Liquids Vol. 1: Fluid Mechanics*, 2nd ed., Wiley: N.Y., 1987a.

Bird, R. B.; Curtiss, C. F.; Armstrong, R. C.; Hassager O. *Dynamics of Polymeric Liquids Vol. 2: Kinetic Theory*, 2nd ed., Wiley: New York, 1987b.

Bird, R. B.; Wiest, J. M. Constitutive Equations for Polymeric Liquids. *Annu. Rev. Fluid Mech.* **1995**, *27*, 169-193.

Blackadder, D. A.; Lewell, P. A. Properties of Polymer Crsytal Aggregates. (1) Comparison of Polyethylene Crystal Aggregates with Bulk Crystallized Polyethylene. *Polymer* **1970a**, *11*, 125-146.

Blackadder, D. A.; Lewell, P. A. Properties of Polymer Crsytal Aggregates. (2) Annealing of Polyethylene Crystal Aggregates. *Polymer* **1970b**, *11*, 147-164.

Boldizar, A.; Jacobsson, S.; Hard, S. Far Infrared Birefringence versus Other Orientational Measurements of High-Pressure Injection-Molded High-Density Polyethylene. *Journal of Applied Polymer Science* **1988**, *36*, 1567-1581.

Broyden, G. C. Quasi-Newton Methods and Their Application to Function Minimization. *Math. Comput.* **1967**, *21*, 368.

Broyden, G. C. The Convergence of a Class of Double-Rank Minimization Algorithms parts I and II. *J. Inst. Math. Appl.* **1970**, *6*(76), 222.

Boon, J.; Challa, G.; Krevelen, D. W. V. Crystallization Kinetics of Isotactic Polystyrene. I. Spherulitic Growth Rate. *Journal of Polymer Science: Part A-2* **1968**, *6*, 1791-1801.

Braibant, V.; Fleury, C. An Approximation-Concepts Approach to Shape Optimal Design. *Computer Methods in Applied Mechanics and Engineering* **1985**, *53*, 119-148.

Bushman, A.C.; McHugh, A. J. A Continuum Model for the Dynamics of Flow-Induced Crystallization. *J. Polymer Science: Part B: Polymer Physics* **1996**, *34*, 2393-2407.

Çabuk, H.; Modi, V. Shape Optimization Analysis: First- and Second-Order Necessary Conditions. *Optimal Control Appl. & Meth.* **1990**, *11*, 173-190.

Çabuk, H.; Modi, V. Optimum Plane Diffuser in Laminar Flow. *J. Fluid Mech.* **1992**, *237*, 373-393.

Cardew, P. T.; Davey, R. J.; Ruddick, A. J. Kinetics of Polymorphic Solid-State Transformations. *J. Chem. Soc., Faraday Trans.* **1984**, *80*, 659-668.

Chen, C.; Jen, P.; Lai, F. S. Optimization of the Coathanger Manifold via Computer Simulation and an Orthogonal Array Method. *Polymer Engineering and Science.* **1997**, *37*(1), 188-196.

Chen, H.-S.; Stadtherr, M. A. Enhancements of the Han-Powell Method for Successive Quadratic Programming. *Comput. Chem. Eng.* **1984**, *8*(3/4), 229-234.

Chen, H.-S.; Stadtherr, M. A. *SQPHP, a Code for Successive Quadratic Programming by the Han-Powell Method: Theory and Performance.* Dept. of Chem. Eng., University of Illinois, Urbana: 1983.

Chen, Z.; Linet, M. C.; Liddell, K.; Thompson, D. P.; White, J. R. Crystal Orientation Distributions in Injection-Molded Polypropylene Compounds. *J. Appl. Polym. Sci.* **1992**, *46*(8), 1429-1437.

Cheng, S. Z. D.; Chen, J.; Heberer, D. P. Extended Chain Crystal Growth of Low Molecular Mass Poly(ethylene oxide) and α,ω-methoxy Poly(ethylene oxide) Fractions Near Their Melting Temperature. *Polymer* **1992**, *33*(7), 1429-1436.

Chew, S.; Griffiths, J. R.; Stachurski, Z. H. The Crystallization Kinetics of Polyethylene under Isothermal and Non-Isothermal Conditions. *Polymer* **1989**, *30*, 874-881.

Cobbs, W. H.; Burton, R. L. Crystallization of Polyethylene Terephthalate. *J. Polym. Sci.* **1952**, *10*(3), 275-290.

Collyer, A. A.; Clegg, D. W., *High Performance Plastics* **1986**, *4*, 1.

Chung, S. T.; Kwon, T. H. Numerical Simulation of Fiber Orientation in Injection Molding of Short-Fiber-Reinforced Thermoplastics. *Polym. Eng. Sci.* **1995**, *36*(7), 604-618.

Davidon, W. C. Variable Metric Method for Minimization, *AEC Res. Dev. Rep.* **1959**, ANL-, 5990.

Dayde, M. Parallel Algorithms for Nonlinear Programming Problems. *JOTA* **1989**, *61*(1), 23-46.

Dems, K.; Morz, Z. Multiparameter Structural Shape Optimization by the Finite Element Method. *International Journal for Numerical Methods in Engineering* **1978**, *13*, 247-263.

Desai, P.; Abhiraman, A. S. Role of Orientation in Kinetics of Nucleation and Growth of Crystals in Polymers. *J. Polym. Sci. - Polym. Phys.* **1989**, *27*, 2469-2478.

Doshi, S. R.; Dealy, J. M.; Charrier, J.-M. Flow Induced Fiber Orientation in an Expanding Channel Tubing Die. *Polym. Eng. Sci.* **1986**, *26*(7), 468-478.

Eder, G.; Janeschitz-Kriegl, H. Theory of Shear-induced Crystallization of Polymer Melts. *Colloid & Polymer Science* **1988**, *266*, 1087-1094.

Eder, G.; Janeschitz-Kriegl, H.; Liedauer, S. Crystallization Process in Quiescent and Moving Polymer Melts under Heat transfer Conditions. *Prog. Polym. Sci.* **1990**, *15*, 629-714.

Edgar, T. F.; Himmelblau, D. M. *Optimization of Chemical Processes*; McGraw-Hill: New York, **1988**.

Eleshaky, M. E.; Baysal, O. Airfoil Shape Optimization Using Sensitivity Analysis on Viscous Flow Equations. *J. Fluids Eng.* **1993**, *115*(75), 75-84.

Fatou, J. G.; Marco, C. The Influence of Molecular Weight on the Regime Crystallization of Linear Polyethylene. *Polymer* **1990**, *31*, 1685-1693.

Fleischmann, E.; Koppelmann, J. Effect of Cooling Rate and Shear-Induced Crystallization on the Pressure-Specific Volume-Temperature Diagram of Isotactic Polypropylene. *J. Applied Polymer Sci.* **1990**, *41*, 1115-1121.

Fletcher, R. A New Approach to Variable Metric Algorithms, *Comput. J.* **1970**, *13*, 317.

Fletcher, R.; Powell, M. J. D. A Rapidly Convergent Descent Method for Minimization, *Comput. J.* **1963**, *6*, 163.

Flory, P. J. Thermodynamics of Crystallization in High Polymers. I. Crystallization Induced by Stretching. *J. Chem. Phys.* **1947**, *15*(6) 397-408.

Flory, P. J. *Statistical Mechanics of Chain Molecules*. N. Y.: Interscience, 1969.

Fraenkel, G. K. *J. Chem. Phys.* **1952**, *20*, 642-647.

Francavilla, A.; Ramakrishnan, C. V.; Zienkiewicz, Optimization of Shape to Minimize Stress Concentration, *J. Strain Anal.* **1975**, *10*, 63-70.

Fritzsche, A. K.; Price, F. P.; Ulrich, R. D. Disruptive Processes in the Shear Crystallization of Poly(ethylene Oxide). *Polym. Eng. Sci.* **1976**, *16*(3), 182-188.

Fritzsche, A. K.; Price, F. P. Crystallization of Polyethylene Oxide Under Shear. *Polym. Eng. Sci.* **1974**, *14*(6), 401-412.

Gagnon, K. D.; Lenz, R. W.; Farris, R. J.; Fuller, R. C. Crystallization Behavior and Its Influence on the Mechanical Properties of a Thermoplastic Elastomer Produced by Pseudomonas Oleovorans. *Macromol.* **1992**, *25*(14), 3723-3728.

Gaylord, R. J; Lohse, D. L. *Polym. Eng. Sci.* **1976**, *16*, 163.

Gaylord, R. J. *J. Polym. Sci.* **1976**, *14*, 1827.

Givler, R. C.; Crochet, M. J.; Pipes, R. B. Numerical Prediction of Fiber Orientation in Dilute Suspensions. *Journal of Composite Materials* **1983**, *17*, 330-343.

Glowinski, R.; Pironneau, O. On the numerical computation of the minimum-drag profile in laminar flow. *J. Fluid Mech.* **1975**, *72*, 385-389.

Godovskii, Y. K. The Effect of Temperature and Molecular Structure on the Rate of Crystallization of Polymers. *Vysokomol. soyed.* **1969**, *10*, 2423-2429.

Goldfarb, D. A Family of Variable Metric Methods Derived by Variational Means. *Math. Comput.* **1970**, *24*, 23.

Gornick, F.; Hoffman, J. D. Nucleation in Polymers. *Industrial and Engineering Chemistry* **1966**, *58*(2), 41-53.

Gould, A. J.; Bleakney, W.; Taylor, H. S., *J. Chem. Phys.* **1934**, *2*, 362.

Goulet, L.; Prud'homme, R. E. Crystallization Kinetics and Melting of Caprolactone Random Copolymers. *J. Polym. Sci.: Polym. Phys.* **1990**, *28*, 2329-2352.

Gutfinger, C.; Broyer, E.; Tadmor, Z. Melt Solidification in Polymer Processing. *Polym. Eng. Sci.* **1975**, *15*(7), 515-524.

Guggenheim, E. A., *Trans. Faraday Soc.* **1941**, *37*, 97.

Han, S. P. Superlinearly Convergent Variable Metric Algorithms for General Nonlinear Programming problems. *Math. Prog.* **1976**, *11*, 263.

Han, S. P. A Globally Convergent Method for Nonlinear Programming. *J. Opt. Theory & Appl.* **1977**, *22*, 297.

Han, C. S.; Grandhi, R. V.; Srinivasan, R. Optimum Design of Forging Die Shapes Using Nonlinear Finite Element Analysis. *AIAA J.* **1993**, *31*(4), 774-781.

Henry de Frahan, D.; Verleye, V.; Dupret, F.; Crochet, M. J. Numerical Prediction of Fiber Orientation in Injection Molding. *Polym. Eng. Sci.* **1992**, *32*(4), 254-266.

Herman, J. J. *Physica* **1943**, *10*, 777-789.

Hermans, P. H. *Contributions to the Physics of Cellulose Fibers*, Elsevier: Amsterdam, 1946.

High, K. C. *Nonlinear Optimization and Parallel Processing for Chemical Process Design*, Ph.D. Thesis, Pennsylvania State University, University Park, 1991.

Hikosaka, M.; Tamaki, S. Growth of Bulky Extended Chain Single Crystals of Polyethylene. *J. Phys. Soc. Jpn* **1981**, *50*(2), 638-641.

Hikosaka, M. Unified Theory of Nucleation of Folded-Chain Crystals and Extended-Chain Crystals of Linear-Chain Polymers. *Polymer* **1987**, *28*, 1257-1264.

Hikosaka, M. Unified Theory of Nucleation of Folded-Chain Crystals (FCCs) and Extended-Chain Crystals (ECCs) of Linear-Chain Polymers: 2. Origin of FCC and ECC. *Polymer* **1990**, *31*, 458-468.

Himmelblau, D. M. *Applied Nonlinear Programming*, McGraw-Hill: New York, 1972.

Hirschfelder, J. O.; Curtiss, C. F.; Bird, R. B. *Molecular Theory of Gases and Liquids*; Second Printing with Corrections, Wiley: New York, 1964; pp 905-912.

Hougen, O. A.; Watson, K. M. *Chemical Process Principles*, Part III, New York: Wiley, 1947, p. 873.

Holland, V. F.; Lindenmeyer, P. H. Morphology and Crystal Growth Rate of Polyethylene Crystalline Complexes. *J. Polym. Sci.* **1962**, *57*, 589-608.

Hongladarom, K.; Ugaz, V. M.; Cinader, D. K.; Burghardt, W. R.; Quintana, J. P.; Hsiao, B. S. Dadmun, M. D.; Hamilton, W. A.; Butler, P. D. Birefringence, X-Ray-Scattering, And Neutron-Scattering Measurements Of Molecular-Orientation In Sheared Liquid-Crystal Polymer-Solutions. *Macromolecules* **1996**, 29(16), 5346-5355.

Hua, C., C.; Scheiber, J. D., Application of Kinetic-Theory Models in Spatiotemporal Flows for Polymer-Solutions, Liquid-Crystals and Polymer Melts Using the Connffessit Approach. *Chem. Eng. Sci.* **1996**, *51*(9), 1473-1485.

Iragorri, J. I.; Rego, J. M.; Katime, I.; Conde Brana, M. T.; Gedde, U. W. A Crystallization Kinetics Study of Binary Blends of Linear and Branched Polyethylene. *Polymer* **1992**, *33*(3), 461-466.

Jackson, W. C.; Advani, S. G.; Tucker, C. L. Predicting the Orientation of Short Fibers in Thin Compression Moldings. *J. Composite Materials* **1986**, *20*, 539-557.

Jeffery, G. B., The Motion of Ellipsoidal Particles Immersed in a Viscous Fluid. *Proc. Roy. Soc.*, **1922**, *A102*, 161-179.

Janimak, J. J.; Cheng, S. Z. D.; Zhang, A.; Hsieh, E. T. Isotacticity Effect on Crystallization and Melting in Polypropylene Fractions: 3. Overall Crystallization and Melting Behaviour. *Polymer* **1992**, *33*(4), 728-735.

Katayama, K.-i.; Murakami, S.; Kobayashi, K. An Apparatus for measuring Flow-Induced Crystallization of Polymers. *Bull. Inst. Chem. Res. Kyoto Univ.* **1976**, *54*(2), 82-90.

Kennard, E. H. *Kinetic Theory of Gases*, New York: McGraw-Hill, 1938.

Kirkwood, J. G. *Macromolecules*, New York: Gordon and Breach, 1967.

Kittel, C. *Solid State Physics*, 2nd ed. New York: Wiley, 1956.

Kowalewski, T.; Galeski, A. Crystallization of Linear Polyethylene from Melt in Isothermal Compression. *J. Appl. Polym. Sci.* **1992**, *44*(1), 95-106.

Kramers, H. A. *Physica* **1944**, *11*, 1-19.

Kuhn, W. *Zeits. f. phys. Chem.* **1932**, *161*, 1-32.

Kuhn, W. *Kolloid-Zeitschrift* **1933**, *62*, 269-285.

Kuhn, W.; Kuhn, H. *Helv. Chim. Acta* **1945**, *28*, 97-127.

Lapersonne, P.; Bower, D. I.; Ward, I. M. Molecular Orientation and Conformational Changes due to Uniaxial-Planar Deformation of Poly(ethylene terephthalate) Films. *Polymer* **1992**, *33*(6), 1277-1283.

Lasdon, L. S.; Waren, A.; Jain, A.; Ratner, M. Design and Testing of a GRG Code for Nonlinear Optimization. *ACM Trans. Math. Software* **1978**, *4*, 34.

Lasdon, L. S.; Waren, A. *GRG2 User's Guide*, Dept. of General Business, University of Texas, Austin, 1982.

Lee, D. K.; Soh, S. K. Prediction of Optimal Preform Thickness Distribution in Blow Molding. *Polymer Engineering and Science* **1996**, *36*(11), 1513-1520.

Liedauer, S.; Eder, G.; Janeschitz-Kriegl, H. On the Limitations of Shear Induced Crystallization in Polypropylene Melts. *Intern. Polymer Processing* **1995**, *10*(3), 243-250.

Magill, J. H. A New Method for Following Rapid Rates of Crystallization I. Poly(hexamethylene adipamide). *Polymer* **1961**, *2*, 221-233.

McQuarrie, D. A. *Statistical Mechanics*. N. Y.: Harper Collins, 1976.

Mandelkern, L. *Crystallization of Polymers. Crystallization Kinetics and Mechanisms*. New York: McGraw-Hill, 1964. 216-289.

Manke, C. W.; Williams, M. C., Transient Stress Responses Predicted by the Internal Viscosity Model in Elongational Flow. *Rheologica Acta* **1991**, *30*, 316-328.

Manke, C. W.; Williams, M. C., Comparison of a New Internal Viscosity Model with Other Constrained-Connector Theories of Dilute Polymer Solution Rheology. *Rheologica Acta* **1993**, *33*, 418-421.

Matsuo, M.; Sato, R.; Yanagida, N.; Shimizu, Y. Deformation Mechanism of Nylon 6 Gel and Melt Films Estimated in Terms of Orientation Distribution Function of Crystallites. *Polymer* **1992**, *33*(8), 1640-1648.

Mayer, J. E.; Mayer, M. G. Statistical Mechanics, New York, Wiley, 1940.

McHugh, A. J. Flow-Induced Crystallization from Solution the Relative Effects of Extension and Shearing Flow Fields. *J. Appl. Polym. Sci.* **1975**, *19*, 125-140.

McHugh, A. J. Mechanisms of Flow Induced Crystallization. *Polym. Eng. Sci.* **1982**, *22*(1), 15-26.

McHugh, A. J.; Blunk, R. H. Studies of Fiber Formation in Tubular Flow: Polypropylene and Poly(ethylene oxide). *Macromol.* **1986**, *19*, 1249-1255.

McHugh, A. J.; Mackay, M. E.; Khomami, B. Measurement of Birefringence by the Method of Isoclinics. *Journal of Rheology* **1987**, *31*(7), 619-634.

McHugh, A. J.; Spevacek, J. A. The Kinetics of Flow-Induced Crystallization from Solution. *Journal of Polymer Science: Part B: Polymer Physics* **1991**, *29*, 969-979.

McHugh, A. J.; Tree, D. A.; Pornnimit, B.; Ehrenstein, G. W. Flow-Induced Crystallization and Self-Reinforcement During Extrusion. *Intern. Polymer Processing VI* **1991**, *3*, 208-211.

McHugh, A. J.; Guy, R. K.; Tree, D. A. Extensional Flow-Induced Crystallization of a Polyethylene Melt. *Colloid Polym. Sci.* **1993**, *271*, 629-645.

Mendes, L. J. unfinished Ph.D. Thesis, Oklahoma State University, Stillwater, 1997.

Mychajluk, G.; Manoochehri, S.; Parnas, R. S. Resin Transfer Molding Process Optimization for Minimum Cycle-Time. *J. Advanced Materials* **1996**, *28*(1), 9-18.

Nakamura, K.; Watanabe, T.; Katayama, K. Some Aspects of Nonisothermal Crystallization of Polymers. I. Relationship Between Crystallization Temperature, Crystallinity, and Cooling Conditions. *Journal of Applied Polymer Science* **1972**, *16*, 1077-1091.

Nakamura, K.; Katayama, K.; Amano, T. Some Aspects of Nonisothermal Crystallization of Polymers. II. Consideration of the Isokinetic Condition. *Journal of Applied Polymer Science* **1973**, *17*, 1031-1041.

Nakamura, K.; Watanabe, T.; Amano, T.; Katayama, K. Some Aspects of Nonisothermal Crystallization of Polymers. III. Crystallization During Melt Spinning. *Journal of Applied Polymer Science* **1974**, *18*, 615-623.

Ng, R. C-Y.; Leal, L. G., A study of the interacting FENE Dumbbell Model for Semi-Dilute Polymer Solutions in Extensional Flows. *Rheologica Acta*, **1993**, *32*, 25-35.

Nicholson, T. M.; Mackley, M. R.; Windle, A. H. Shear-induced Crystallization in a Liquid Crystalline Random Copolyester. *Polymer* **1992**, *33*(2), 434-435.

Nonhof, C. J. Optimization of Hot Plate Welding for Series and Mass Production. *Polym. Eng. Sci.* **1996**, *36*(9), 1184-1195.

Pennings, A. J.; van der Mark, J. M. A. A.; Booij, H. C. Hydrodynamically Induced Crystallization of Polymers from Solution II. The Effect of Secondary Flow. *Kolloid-Z. u. Z. Polymere* **1969**, *236*(2), 99-111.

Philippoff, W. *Kolloid Z.* **1935**, *71*, 1-16.

Pironneau, O. On Optimum Profiles in Stokes Flow. *J. Fluid Mech.* **1973**, *59*(1), 117-128.

Pironneau, O. On Optimum Design in Fluid Mechanics. *J. Fluid Mech.* **1974**, *64*(1), 97-110.

Point, J. J.; Dosiere, M. Crystal Growth Rate as a Function of Molecular Weight in Polyethylene Crystallized from the Melt: An Evaluation of the Kinetic Theory of Polymer Crystallization. *Polymer* **1989**, *30*, 2292-2296.

Poisson, S. D. Sur la variation des constantes arbitraires dans les questions de mécanique. *J. de l'École Polytechnique* **1809**, *8*, 266-344.

Powell, M. J. D. A New Algorithm for Unconstrained Optimization, in *Nonlinear Programming*, J. B. Rosen, O. L. Mangasarian, and K. Ritter eds., Academic Press, New York, 1970, pp 31.

Powell, M. J. D. A Fast Algorithm for Nonlinear Programming, In *Numerical Analysis*, Watson, G. A. ed., Lecture Notes in Mathematics, Springer-Verlag: Belin, 1978; pp 144-157.

Rittenberg, D.; Bleakney, W.; Urey, H. C. *J. Chem. Phys.* **1934**, *2*, 362.

Rasaiah, J. C.; Friedman, H. L. *J. Chem. Phys.* **1968**, *48*, 2742.

Rasaiah, J. C.; Friedman, H. L. *J. Chem. Phys.* **1969**, *50*, 3965.

Rasaiah, J. C. *Chem. Phys. Lett.* **1970a**, *7*, 260.

Rasaiah, J. C. *J. Chem. Phys.* **1970b**, *52*, 704.

Shanno, D. F. Conditioning of Quasi-Newton Methods for Function Minimization. *Math. Comput.* **1970**, *24*, 647.

Sherwood, C. H.; Price, F. P.; Stein, F. P. Effect of Shear on the Crystallization Kinetics of Poly(ethylene oxide) and Poly(epslon-Caprolactone) melts. *J. Polym. Sci. - Polym. Symposium* **1978**, *63*, 77-94.

Shyy, Y. K.; Fleury, C.; Izadpanah, K. Shape Optimal Design Using High-Order Elements. *Computer Methods in Applied Mechanics and Engineering* **1988**, *71*, 99-116.

Riggs, J. B. *An Introduction to Numerical Methods for Chemical Engineers*, Texas Tech University Press: Lubbock, TX, 1988.

Rouse, P. E., Jr., *J. Chem. Phys.*, **1953**, *21*, 1272-1280.

Smith, D. E.; Tortorelli, D. A.; Tucker, C. L., III Sensitivity Analysis and Optimization of Polymer Sheet Extrusion Dies. *ASME Winter Annual Meeting*, Chicago, IL: **1994**, 307-318.

Smith, F. S.; Steward, R. D. The Crystallization of Oriented Poly(ethylene terephthalate). *Polymer* **1974**, *15*, 283-286.

Southern, J. H.; Porter, R.; Bair, H. E. Melting Behavior of Polyethylene Crystallized in a Pressure Capillary Viscometer. *Journal of Polymer Science: Pat A-2* **1972**, *10*, 1135-1143.

Southern, J. H.; Porter, R. S. The Properties of Polyethylene Crystallized Under the Orientation and Pressure Effects of a Pressure Capillary Viscometer. *J. Appl. Polym. Sci.* **1970**, *14*, 2305-2317.

Spevacek, J. A. Ph.D. Thesis, University of Illinois, Urbana, 1989.

Steward, W. E.; Sørensen, J. P. Hydrodynamic Interaction Effects in Rigid Dumbbell Suspensions. II. Computations for Steady Shear Flow. *Trans. Soc. Rheol.*, **1972**, *16*, 1-13.

Sun, Z.; Morgan, R. Z.; Lewis, D. N. Crystallization of Syndiotactic Polystyrene under Pressure. *Polymer* **1992**, *33*(3), 660-661.

Tanzawa, Y. Growth Rate and Morphology of Isotactic Polystyrene Crystals in Solution at High Supercoolings. *Polymer* **1992**, *33*(13), 2659-2665.

Taylor, C.; Hughes, T. G. *Finite Element Programme of Navier-Stokes Equations.* Swansea: Pineridge Press Limited, 1981.

Tolman, R. C. *The Principles of Statistical Mechanics*, London: Oxford University Press, 1938.

Tree, D. A. *Crystallization Kinetics of Polymer Melts in Extensional Flow*. Ph.D. Thesis, University of Illinois, Urbana-Champaign, Illinois, 1990.

Tucker, C. L., III Predicting Fiber Orientation in Short Fiber Composites. *Proceedings of Manufacturing International, Manufacturing Science of Composite*, ASME, **1988**, *4*, 95-104.

Tucker, C. L., III; Smith, D. E.; Tortorelli, D. A. Sensitivity Analysis and Optimization for Extrusion Dies Design, *SPE Eleventh Annual Meeting*. Seoul, Korea, **1995**, 27-30.

van den Brule, B. H. A. A., Brownian Dynamics Simulation of Finitely Extensible Bead-Spring Chains. *J. Non-Newtonian Fluid Mech*. **1993a**, *47*, 357-378.

van den Brule, B. H. A. A., in *Topics in Applied Mechanics*, Dijksman, J. D., Nieuwstadt, F. T. M. (Editors), 1993b; pp. 213-221.

van Wijk, H.; Luiten, G. A.; van Engen, P. G.; Nonhof, C. J., Process Optimization of Ultrasonic Welding. *Polymer Engineering and Science*. **1996**, *36*(9), 1165-1176.

Volkenstein, M. V.; Timasheff, S. N.; Timasheff, M. J. Configurational Statistics of Polymeric Chains N. Y.: Interscience, 1963.

Watson, S. R. Towards the Minimum Drag on a Body of Given Volume in Slow Viscous Flow, *J. Inst. Maths Applics* **1971**, *7*, 367-376.

Wedgewood, L. E.; Bird, R. B. From Molecular Models to the Solution of Flow Problems. *Ind. Eng. Chem. Res.* **1988**, *27*, 1313-1320.

Wiest, J. M.; Tanner, R. I. Rheology of Bead-nonlinear Spring Chain Macromolecules. *J. Rheology* **1989**, *33*, 281-316.

Wilson, E. B., Jr. *Adv. Chem. Phys*., **1959**, *2*, 367.

Wilson, R. B. *A Simplical Method for Convex Programming*. Ph.D. Thesis, Harvard University, Cambridge, Mass., 1966.

Ziabicki, A. Theoretical Analysis of Oriented and Non Isothermal Crystallization I. Phenomenological Considerations. Isothermal Crystallization Accompanied by Simultaneous Orientation or Disorientation. *Colloid & Polymer Sci.* **1974**, *252*, 207-221.

Zienkiewicz, O. C.; Campbell, J. S. Shape Optimization and Sequential Linear Programming in *Optimum Structural Design*, Gallagher, R.H., Zienkiewicz, (Editors), Wiley, London, 1973.

Zienkiewicz, O. C.; Taylor, R. L. *The Finite Element Method.* 4th ed. 2 vols. London: McGraw-Hill Book Company, **1989**.

Zimm, B. H. *J. Chem. Phys.* **1956**, *24*, 269-278.

APPENDIX A

SPHERICAL COORDINATES AND EXPRESSIONS

Spherical coordinates are useful in the derivation of working equations for problems with spherical boundaries. Chapter III a dumbbell is considered. The length of the dumbbell is fixed. Consequently, if the origin is on the dumbbell, the motion of the ends of the dumbbell will be on the surface of a sphere. Hence, spherical coordinates are the most suitable coordinate system for describing the position of the ends of the dumbbell.

Figure A-1 shows a Cartesian frame of reference and the definitions of the angles associated with the spherical coordinate system. The quantity r is the length of the position vector. θ is the angle ($0 \le \theta \le \pi$) between the position vector and the z-axis in the plane containing the position vector and the z-axis (spherical polar angle). ϕ ($0 \le \phi \le 2\pi$) is the angle between the x-axis and the projection of the position vector on the x-y plane (spherical azimuthal angle).

In working with bead-rod models a nomenclature has developed by analogy to the earth. The spherical coordinates θ and ϕ are similar to the geographic coordinates of latitude and longitude. If the earth's axis of rotation is taken to be the z-axis, the north and south pole correspond to the points where $\theta = 0$ and $\theta = \pi$, respectively. The equator corresponds to the line where $\theta = \pi/2$.

117
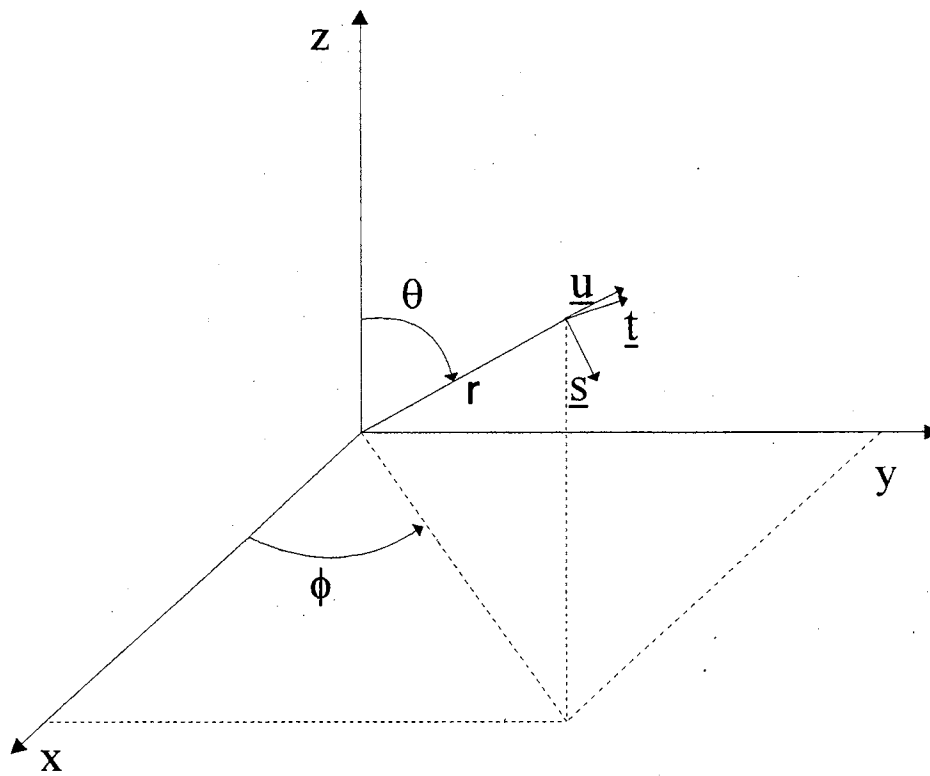
Figure A-1. Spherical Coordinate System

Spherical coordinates are related to rectangular coordinates as follows:

$$x = r\sin\theta\cos\phi, \quad r = \sqrt{x^2 + y^2 + z^2},$$
$$y = r\sin\theta\sin\phi, \quad \theta = \arctan\left(\sqrt{x^2 + y^2}\big/z\right), \tag{A-1}$$
$$z = r\cos\theta, \quad \phi = \arctan(y/x).$$

Unit vectors are defined as vectors of unit magnitude in the direction of each coordinate. They are denoted by $\underline{\delta}_i$ where the subscript i refers to the coordinate direction. For example, $\underline{\delta}_x$ represents the unit vector in the x-direction. The relationship between unit vectors in the rectangular and spherical coordinate systems is shown in Eq. A-2

$$\underline{\delta}_r = (\sin\theta\cos\phi)\underline{\delta}_x + (\sin\theta\sin\phi)\underline{\delta}_y + (\cos\theta)\underline{\delta}_z,$$
$$\underline{\delta}_\theta = (\cos\theta\cos\phi)\underline{\delta}_x + (\cos\theta\sin\phi)\underline{\delta}_y + (-\sin\theta)\underline{\delta}_z, \tag{A-2}$$
$$\underline{\delta}_\phi = (-\sin\phi)\underline{\delta}_x + (\cos\phi)\underline{\delta}_y.$$

In order to be consistent with the notation in Bird *et al.* (1987), the unit vectors $\underline{\delta}_r$, $\underline{\delta}_\theta$, and $\underline{\delta}_\phi$ will henceforth be represented as $\underline{u}$, $\underline{s}$, and $\underline{t}$, respectively. Unlike Cartesian coordinates, the unit vectors in spherical coordinates are not constant. The spatial derivatives of unit vectors $\underline{u}$, $\underline{s}$ and $\underline{t}$ with respective to spherical coordinates are shown below in Eq. A-3

$$\begin{bmatrix} \dfrac{\partial}{\partial r}\underline{u} & \dfrac{\partial}{\partial r}\underline{s} & \dfrac{\partial}{\partial r}\underline{t} \\[2mm] \dfrac{\partial}{\partial\theta}\underline{u} & \dfrac{\partial}{\partial\theta}\underline{s} & \dfrac{\partial}{\partial\theta}\underline{t} \\[2mm] \dfrac{\partial}{\partial\phi}\underline{u} & \dfrac{\partial}{\partial\phi}\underline{s} & \dfrac{\partial}{\partial\phi}\underline{t} \end{bmatrix} = \begin{bmatrix} 0 & 0 & 0 \\ \underline{s} & -\underline{u} & 0 \\ \underline{t}\sin\theta & \underline{t}\cos\theta & -\underline{u}\sin\theta - \underline{s}\cos\theta \end{bmatrix} \tag{A-3}$$

The following linear operators are needed for development of models in spherical coordinates:

The gradient operator, $\underline{\nabla}$, in the spherical coordinate system is defined as

$$\underline{\nabla} \equiv \underline{u}\frac{\partial}{\partial r} + \underline{s}\frac{1}{r}\frac{\partial}{\partial \theta} + \underline{t}\frac{1}{r\sin\theta}\frac{\partial}{\partial \phi}.$$ (A-4)

The partial derivative with respect to the r-directional unit vector is similar to $\underline{\nabla}$ except

that the θ-, and ϕ- components are projected out by multiplying the $\underline{\nabla}$ by $\left(\underline{\underline{\delta}} - \underline{u}\underline{u}\right)$ and $\underline{r}$:

$$\frac{\partial}{\partial \underline{u}} = r\left[\left(\underline{\underline{\delta}} - \underline{u}\underline{u}\right) \cdot \underline{\nabla}\right] = \underline{s}\frac{\partial}{\partial \theta} + \underline{t}\frac{1}{\sin\theta}\frac{\partial}{\partial \phi}$$ (A-5)

The time derivative of the unit vectors can be obtained using the chain rule.

$$\underline{\dot{u}} \equiv \frac{d\underline{u}}{dt} = \frac{\partial r}{\partial t}\frac{\partial \underline{u}}{\partial r} + \frac{\partial \theta}{\partial t}\frac{\partial \underline{u}}{\partial \theta} + \frac{\partial \phi}{\partial t}\frac{\partial \underline{u}}{\partial \phi}$$ (A-6)

The relationships for $\dfrac{\partial \underline{u}}{\partial r}$, $\dfrac{\partial \underline{u}}{\partial \theta}$, and $\dfrac{\partial \underline{u}}{\partial \phi}$ in Eq. A-3 can be substituted into Eq. A-6 to

obtain

$$\underline{\dot{u}} = \underline{s}\dot{\theta} + \underline{t}\dot{\phi}\sin\theta .$$ (A-7)

Vector operations in spherical coordinate are different than those in the more

familiar Cartesian coordinates. The following vector operations are used in the derivation

in Chapter III. A detailed derivation will be helpful for understanding the context of this

study.

(1) $\underline{\underline{\kappa}} \cdot \underline{u} - \underline{\underline{\kappa}} : \underline{u}\underline{u}\underline{u}$

The expression $\underline{\underline{\kappa}} \cdot \underline{u} - \underline{\underline{\kappa}} : \underline{u}\underline{u}\underline{u}$ looks complicated. However, it can be simplified to

terms that are easily understood. The idea can be easily explained by adopting an

analytical viewpoint. Tensor $\underline{\underline{\kappa}}$ can be expressed as the summation of each component of

the tensor times the dyadic products $\underline{\delta}_i\underline{\delta}_j$. That is

$$\underline{\underline{\kappa}} = \sum_i \sum_j \underline{\delta}_i \underline{\delta}_j \kappa_{ij} \qquad\qquad (A\text{-}8)$$

Note that the dyadic products are tensors with unit magnitude. For the following

manipulation, the unit vectors $\underline{u}$, $\underline{s}$, and $\underline{t}$ are written as $\underline{\delta}_1$, $\underline{\delta}_2$ and $\underline{\delta}_3$, respectively.

$$\begin{aligned}
\underline{\underline{\kappa}} \cdot \underline{u} &= \sum_i \sum_j \underline{\delta}_i \underline{\delta}_j \kappa_{ij} \cdot \underline{\delta}_1 \\
&= \sum_i \sum_j \delta_i \delta_j \cdot \delta_1 \kappa_{ij} \qquad\qquad (A\text{-}9) \\
&= \sum_i \sum_j \delta_i \delta_{j1} \kappa_{ij}
\end{aligned}$$

in which δ_{j1} is the Kronecker delta and has the following properties

$$\begin{cases} \delta_{j1} = 1, & j = 1 \\ \delta_{j1} = 0, & j \neq 1 \end{cases} \qquad\qquad (A\text{-}10)$$

Hence, $\delta_{j1}\kappa_{ij}$ will be zero except $\delta_{11}\kappa_{I1}$, Eq. A-9 becomes

$$\underline{\underline{\kappa}} \cdot \underline{u} = \sum_i \underline{\delta}_i \kappa_{i1} \qquad\qquad (A\text{-}11)$$

$$\begin{aligned}
\underline{\underline{\kappa}} : \underline{u}\underline{u}\underline{u} &= \sum_i \sum_j \underline{\delta}_i \underline{\delta}_j \kappa_{ij} : \underline{\delta}_1 \underline{\delta}_1 \underline{\delta}_1 \\
&= \sum_i \sum_j \underline{\delta}_i \underline{\delta}_j : \underline{\delta}_1 \underline{\delta}_1 \kappa_{ij} \underline{\delta}_1 \qquad\qquad (A\text{-}12) \\
&= \sum_i \sum_j \delta_{i1} \delta_{j1} \kappa_{ij} \underline{\delta}_1
\end{aligned}$$

Combining Eqs. A-11 and A-12

$$\underline{\underline{\kappa}} \cdot \underline{u} - \underline{\underline{\kappa}} : \underline{u}\underline{u}\underline{u} = \sum_i \sum_j \underline{\delta}_i \underline{\delta}_j \kappa_{ij} \cdot \underline{\delta}_1 - \sum_i \sum_j \underline{\delta}_i \underline{\delta}_j \kappa_{ij} : \underline{\delta}_1 \underline{\delta}_1 \underline{\delta}_1$$

$$= \sum_i \underline{\delta}_i \kappa_{i1} - \sum_i \sum_j \delta_{i1} \delta_{j1} \kappa_{ij} \underline{\delta}_1 \tag{A-13}$$

$$= \left(\underline{\delta}_1 \kappa_{11} + \underline{\delta}_2 \kappa_{21} + \underline{\delta}_3 \kappa_{31} \right) - \underline{\delta}_1 \kappa_{11}$$

$$= \underline{\delta}_2 \kappa_{21} + \underline{\delta}_3 \kappa_{31}$$

The unit vectors $\underline{\delta}_2$ and $\underline{\delta}_3$ are $\underline{s}$ and $\underline{t}$, respectively.

$$\underline{\underline{\kappa}} \cdot \underline{u} - \underline{\underline{\kappa}} : \underline{u}\underline{u}\underline{u} = \underline{s}\kappa_{21} + \underline{t}\kappa_{31} \tag{A-14}$$

$\dfrac{\partial}{\partial \underline{u}} \cdot [\underline{\underline{\kappa}} \cdot \underline{u} - \underline{\underline{\kappa}} : \underline{u}\underline{u}\underline{u}]\psi$ can be obtained from Eqs. A-5 and A-14

$$\frac{\partial}{\partial \underline{u}} \cdot [\underline{\underline{\kappa}} \cdot \underline{u} - \underline{\underline{\kappa}} : \underline{u}\underline{u}\underline{u}]\psi = \left(\underline{s} \frac{\partial}{\partial \theta} + \underline{t} \frac{1}{\sin \theta} \frac{\partial}{\partial \phi} \right) \cdot \left(\underline{s}\kappa_{21}\psi + \underline{t}\kappa_{31}\psi \right) \tag{A-15}$$

Taking dot product of Eq. A-15

$$\frac{\partial}{\partial \underline{u}} \cdot [\underline{\underline{\kappa}} \cdot \underline{u} - \underline{\underline{\kappa}} : \underline{u}\underline{u}\underline{u}]\psi = \underline{s} \cdot \left(\frac{\partial \underline{s}}{\partial \theta} \right) \kappa_{21}\psi + \underline{s} \cdot \underline{s} \frac{\partial}{\partial \theta}(\kappa_{21}\psi) +$$

$$\underline{s} \cdot \left(\frac{\partial \underline{t}}{\partial \theta} \right) \kappa_{31}\psi + \underline{s} \cdot \underline{t} \frac{\partial}{\partial \theta}(\kappa_{31}\psi) +$$

$$\frac{\underline{t}}{\sin \theta} \cdot \left(\frac{\partial \underline{s}}{\partial \phi} \right) \kappa_{21}\psi + \underline{t} \cdot \underline{s} \frac{\partial}{\partial \phi}(\kappa_{21}\psi) + \tag{A-16}$$

$$\frac{\underline{t}}{\sin \theta} \cdot \left(\frac{\partial \underline{t}}{\partial \phi} \right) \kappa_{31}\psi + \frac{\underline{t}}{\sin \theta} \cdot \underline{t} \frac{\partial}{\partial \phi}(\kappa_{31}\psi)$$

Using the relation given in Eq. A-3 to evaluate the derivative of the unit vector with

respect to the coordinates

$$\frac{\partial}{\partial \underline{u}} \cdot [\underline{\underline{\kappa}} \cdot \underline{u} - \underline{\underline{\kappa}} : \underline{uuu}] \psi = \underline{s} \cdot (-\underline{u}) \kappa_{21} \psi + \underline{s} \cdot \underline{s} \frac{\partial}{\partial \theta} (\kappa_{21} \psi) +$$

$$\underline{s} \cdot (0) \kappa_{31} \psi + \underline{s} \cdot \underline{t} \frac{\partial}{\partial \theta} (\kappa_{31} \psi) +$$

$$\frac{\underline{t}}{\sin \theta} \cdot (\underline{t} \cos \theta) \kappa_{21} \psi + \underline{t} \cdot \underline{s} \frac{\partial}{\partial \phi} (\kappa_{21} \psi) + \tag{A-17}$$

$$\frac{\underline{t}}{\sin \theta} \cdot (-\underline{u} \sin \theta - \underline{s} \cos \theta) \kappa_{31} \psi + \frac{\underline{t}}{\sin \theta} \cdot \underline{t} \frac{\partial}{\partial \phi} (\kappa_{31} \psi)$$

Keeping the non-zero terms which contain dot product of unit vector and itself

$$\frac{\partial}{\partial \underline{u}} \cdot [\underline{\underline{\kappa}} \cdot \underline{u} - \underline{\underline{\kappa}} : \underline{uuu}] \psi = \frac{\partial}{\partial \theta} (\kappa_{21} \psi) + \frac{\cos \theta}{\sin \theta} \kappa_{21} \psi + \frac{1}{\sin \theta} \frac{\partial}{\partial \phi} (\kappa_{31} \psi) \tag{A-18}$$

(2) $\dfrac{\partial}{\partial \underline{u}} \cdot \dfrac{\partial}{\partial \underline{u}} \psi$

$$\frac{\partial}{\partial \underline{u}} \cdot \frac{\partial}{\partial \underline{u}} \psi = \left(\underline{s} \frac{\partial}{\partial \theta} + \underline{t} \frac{1}{\sin \theta} \frac{\partial}{\partial \phi} \right) \cdot \left(\underline{s} \frac{\partial \psi}{\partial \theta} + \underline{t} \frac{1}{\sin \theta} \frac{\partial \psi}{\partial \phi} \right) \tag{A-19}$$

Expanding Eq. A-19, the following equation can be obtained

$$\frac{\partial}{\partial \underline{u}} \cdot \frac{\partial}{\partial \underline{u}} \psi = \underline{s} \cdot \frac{\partial}{\partial \theta} \left(\underline{s} \frac{\partial \psi}{\partial \theta} \right) + \underline{s} \cdot \frac{\partial}{\partial \theta} \left(\underline{t} \frac{1}{\sin \theta} \frac{\partial \psi}{\partial \phi} \right)$$

$$+ \frac{1}{\sin \theta} \underline{t} \cdot \frac{\partial}{\partial \phi} \left(\underline{s} \frac{\partial \psi}{\partial \theta} \right) + \frac{1}{\sin \theta} \underline{t} \cdot \frac{\partial}{\partial \phi} \left(\underline{t} \frac{1}{\sin \theta} \frac{\partial \psi}{\partial \phi} \right) \tag{A-20}$$

Expanding the derivative in every terms of Eq. A-20

$$\frac{\partial}{\partial \underline{u}} \cdot \frac{\partial}{\partial \underline{u}} \psi = \underline{s} \cdot \left(\frac{\partial \underline{s}}{\partial \theta} \right) \frac{\partial \psi}{\partial \theta} + \underline{s} \cdot \underline{s} \frac{\partial^2 \psi}{\partial \theta^2} + \underline{s} \cdot \left(\frac{\partial \underline{t}}{\partial \theta} \right) \frac{1}{\sin \theta} \frac{\partial \psi}{\partial \phi}$$

$$+ \frac{1}{\sin \theta} \underline{s} \cdot \underline{t} \left(\frac{\partial^2 \psi}{\partial \theta \partial \phi} \right) + \frac{1}{\sin \theta} \underline{t} \cdot \frac{\partial \underline{s}}{\partial \phi} \frac{\partial \psi}{\partial \theta} + \frac{1}{\sin \theta} \underline{t} \cdot \underline{s} \frac{\partial \psi}{\partial \theta} \tag{A-21}$$

$$+ \frac{1}{\sin^2 \theta} \underline{t} \cdot \frac{\partial \underline{t}}{\partial \phi} \frac{\partial \psi}{\partial \phi} + \frac{1}{\sin^2 \theta} \underline{t} \cdot \underline{t} \frac{\partial^2 \psi}{\partial \phi^2}$$

Using the relation given in Eq. A-3 to evaluate the derivative of the unit vectors with respect to the coordinates

$$\frac{\partial}{\partial \underline{u}} \cdot \frac{\partial}{\partial \underline{u}} \psi = \underline{s} \cdot (-\underline{u}) \frac{\partial \psi}{\partial \theta} + \underline{s} \cdot \underline{s} \frac{\partial^2 \psi}{\partial \theta^2} + \underline{s} \cdot (0) \frac{1}{\sin \theta} \frac{\partial \psi}{\partial \phi}$$

$$+ \frac{1}{\sin \theta} \underline{s} \cdot \underline{t} \left(\frac{\partial^2 \psi}{\partial \theta \partial \phi} \right) + \frac{1}{\sin \theta} \underline{t} \cdot \underline{t} \cos \theta \frac{\partial \psi}{\partial \theta} \qquad \text{(A-22)}$$

$$+ \frac{1}{\sin \theta} \underline{t} \cdot \underline{s} \frac{\partial \psi}{\partial \theta} + \frac{1}{\sin^2 \theta} \underline{t} \cdot (0) \frac{\partial \psi}{\partial \phi} + \frac{1}{\sin^2 \theta} \underline{t} \cdot \underline{t} \frac{\partial^2 \psi}{\partial \phi^2}$$

Since the unit vectors are perpendicular to each other, the dot product of unit vectors is zero, except when doted into itself, we obtain.

$$\frac{\partial}{\partial \underline{u}} \cdot \frac{\partial}{\partial \underline{u}} \psi = \frac{\partial^2 \psi}{\partial \theta^2} + \frac{\cos \theta}{\sin \theta} \frac{\partial \psi}{\partial \theta} + \frac{1}{\sin^2 \theta} \frac{\partial^2 \psi}{\partial \phi^2} \qquad \text{(A-23)}$$

$$(3) \quad \frac{\partial}{\partial \underline{u}} \cdot \underline{\dot{u}} = \frac{1}{\sin \theta} \frac{\partial \dot{\theta} \sin \theta}{\partial \theta} + \frac{1}{\sin \theta} \frac{\partial \dot{\phi}}{\partial \phi} \qquad \text{(A-24)}$$

The expressions $\dfrac{\partial}{\partial \underline{u}}$ and $\underline{\dot{u}}$ were defined in Eqs. A-5 and A-7, respectively. Therefore

$$\frac{\partial}{\partial \underline{u}} \cdot \underline{\dot{u}} = \left(\underline{s} \frac{\partial}{\partial \theta} + \underline{t} \frac{1}{\sin \theta} \frac{\partial}{\partial \phi} \right) \cdot \left(\underline{s} \dot{\theta} + \underline{t} \dot{\phi} \sin \theta \right) \qquad \text{(A-25)}$$

$$\frac{\partial}{\partial \underline{u}} \cdot \underline{\dot{u}} = \underline{s} \cdot \frac{\partial}{\partial \theta} (\underline{s} \dot{\theta}) + \underline{s} \cdot \frac{\partial}{\partial \theta} (\underline{t} \dot{\phi} \sin \theta)$$

$$+ \frac{\underline{t}}{\sin \theta} \cdot \frac{\partial}{\partial \phi} (\underline{s} \dot{\theta}) + \frac{\underline{t}}{\sin \theta} \cdot \frac{\partial}{\partial \phi} (\underline{t} \dot{\phi} \sin \theta) \qquad \text{(A-26)}$$

Expanding the derivatives on the right hand side of Eq. A-26:

$$\frac{\partial}{\partial \underline{u}} \cdot \underline{\dot{u}} = \underline{s} \cdot \left(\frac{\partial}{\partial \theta} \underline{s} \right) \dot{\theta} + \underline{s} \cdot \underline{s} \frac{\partial \dot{\theta}}{\partial \theta} + \underline{s} \cdot \left(\frac{\partial}{\partial \theta} \underline{t} \right) \dot{\phi} \sin \theta + \underline{s} \cdot \underline{t} \frac{\partial (\dot{\phi} \sin \theta)}{\partial \theta}$$

$$+ \frac{\underline{t}}{\sin \theta} \cdot \left(\frac{\partial}{\partial \phi} \underline{s} \right) \dot{\theta} + \frac{\underline{t}}{\sin \theta} \cdot \underline{s} \frac{\partial \dot{\theta}}{\partial \phi} + \frac{\underline{t}}{\sin \theta} \cdot \left(\frac{\partial}{\partial \phi} \underline{t} \right) \dot{\phi} \sin \theta \qquad \text{(A-27)}$$

$$+ \frac{\underline{t}}{\sin \theta} \cdot \underline{t} \frac{\partial (\dot{\phi} \sin \theta)}{\partial \phi}$$

The derivatives of unit vectors with respect to the coordinates on the right hand side of

Eq. A-27 can be substituted from Eq. A-3, and rearranged to obtain

$$\frac{\partial}{\partial \underline{u}} \cdot \dot{\underline{u}} = \frac{1}{\sin\theta} \frac{\partial \dot{\theta} \sin\theta}{\partial \theta} + \frac{1}{\sin\theta} \frac{\partial \dot{\phi}}{\partial \phi}$$

(A-28)

APPENDIX B

PHASE-SPACE THEORY AND BROWNIAN FORCE

PHASE-SPACE THEORY

The position of bead v in the space can be represented by the position vector $\underline{r}_v$ with respect to an arbitrary reference point as shown in Figure B-1a. The velocity of the bead can be represented by $\underline{\dot{r}}_v$ with respect to the fixed arbitrary reference point, and defined as the time derivative of the vector $\underline{r}_v$, as shown below:

$$\underline{\dot{r}}_v = \frac{d\underline{r}_v}{dt} \qquad \text{(B-1)}$$

The momentum of bead v is

$$\underline{p}_v = m_v \underline{\dot{r}}_v . \qquad \text{(B-2)}$$

The total momentum of the molecule can be found as the sum of the momenta of all beads or the total momentum can be described by the velocity of the center of mass of the molecule:

$$\underline{p}_c = \sum_v m_v \underline{\dot{r}}_v = m_p \underline{\dot{r}}_c \qquad \text{(B-3)}$$

where

$$m_p = \sum_v m_v \qquad \text{(B-4)}$$

126

(a)

(b)
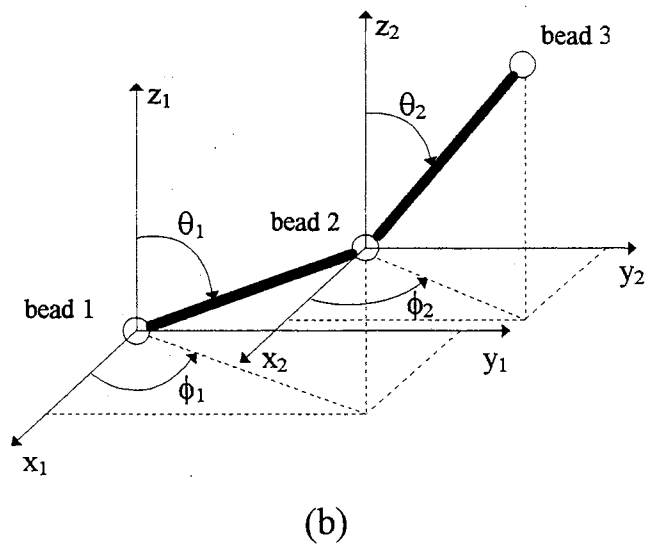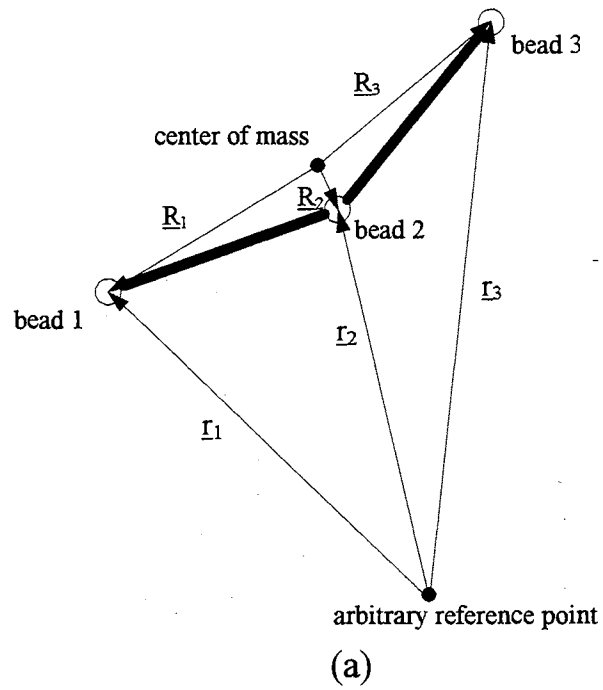
Figure B-1. Definition of Position Vectors and Coordinates

$$\dot{\underline{r}}_c = \frac{1}{m_p} \sum_v m_v \dot{\underline{r}}_v \qquad \text{(B-5)}$$

If the reference point of the coordinate system is on the center of mass of the molecule, the position vectors $\underline{R}_v$ and velocity vector $\dot{\underline{R}}_v$ can be defined with respect to the center of the mass as shown in Figure B-1a. Thus, $\underline{R}_v$ is the position vector from the center of mass of the entire molecule to the center of mass of the vth bead, and $\dot{\underline{R}}_v$ is the bead velocity with respect to the center of mass of the molecule.

The total kinetic energy $\mathcal{X}^{(T)}$ is the sum of the kinetic energy of every bead. Total kinetic energy can also be treated as the kinetic energy of the center of mass and the kinetic energy of beads with respect to the center of mass

$$\begin{aligned} \mathcal{X}^{(T)} &= \tfrac{1}{2} \sum_s m_v \dot{\underline{r}}_v^2 \\ &= \tfrac{1}{2} m_p \dot{\underline{r}}_c^2 + \tfrac{1}{2} \sum_s m_v \dot{\underline{R}}_v^2 \end{aligned} \qquad \text{(B-6)}$$

The momentum $\underline{p}_c$ in Equation (B-3) can be also treated as

$$\underline{p}_c = \frac{\partial}{\partial \dot{\underline{r}}_c} \mathcal{X}^{(T)} \qquad \text{(B-7)}$$

Generalized Coordinate System:

The Cartesian coordinate system is the most easy to understand; however, for the problem at hand, a spherical coordinate system is more convenient. One example of the generalized coordinates required to describe the orientation of the rods for a three bead rod model are the coordinates θ_1, ϕ_1, θ_2, and ϕ_2 which are shown in Figure B-1b. The

subscripts refer to the bead as reference point. Before further derivation, the base vector and metric matrix need to be defined as:

$$\underline{b}_{vs} = \sqrt{m_v}\, \frac{\partial}{\partial Q_s}\underline{R}_v \tag{B-8}$$

$$g_{st} = \sum_v (\underline{b}_{vs} \cdot \underline{b}_{vt}) \tag{B-9}$$

The conjugate momentum, P_s, associated with generalized coordinate Q_s can be defined in a manner similar to the definition of momentum, $\underline{p}_c$, in Equation (B-7)

$$P_s = \frac{\partial}{\partial \dot{Q}_s}\mathcal{K}^{(T)} = \sum_t g_{st}\dot{Q}_t \tag{B-10}$$

The internal kinetic energy can also be represented by the metric matrix g_{st} and generalized coordinates as

$$
\begin{aligned}
\mathcal{K}_{int} &= \tfrac{1}{2}\sum_s m_v \dot{\underline{R}}_v^2 \\
&= \frac{1}{2}\sum_s \sum_t \sum_v \left(\sqrt{m_v}\,\frac{\partial}{\partial Q_s}\underline{R}_v\right)\cdot\left(\sqrt{m_v}\,\frac{\partial}{\partial Q_t}\underline{R}_v\right)\dot{Q}_s\dot{Q}_t \\
&= \frac{1}{2}\sum_s \sum_t g_{st}\dot{Q}_s\dot{Q}_t
\end{aligned}
\tag{B-11}
$$

By using Equation (B-10) the internal kinetic energy can be represented in term of generalized momentum as follows

$$\mathcal{K}_{int} = \tfrac{1}{2}\sum_s \sum_t G_{st}P_s P_t \tag{B-12}$$

where

G_{st}: is the inverse of the metric matrix

The Hamiltonian of a single molecule is defined as the sum of internal kinetic and potential energy, as shown below:

$$\mathcal{H}'_{int} = \mathcal{H}_{int} + \phi \tag{B-13}$$

The Hamiltonian of the entire system is given by

$$\mathcal{H}^{(T)} = \sum_{\alpha} \sum_{i} \left[\frac{1}{2m^{\alpha}} \left(\underline{p}^{\alpha i} \right)^{2} + \mathcal{H}_{int}^{\alpha i} + \phi^{(e)\alpha i} \right] + \Phi \tag{B-14}$$

where

$\phi^{(e)}$: potential which describe the "external" force on a molecule of species α

Φ : intermolecular potential associated with the forces between the molecules

The Greek indices $(\alpha, \beta, \gamma, ...)$ are used to indicate the molecular species, and the Italic indices $(i, j, k, ...)$ are used to label the various molecules of each species.

Definition of Forces

The force on the center of mass of molecule i of species α due to the external force is given by

$$F^{(e)\alpha i} = -\frac{\partial}{\partial \underline{r}^{\alpha i}} \phi^{(e)\alpha i} \tag{B-15}$$

The force on the center of mass of molecule i of species α due to all the other molecules is given by

$$F^{\alpha i} = -\frac{\partial}{\partial \underline{r}^{\alpha i}} \Phi \tag{B-16}$$

The following forces are associated with the coordinate Q_s:

Force $\mathcal{J}_s^{(k)\alpha i}$ arising from the use of non-Cartesian coordinates

$$\mathcal{J}_s^{(k)\alpha i} = -\frac{1}{2} \sum_{tu} P_t^{\alpha i} P_t^{\alpha i} \frac{\partial}{\partial Q_s^{\alpha i}} G_{tu}^{\alpha i} \tag{B-17}$$

Intramolecular forces: $\mathcal{J}_s^{(\phi)\alpha i} = -\dfrac{\partial}{\partial \mathcal{Q}_s^{\alpha i}}\phi^{\alpha i}$ (B-18)

External forces: $\mathcal{J}_s^{(e)\alpha i} = -\dfrac{\partial}{\partial \underline{\mathcal{Q}}_s^{\alpha i}}\phi^{(e)\alpha i}$ (B-19)

Intermolecular forces $\mathcal{J}_s^{(d)\alpha i} = -\dfrac{\partial}{\partial \mathcal{Q}_s^{\alpha i}}\Phi$ (B-20)

Hamilton's equation of motion can be written as

$$\dot{\underline{r}}^{\alpha i} = \frac{\partial \mathcal{H}^{(T)}}{\partial \underline{p}_c^{\alpha i}} = \frac{1}{m^\alpha}\underline{p}_c^{\alpha i}$$ (B-21)

$$\dot{Q}_s^{\alpha i} = \frac{\partial \mathcal{H}^{(T)}}{\partial P_s^{\alpha i}} = \sum_t G_{st}^{\alpha i} P_t^{\alpha i}$$ (B-22)

$$\dot{\underline{p}}_c^{\alpha i} = -\frac{\partial \mathcal{H}^{(T)}}{\partial \underline{r}^{\alpha i}} = \underline{F}^{(e)\alpha i} + \underline{F}^{\alpha i}$$ (B-23)

$$\dot{P}_s^{\alpha i} = -\frac{\partial \mathcal{H}^{(T)}}{\partial \mathcal{Q}_s^{\alpha i}} = \mathcal{J}_s^{\alpha i}$$ (B-24)

where

$$\mathcal{J}_s^{\alpha i} = \mathcal{J}_s^{(k)\alpha i} + \mathcal{J}_s^{(\phi)\alpha i} + \mathcal{J}_s^{(e)\alpha i} + \mathcal{J}_s^{(d)\alpha i}$$ (B-25)

The general equation of change for an arbitrary dynamical variable B(x) is given by

$$\frac{\partial \langle B \rangle}{\partial t} = \langle \mathcal{L}B \rangle$$ (B-26)

$\mathcal{L}$ is the Liouville operator and is defined as

$$\mathcal{L} = \sum_\alpha \sum_i \left(\frac{1}{m^\alpha}\underline{p}^{\alpha i} \cdot \frac{\partial}{\partial \underline{r}^{\alpha i}} + \sum_s \sum_t G_{st}^{\alpha i} P_t^{\alpha i} \frac{\partial}{\partial \mathcal{Q}_s^{\alpha i}} \right.$$
$$\left. + [\underline{F}^{(e)\alpha i} + \underline{F}^{\alpha i}] \cdot \frac{\partial}{\partial \underline{p}_c^{\alpha i}} + \sum_s \mathcal{J}_s^{\alpha i} \frac{\partial}{\partial P_s^{\alpha i}} \right)$$ (B-27)

The dynamic variables B, after taking the average over the phase-space, is represented as follows

$$\langle B \rangle = f_\alpha(\underline{r}, Q, \underline{p}_c, P, t)$$

$$= \left\langle \sum_i \delta(\underline{r}^{\alpha i} - \underline{r})\delta(Q^{\alpha i} - Q)\delta(\underline{p}_c^{\alpha i} - \underline{p}_c)\delta(P^{\alpha i} - P) \right\rangle \qquad (B-28)$$

The angular bracket represents the average of the quantity over the phase-space which is defined as

$$\langle B \rangle = \frac{1}{nV} \int \int \int \int B f \, d\underline{r}_c \, dQ_s \, d\underline{p}_c \, dP_s \qquad (B-29)$$

where

f: phase-space distribution function

n: number of polymer molecules per unit volume

V: volume

The Direc delta function has the property that

$$\int \delta(x - a) f(x) dx = f(a) \qquad (B-30)$$

Equation (B-26) becomes:

$$\frac{\partial f_\alpha}{\partial t} + \left(\frac{1}{m^\alpha} \underline{p}_c \cdot \nabla f_\alpha \right) + \sum_{st} P_s \frac{\partial}{\partial Q_t} (G_{st} f_\alpha) + \left(\underline{F}^{(e)} \cdot \frac{\partial}{\partial \underline{p}_c} f_\alpha \right)$$

$$+ \left(\frac{\partial}{\partial \underline{p}_c} \cdot \left\langle \sum_i \underline{F}^\alpha B_i \right\rangle \right) + \sum_s \frac{\partial}{\partial P_s} \left\langle \sum_i \mathcal{J}_s^{\alpha i} B_i \right\rangle = 0 \qquad (B-31)$$

where:

$$F^{\alpha\beta} = -\frac{\partial}{\partial \underline{r}^\alpha} \Phi^{\alpha\beta} = \text{total force on a molecule of } \alpha \text{ by a molecule of } \beta \qquad (B-32)$$

$$\left\langle \sum_i \underline{F}^{\alpha} B_i \right\rangle = \sum_{\beta} \int F^{\alpha\beta} f_{\alpha\beta}(\underline{r}, \underline{Q}, \underline{r}_{\beta}, \underline{Q}_{\beta}, \underline{p}_c, P, \underline{p}_{\beta}, P_{\beta}, t) dr_{\beta} dQ_{\beta} dp_{\beta} dP_{\beta} \quad \text{(B-33)}$$

$$\left\langle \sum_i \mathfrak{J}_s^{\alpha} B_i \right\rangle = (\mathfrak{J}_s^{(e)} + \mathfrak{J}_s^{(k)} + \mathfrak{J}_s^{(\phi)}) f_{\alpha}$$

$$+ \sum_{\beta} \int f_{\alpha\beta} \mathfrak{J}^{\alpha\beta} f_{\alpha\beta}(\underline{r}, \underline{Q}, \underline{r}_{\beta}, \underline{Q}_{\beta}, \underline{p}_c, P, \underline{p}_{\beta}, P_{\beta}, t) dr_{\beta} dQ_{\beta} dp_{\beta} dP_{\beta} \quad \text{(B-34)}$$

$$\mathfrak{J}_s^{\alpha\beta} = -\frac{\partial}{\partial \underline{Q}_{\beta}^{\alpha}} \Phi^{\alpha\beta} = \text{generalized force on bead s of a molecule of species } \alpha$$

$$\text{due to a molecule of species } \beta \quad \text{(B-35)}$$

When Equation (B-31) is multiplied by $\underline{p}$ and then integrated over the momenta, the

equation becomes:

$$\frac{\partial}{\partial t}\left(\llbracket \underline{p}_c \rrbracket^{\alpha} \Psi_{\alpha}\right) + \frac{1}{m_p} \nabla \cdot \left(\llbracket \underline{p}_c \underline{p}_c \rrbracket^{\alpha} \Psi_{\alpha}\right) + \sum_{st} \frac{\partial}{\partial \underline{Q}_t}\left(G_{st} \llbracket P_s \underline{p}_c \rrbracket^{\alpha} \Psi_{\alpha}\right)$$

$$= \left(\underline{F}^{(e)\alpha} + \overline{N} \underline{F}^{(h)\alpha}\right) \Psi_{\alpha} \quad \text{(B-36)}$$

where

$$F^{(h)\alpha} = \frac{1}{\overline{N} \Psi_{\alpha}} \sum_{\beta} \iint F^{\alpha\beta} \Psi_{\alpha\beta}(\underline{r}, \underline{Q}, \underline{r}_{\beta}, \underline{Q}_{\beta}, t) dr_{\beta} dQ_{\beta} \quad \text{(B-37)}$$

$\overline{N}$: average number of beads per molecule of species α

$$\overline{N} = \sum_{\alpha} x_a N_{\alpha} \quad \text{(B-38)}$$

N_{α} : the number of beads making up a molecule of species α

x_{α} : mole fraction of species α

$$x_{\alpha} = \frac{n_{\alpha}}{\sum_{\beta} n_{\beta}} \quad \text{(B-39)}$$

Equation B-36 is also called the equation of motion for the centers of mass of molecules of species α. After rearranging, Equation (B-36) becomes

$$m^\alpha \left[\frac{\partial}{\partial t}(\underline{v}\Psi_\alpha) + \underline{\nabla} \cdot (\underline{v}\underline{v}\Psi_\alpha) \right] + \frac{\partial}{\partial t}\left([\![\underline{p}_c - m^\alpha \underline{v}]\!]^\alpha \Psi_\alpha \right) +$$

$$\underline{\nabla} \cdot \left(\underline{v}[\![\underline{p}_c - m^\alpha \underline{v}]\!]^\alpha \Psi_\alpha \right) + \underline{\nabla} \cdot \left([\![\underline{p}_c - m^\alpha \underline{v}]\!]^\alpha \underline{v}\Psi_\alpha \right) \tag{B-40}$$

$$= \left(\underline{F}^{(b)\alpha} + \underline{F}^{(e)\alpha} + \overline{N}\underline{F}^{(h)\alpha} \right) \Psi_\alpha$$

$$F^{(b)\alpha} = -\frac{1}{m^\alpha \psi_\alpha} \underline{\nabla} \cdot \left([\![(\underline{p}_c - m^\alpha \underline{v})(\underline{p}_c - m^\alpha \underline{v})]\!]^\alpha \psi_\alpha \right)$$

$$-\frac{1}{\psi_\alpha} \sum_{st} \frac{\partial}{\partial Q_s} \left(G_{st} [\![P_t \underline{p}_c]\!]^\alpha \psi_\alpha \right) \tag{B-41}$$

The Brownian force has the form of the divergence of a momentum flux with respect to the solution velocity $\underline{v}$ at the center of mass of the molecule.

Brownian Force for Equilibration in Momentum Space:

If the phase space distribution function is assumed to be in equilibrium (i.e., the velocity distribution function is the same as Eq. 2-1 for elastic dumbbell model), the momentum space distribution is:

$$f_{eq} = \frac{\exp\left\{ -\frac{1}{2}\left[(\underline{p}_c - m_p \underline{v})(\underline{p}_c - m_p \underline{v}) \right] / kT \right\}}{\iint \exp\left\{ -\frac{1}{2}\left[(\underline{p}_c - m_p \underline{v})(\underline{p}_c - m_p \underline{v}) \right] / kT \right\} d\underline{p}dP} \tag{B-42}$$

The following expressions hold by using Equation (B-42)

$$[\![(\underline{p}_c - m_p \underline{v})(\underline{p}_c - m_p \underline{v})]\!] =$$

$$\iint \frac{(\underline{p}_c - m_p \underline{v})^2 \exp\left\{ -\frac{1}{2}\left[(\underline{p}_c - m_p \underline{v})^2 \right] / kT \right\}}{\iint \exp\left\{ -\frac{1}{2}\left[(\underline{p}_c - m_p \underline{v})^2 \right] / kT \right\} d\underline{p}dP} d\underline{p}dP \tag{B-43}$$

$$[\![(\underline{p}_c - m_p \underline{v})(\underline{p}_c - m_p \underline{v})]\!] = m_p kT \underline{\underline{\sigma}} \tag{B-44}$$

$$\llbracket P_t \underline{p}_c \rrbracket = \iint \frac{P_t \underline{p}_c \exp\left\{-\frac{1}{2}\left[(\underline{p}_c - m_p \underline{v})^2\right] / kT\right\}}{\iint \exp\left\{-\frac{1}{2}\left[(\underline{p}_c - m_p \underline{v})^2\right] / kT\right\} d\underline{\dot{p}} dP} d\underline{\dot{p}} dP_t \qquad \text{(B-45)}$$

$$\llbracket P_t \underline{p}_c \rrbracket = 0 \qquad \text{(B-46)}$$

Then, the Brownian force becomes

$$F^{(b)\alpha} = -\frac{1}{m^\alpha \psi_\alpha} \underline{\nabla} \cdot \left(m^\alpha kT \psi_\alpha\right) \qquad \text{(B-47)}$$

$$\underline{F}^{(b)} = -kT \underline{\nabla} \ln \psi_\alpha \qquad \text{(B-48)}$$

APPENDIX C

TEST PROBLEMS

Problem 1 (Himmelblau, 1972; Dayde, 1989)

Minimize: $f(\underline{x}) = 1000 - x_1^2 - 2x_2^2 - x_3^2 - x_1x_2 - x_1x_3$

subject to: $x_1^2 + x_2^2 + x_3^2 - 25 = 0$

$8x_1 + 14x_2 + 7x_3 - 56 = 0$

$0 \le x_i \le 100, \quad i = 1, 2, 3$

$\underline{x}_o = [2, 2, 2]^T$ — Infeasible

$f(\underline{x}_o) = 976$

$\underline{x}^* = [3.5121, 0.21698, 3.5522]^T$

$f(\underline{x}^*) = 961.715$

Problem 2 (Himmelblau, 1972; Betts, 1978; Dayde, 1989)

Minimize: $f(\underline{x}) = (x_1 - 2)^2 + (x_2 - 1)^2$

Subject to: $-x_1^2 + x_2 \ge 0$

$-x_1 - x_2 + 2 \ge 0$

$\underline{x}_o = [2, 2]^T$ — Infeasible

$f(\underline{x}_o) = 1$

$\underline{x}^* = [1, 1]$

$f(\underline{x}^*) = 1$

Problem 3 (Himmelblau, 1972; Betts, 1978; Dayde, 1989)

Minimize: $f(\underline{x}) = (x_1 - 2)^2 + (x_2 - 1)^2$

Subject to: $x_1 - 2 x_2 + 1 = 0$

$-x_1^2/4 - x_2^2 + 1 \ge 0$

$\underline{x}_o = [2, 2]^T$ — Infeasible

$f(\underline{x}_o) = 1$

$\underline{x}^* = [0.82287, 0.91143]^T$

$f(\underline{x}^*) = 1.3934$

Problem 4 (Dayde, 1989)

Minimize: $f(\underline{x}) = 100(x_2 - x_1^2)^2 + (1 - x_1)^2 + 100(x_3 - x_2^2)^2 + (1 - x_2)^2$

Subject to: $9x_1 + 6x_2 + x_3 - 100 = 0$

$10x_1 + 20x_2 + x_3 - 100 \geq 0$

$40 - x_1 - 2x_2 - 4x_3 \geq 0$

$x_i \geq 0, \quad i = 1, 2, 3$

$\underline{x}_o = [1, 1, 1]^T \quad$ — Infeasible

$f(\underline{x}_o) = 0$

$\underline{x}^* = [6.67, 6.67, 0]^T$

$f(\underline{x}^*) = 3.3 \times 10^5$

SQPHP results, same as High (1991)

$\underline{x}^* = [6.5983, 5.8663, 5.4173]$

$f(\underline{x}^*) = 2.26 \times 10^5$

Problem 5 (Himmelblau, 1972; Betts, 1978)

Minimize: $f(\underline{x}) = 100(x_2 - x_1^2)^2 + (1 - x_1)^2 + 90(x_4 - x_3^2)^2$
$+ (1 - x_3)^2 + 10.1[(x_2 - 1)^2 + (x_4 - 1)^2] + 19.8(x_2 - 1)(x_4 - 1)$

Subject to: $-10 \leq x_i \leq 10, \quad i = 1, 2, 3, 4$

$\underline{x}_o = [-3, -1, -3, -1]^T \quad$ — Feasible

$f(\underline{x}_o) = 19192$

$\underline{x}^* = [1, 1, 1, 1]^T$

$f(\underline{x}^*) = 0$

Problem 6 (Betts, 1978; Dayde, 1989)

Minimize: $f(\underline{x}) = 0.001x_1 + x_2$

Subject to: $10^5(x_2 - x_1^2) = 0$

$-100 \leq x_i \leq 100, \quad i = 1, 2$

$\underline{x}_o = [1, 1]^T \quad$ — Feasible

$f(\underline{x}_o) = 1.001$

$\underline{x}^* = [-0.49999 \times 10^{-3}, 0.25 \times 10^{-6}]^T$

$f(\underline{x}^*) = -0.249999 \times 10^{-6}$

Problem 7 (Dayde, 1989)

Minimize: $f(\underline{x}) = 0.001x_1 + x_2$

Subject to: $-1000x_1^2 - 100x_2^2 + x_3 = 0$

$100x_1^2 + 400x_2^2 + x_3 - 0.01 = 0$

$-10 \leq x_i \leq 10, \quad i = 1, 2, 3$

$\underline{x}_o = [1, 1, 1]^T \quad$ — Infeasible

$$f(\underline{x}_o) = 1.001$$

$\underline{x}^* = [-0.20908 \times 10^{-5}, -0.44721 \times 10^{-2}, 0.2 \times 10^{-2}]^T$

$f(\underline{x}^*) = -4.7721 \times 10^{-3}$

Problem 8 (Dayde, 1989)

Minimize: $f(\underline{x}) = 5\exp(x_1 x_6) + x_2 x_4^2 - x_3 \sin(2x_7) + x_5^2 - 10x_8 x_5$

Subject to: $-x_2 + 15x_3 + x_6 - x_7 + 3x_8 - 25 = 0$

                   $x_4 - x_5 + 5x_6 - 10x_8 - 27 = 0$

                   $35 - x_2 - 10x_4 - x_8 \geq 0$

                   $8 - x_3 + 5x_5 - x_6 + x_7 \geq 0$

                   $200 - x_1 - x_2 - 3x_4 - x_5 - 7x_7 \geq 0$

                   $-3x_2 - 8x_3 + x_5 + 6x_7 - 10 \geq 0$

                   $x_1 + 15x_2 + x_5 + 8x_6 - 17 \geq 0$

                   $x_1 - 2x_2 - 8x_3 + 5x_4 + x_5 - 7x_6 + 10x_7 + 3x_8 - 50 \geq 0$

                   $x_i \geq 0, \quad i = 1, 2, 3, 4, 5, 6, 7, 8$

                   $\underline{x}_o = [-1, 0, -1, 0, -1, 0, -1, 0]^T$ — Infeasible

                   $f(\underline{x}_o) = 5.091$

$\underline{x}^* = [0, 0, 1.89014, 3.5, 0, 4.7, 8.05211, 0]^T$

$f(\underline{x}^*) = 5.727$

Problem 9 (Betts, 1978; Dayde, 1989)

Minimize: $f(x) = \sum_{i=1}^{10} x_i \left[A_i + \ln\left(x_i \sum_{j=1}^{10} x_j \right) \right]$

                   $A_1 = -6.089 \quad A_2 = -17.164 \quad A_3 = -34.054$

                   $A_4 = -5.914 \quad A_5 = -24.721 \quad A_6 = -14.986$

                   $A_7 = -24.10 \quad A_8 = -10.708 \quad A_9 = -26.662$

                   $A_{10} = -22.179$

Subject to: $x_1 + 2x_2 + 2x_3 + x_6 + x_{10} - 2 = 0$

                   $x_4 + 2x_5 + x_6 + x_7 - 1 = 0$

                   $x_3 + x_7 + x_8 + 2x_9 + x_{10} - 1 = 0$

                   $10^{-5} \leq x_i \leq 10, \quad i = 1, 2, 3, \ldots, 10$

                   $x_i = 0.1, \quad\quad\quad i = 1, \ldots, 10$ — Infeasible

                   $f(\underline{x}_o) = -20.961$

$\underline{x}^* = [0.040668, 0.14773, 0.78315, 0.0014142, 4.8524, 0.00069317, 0.027399,$

         $0.017947, 0.037314, 0.096871]^T$

$f(\underline{x}^*) = -47.761$

Problem 10 (Himmelblau, 1972; Betts, 1978; Dayde, 1989)

Minimize: $\quad f(x) = \sum_{i=1}^{10} \exp(x_i) \left[A_i + x_i - \ln\left(\sum_{j=1}^{10} \exp(x_j) \right) \right]$

$\quad A_1 = -6.089 \quad A_2 = -17.164 \quad A_3 = -34.054$

$\quad A_4 = -5.914 \quad A_5 = -24.721 \quad A_6 = -14.986$

$\quad A_7 = -24.10 \quad A_8 = -10.708 \quad A_9 = -26.662$

$\quad A_{10} = -22.179$

Subject to: $\quad \exp(x_1) + 2\exp(x_2) + 2\exp(x_3) + \exp(x_6) + \exp(x_{10}) - 2 = 0$

$\quad \exp(x_4) + 2\exp(x_5) + \exp(x_6) + \exp(x_7) - 1 = 0$

$\quad \exp(x_3) + \exp(x_7) + \exp(x_8) + 2\exp(x_9) + \exp(x_{10}) - 1 = 0$

$\quad -100 \le x_i \le 100, \qquad i = 1, 2, 3, \dots, 10$

$\quad x_i = -2.3, \qquad i = 1, \dots, 10 \quad$ — Infeasible

$\quad f(\underline{x}_o) = -21.0145$

$x^* = [-3.2024, -1.9123, -0.24441, -6.5606, -0.72166, 7.2736, -3.5965, -4.0206,$
$\qquad -3.2885, -2.3344]^T$

$f(\underline{x}^*) = -47.760$

Problem 11 (Himmelblau, 1972; Betts, 1978; Dayde, 1989)

Minimize : $f(\underline{x}) = -0.5(x_1x_4 - x_2x_3 + x_3x_9 - x_5x_9 + x_5x_8 - x_6x_7)$

Subject to: $\quad 1 - x_3^2 - x_4^2 \ge 0$

$\quad 1 - x_9^2 \ge 0$

$\quad 1 - x_5^2 - x_6^2 \ge 0$

$\quad 1 - x_1^2 - (x_2 - x_9)^2 \ge 0$

$\quad 1 - (x_1 - x_5)^2 - (x_2 - x_6)^2 \ge 0$

$\quad 1 - (x_1 - x_7)^2 - (x_2 - x_8)^2 \ge 0$

$\quad 1 - (x_3 - x_5)^2 - (x_4 - x_6)^2 \ge 0$

$\quad 1 - (x_3 - x_7)^2 - (x_4 - x_8)^2 \ge 0$

$\quad 1 - x_7^2 - (x_8 - x_9)^2 \ge 0$

$\quad x_1x_4 - x_2x_3 \ge 0$

$\quad x_3x_9 \ge 0$

$\quad -x_5x_9 \ge 0$

$\quad x_5x_8 - x_6x_7 \ge 0$

$\quad x_9 \ge 0$

$\quad x_i = 1, \quad i = 1, \dots, 9 \quad$ — Infeasible

$\quad f(\underline{x}_o) = 0$

$\underline{x}^* = [0.9971, -0.0758, 0.5530, 0.8331, 0.9981, -0.0623, 0.5642, 0.8256,$
$\qquad 0.0000024]^T$ Himmelblau (1972)

$\underline{x}^* = [0.91878, 0.39476, 0.11752, 0.99307, 0.91878, 0.39476, 0.11752, 0.99307,$
$\qquad -0.60445 \times 10^{-14}]^T$ Dayde (1989); Betts, (1978)

$f(\underline{x}^*) = -0.8660$

SQPHP results

$\underline{x}^* = [0.86602, 0.5, 0, 1.0, 0.86602, 0.5, 0, 1, 0]^T$

$f(\underline{x}^*) = -0.86602$

Problem 12 (Himmelblau, 1972; Betts, 1978)

Minimize: $f(x) = -75.196 + 3.8112\ x_1 - 0.12694x_1^2 + 2.0567 \times 10^{-3} x_1^3$

$- 1.0345 \times 10^{-5} x_1^4 + 6.8306x_2 - 0.030234x_1x_2 + 1.28134 \times 10^{-3} x_2 x_1^2$

$- 3.5256 \times 10^{-5} x_2 x_1^3 + 2.266 \times 10^{-7} x_2 x_1^4 - 0.25645 x_2^2 + 3.4604 \times 10^{-3} x_2^3$

$- 1.3514 \times 10^{-5} x_2^4 + 28.106/(x_2 + 1) + 5.2375 \times 10^{-6} x_1^2 x_2^2$

$+ 6.3 \times 10^{-8} x_1^3 x_2^2 - 7 \times 10^{-10} x_1^3 x_2^3 - 3.4054 \times 10^{-4} x_1 x_2^2$

$+ 1.6638 \times 10^{-6} x_1 x_2^3 + 2.8673 \exp(0.0005 x_1 x_2)^-$

Subject to: $0 \le x_1 \le 75$

$0 \le x_2 \le 65$

$x_1 x_2 - 700 \ge 0$

$x_2 - 5(x_1 / 25)^2 \ge 0$

$(x_2 - 50)^2 - 5(x_1 - 55) \ge 0$

$\underline{x}_o = [90, 10]^T$ — Infeasible

$f(\underline{x}_o) = 82.828$

$\underline{x}^* = [75, 65]^T$

$f(\underline{x}^*) = -58.903$

SQPHP results

$\underline{x}^* = [46.2, 50.63]^T$

$f(\underline{x}^*) = -6.58$

Problem 13 (Himmelblau, 1972; Betts, 1978)

Minimize: $f(x) = 5.3578547x_3^2 + 0.8356891x_1x_5 + 37.293239x_1 - 40792.141$

Subject to:

$0 \le 85.334407 + 0.0056858x_2x_5 + 0.0006262x_1x_4 - 0.0022053x_3x_5 \le 92$

$90 \le 80.51249 + 0.0071317x_2x_5 + 0.0029955x_1x_2 + 0.0021813x_3^2 \le 110$

$20 \le 9.300961 + 0.0047026x_3x_5 + 0.0012547x_1x_3 + 0.0019085x_3x_4 \le 25$

$78 \le x_1 \le 102$

$33 \le x_2 \le 45$

$27 \le x_3 \le 45$

$27 \le x_4 \le 45$

$27 \le x_5 \le 45$

$\underline{x}_o = [78.62, 33.44, 31.07, 44.18, 35.22]^T$ — Feasible

$f(\underline{x}_o) = -33217$

$\underline{x}^* = [78, 33, 29.995, 45, 36.776]^T$

$f(\underline{x}^*) = -30665.5$

APPENDIX D

COMPUTER CODES

The optimizations in this study required several programs as listed below:

```
opt.f
sqphp.f
opt.FDREAD
rdbase.f
psi.f
linpac.f
```

An utility program called "make" which is very common in UNIX system and clone was used to determine automatically which pieces of a large program need to be recompiled and issue the commands to recompile them. A file called the "Makefile" that describes the relationships among files in the program, and the states the commands for updating each file was written and list below.

Makefile:

```
SHELL          = /bin/sh

INC            =    $(PLAT)/include
LIB_DIR        =    $(PLAT)/lib
BIN_DIR        =
SRC_DIR        =    $(PLAT)/src/utility/rdbase
MSRC_INC       =    $(FIDAPSOURCE)/include
MSRC_DIR       =

CFLAGS = $(STD_CFLAGS) $(NOPTL_CFLAGS) -I$(INC) -
I$(INC)/fidap
FFLAGS = $(STD_FFLAGS) $(NOPTL_FFLAGS) -I$(INC) -
I$(INC)/fidap
```

141

```
FFILES =  $(SRC_DIR)/futility.o     rdbase.o linpac.o psi.o
CFILES =  $(SRC_DIR)/cutility.o

##### Machine specific definitions #########################

LDFLAGS = -L$(PLAT)/lib -lint -ldb -lm

OPTFILE = opt.o sqphp.o

### Turn off implicit rules for o files from c files

#%.o : %.c
#%.o : %.f

#########################
### Build executable ###
#########################

opt: $(OPTFILE) objfun
     @echo COMPILING opt
     xlf -o opt $(OPTFILE)

objfun: rdbase.o psi.o linpac.o
     @echo LINKING objective function ...
     xlf -o objfun $(FFILES)  $(CFILES)  $(LDFLAGS)

rdbase.o: rdbase.f
     @echo COMPILING rdbase.f
     xlf -c -I$(INC)/fidap rdbase.f
```

The opt file which was compiled from opt.f and sqphp.f is the main

program for the optimization. The opt perform SQPHP (Chen and Stadtherr, 1983)

optimization algorithm and evaluate objective function and derivatives for SQPHP. The

objective function was evaluated the flow field by FIDAP first and calucalte the x-

directional strength based on the output file from FIDAP. The FIDAP input file is

opt.FDREAD. The rdbase.f program read the database from FIDAP, while the

subroutine in psi.f was called to evaluate the probability distribution function. The file

linpac.f (Riggs, 1988) was used for evaluating the matrix when caluclates probability

distribution function. The objective files: futility.o, futility.o; libraries and

include files under $(PLAT)/ sub-directory are provided by Fluid Dynamics

International (or Fluent Inc. after been purchased) without providing source codes.

opt.f

```
C   8/25/96 PROGRAM  opt.f
      IMPLICIT REAL*8 (A-H, O-Z), INTEGER*4 (I-N)
C  Maximum number of variables
      PARAMETER (MNV = 35)
      Dimension MTYPE(3)
      Dimension X(MNV),XMIN(MNV),XMAX(MNV),DELTA(MNV),
     $ WVF(775),WQP(2220),G(MNV),CN(36,3),C(3)
      CALL READATA(M,MEQ,MXITER,ACC,IPRINT,STEPBD,MODE,MTYPE,N,X)
      LCN=N+1
      NP =N+1
      NR =NP-MEQ
      LWVF=1+2*M+N*(N+9)/2
      LWQP=4*NP+3*M + NR*(3*NR+7)/2
      WRITE(*,1200) LWVF, LWQP
      do 50 i=1,n
      xmin(i)=0.5
      xmax(i)=3.0
      delta(i)=1.
50    continue
      delta(n+1)=1.
      CALL SQPHP5(N, X, XMIN,XMAX)
      INF=0
100   CALL FUNCONS(X,F,C)
      IF(INF .EQ. -1) GO TO 300
200   CALL FDGRAD(M,LCN,X,G,CN)

300   CALL SQPHP(N,M,MTYPE,X,F,G,C,CN,LCN,MXITER,ACC,IPRINT,INF,
     $ WVF,LWVF,WQP,LWQP,XMIN,XMAX,DELTA,STEPBD,MODE)
c       do 400 i=1,n
c       write(*,'(f10.8,1x,i3)')x(i),inf
c400    continue
      IF(INF .EQ. -1) GO TO 100
      IF(INF .EQ. -2) GO TO 200
      WRITE(6,1000)F
      WRITE(6,1100)(I,X(I),I=1,N)
1000  FORMAT(3X,4HF = ,G15.8)
1100  FORMAT(3X,2HX(,I2,2H)=,F8.4)
1200  FORMAT(3X,'LWVF= (', I4, ')   LWQP = (', I4, ')')
      STOP
      END
C
C       EVALUATE OBJECTIVE FUNCTION & CONSTRAINTS
C
      SUBROUTINE FUNCONS(X,F,C)
      IMPLICIT REAL*8 (A-H, O-Z), INTEGER*4 (I-N)
      dimension C(*),X(*)
      open(11,file='geo',status='old')
c     rewind 11
      write(11,*) '/geometry'
      write(11,*) '$Y1= ', x(1)
      write(11,*) '$Y2= ', x(2)
      write(11,*) '$Y3= ', x(3)
      close(11)
      call system("fidap -id conv -new -in opt.FDREAD")
      open(12,file='obj',status='old')
      read(12,*) F
c     F=-F
      C(1)  = X(3)-3.
      close(12)
      RETURN
      END


      SUBROUTINE FDGRAD(M,LCN,X,G,CN)
C
C     FORWARD DIFFERENCE METHOD TO FIND G AND CN
C
      IMPLICIT REAL*8 (A-H, O-Z), INTEGER*4 (I-N)
      PARAMETER (MNV = 35)
      dimension X(*), G(*),CN(LCN,*)
      dimension BX(MNV),C(3),BC(3)
```

```fortran
      N=LCN-1
      DELX = 1.0D-2
      CALL FUNCONS(X,F,C)
      BF=F
      DO 10 I = 1,N
      BX(I) = X(I)
10    CONTINUE
      DO 20 I = 1,M
      BC(I) = C(I)
20    CONTINUE
      DO 30 I = 1,N
      X(I)=X(I)+DELX
      CALL FUNCONS(X,F,C)
C     GRADIENT VECTOR OF OBJECTIVE FUNCTION
      G(I) = (F-BF)/(X(I)-BX(I))
      X(I)=BX(I)
30    CONTINUE
      DO 40 I = 1, N
      DO 40 J = 1, M
C     MATRIX OF CONSTRAINT NORMALS
C     CN(I,J) = (C(J)-BC(J))/(X(I)-BX(I))
      CN(I,J) = 0.0
40    CONTINUE
      CN(1,1)=1.
C     CN(N,2)=1.
      RETURN
      END


      SUBROUTINE READATA(M,MEQ,MXITER,ACC,IPRINT,STEPBD,MODE
     & ,MTYPE,N,X)
      IMPLICIT REAL*8 (A-H, O-Z), INTEGER*4 (I-N)
      Dimension MTYPE(*),X(*)
      CHARACTER INAME*80
C     PRINT *, 'PLEASE TYPE INPUT FILE NAME'
C     READ( *, 100) INAME
      INAME='opt.dat'
100   FORMAT(80A)
      OPEN( 10, FILE=INAME, STATUS= 'OLD')
      READ(10,*) M,MEQ,MXITER,ACC,IPRINT,STEPBD,MODE
      WRITE(*,*) M,MEQ,MXITER,ACC,IPRINT,STEPBD,mode
      READ(10,*) (MTYPE(I), I= 1, M)
      WRITE(*,*) (MTYPE(I), I= 1, M)
      READ(10,*) N
      WRITE(*,*) N
      OPEN( 11, FILE="geo", STATUS= 'OLD')
      DO 200 I=1,N
      READ(11,*) INAME, X(I)
200   CONTINUE
      CLOSE(10)
      CLOSE(11)
      RETURN
      END
```

opt.FDREAD

```
/ Any input data beginning with the character "/" is a comment.
FI-GEN ( ELEMENT=1,POINT=1,CURVE=1,SURFACE=1,NODE=0,MEDGE=1,MLOOP=1,MFACE=1,
BEDGE=1,SPAVE=1,MSHELL=1,MSOLID=1,COORDINATE=1 )
readfile(file="geo",nointeractive)
/Generate the points necessary to define the geometry.
point(add,coordinates,x=0,y=0)
point(add,coordinates,x=3,y=0)
point(add,coordinates,x=3,y=1)
point(add,coordinates,x=1.5,y=$y1)
point(add,coordinates,x=0. ,y=$y2)
/connect the points to lines
point(select,ID,window=1)
 5
 1
 2
 3
curve(add,line)
/Define the shape of the die to be optimized.
point(select,ID,window=1)
 3
 4
 5
curve(add)
/Create a surface on which node points are to be created
curve(select,id,window=1)
 1
 2
 3
 4
surface(add,wireframe,edg1cnt=1,edg2cnt=1,edg3cnt=1,edg4cnt=1)
/Define the number and location of points on the edges
curve(select,id,window=1)
 1
 3
medge(add,successive,intervals=20,ratio=0.000000,2ratio=0.000000,
pcentr=0.000000)
curve(select,id,window=1)
 2
 4
medge(add,successive,intervals=40,ratio=0.000000,2ratio=0.000000,
pcentr=0.000000)
/Specify groups of curves which define bounding edges
curve(select,id,window=1)
 1
 2
 3
 4
mloop(add,map,visible,noshowlabel,edg1cnt=1,edg2cnt=1,edg3cnt=1,edg4cnt=1)
/Identify the faces on which mesh generation is to occur
surface(select,id,window=1)
 1
utility(highlight=9)
mloop(select,id,window=1)
 1
utility(highlight=3)
mface(add)
/Generate the mesh
mface(select,ID,window=1)
 1
element(setdefaults,quadrilateral,nodes=9)
/element(setdefaults,triangle,nodes=3)
mface(mesh,map,entity="fluid")
END
options(cnrag1=14)
FI-BC
bgadd(select,edge,include,id,window=1)
 1
bgadd(add,edge,entity="inlet",include)
bgadd(select,edge,include,ID,window=1)
 4
bgadd(add,edge,entity="wall",include)
```

```
bgadd(select,edge,include,ID,window=1)
  3
bgadd(add,edge,entity="outlet",include)
bgadd(select,edge,include,ID,window=1)
  2
bgadd(add,edge,entity="symmetry",include)
/Inlet Boundary Condition: Total normal stress
bcsgroup(bcflux)
bcsgroup(select,ID ,window=1)
  2
BCFLUX(X, GSELECT, constant=5.e6)
utility(unselect,all)
/Inlet Boundary Condition: Uy = 0
bcsgroup(bcnode)
bcsgroup(select,ID ,window=1)
  2
BCNODE( UY, GSELECT, ZERO)
utility(unselect,all)
/Wall Boundary Condition: Ux = Uy = 0
bcsgroup(bcnode)
bcsgroup(select,ID,window=1)
  3
BCNODE( VELOCITY, GSELECT, ZERO )
utility(unselect,all)
bcsgroup(bcnode)
/Symmetric Boundary Condition: Uy = 0
bcsgroup(select,ID ,window=1)
  5
BCNODE( UY, GSELECT, ZERO)
utility(unselect,all)
END
FIPREP
DATAPRINT( ADD, NORMAL )
PRINTOUT( ADD, ALL, BOUNDARY )
PROBLEM( ADD, 2-D, INCOMPRESSIBLE, STEADY, LAMINAR, NONLINEAR, NEWTONIAN,
MOMENTUM, ISOTHERMAL, FIXED, SINGLEPHASE )
SOLUTION(N.R. = 10)
EXECUTION( ADD, NEWJOB )
ENTITY( ADD, NAME="fluid", FLUID )
ENTITY( ADD, NAME="inlet", PLOT )
ENTITY( ADD, NAME="wall", PLOT )
ENTITY( ADD, NAME="outlet", PLOT )
ENTITY( ADD, NAME="symmetry", PLOT )
DENSITY( CONSTANT=0.9 )
VISCOSITY( CONSTANT=7.083e4 )
pressure(MIXED=0.1e-9, CONTINUOUS)
END
CREATE(FISOLV)
RUN( FISOLV)
/Evaluate objective function
config(user="objfun")
system(user)
END
```

rdbase.f

```
        PROGRAM RDBASE
C
C-------------------------------------------------------------------------------
C
C     THE PURPOSE OF THIS PROGRAM IS TO CALCULATE THE OBJECTION FUNCTION
C     BY THE FIDAP MODEL DATABASE (FDBASE) AND THE RESULTS DATABASE (FDPOST)
C
C     THE DEFINATION OF THE VARIABLE CAN BE REFERRING TO
C     $FIDAPROOT/src/utility/rdbase/rdbase.f
C
C     THE PROGRAM ASSUMES THE FOLLOWING FILE NAMES:
C
C        1. FDBASE IS THE FIDAP MODEL DATABASE
C        2. FDPOST ID THE FIDAP RESULTS DATABASE
C        3. FDNEUT IS THE FIDAP NEUTRAL FILE
C
C-------------------------------------------------------------------------------
C
        INCLUDE 'IMPLCT.COM'
        INCLUDE 'CNTRLC.COM'
        INCLUDE 'LEVEL.COM'
C     MAXIMUM NUMBER OF NODAL POINTS (THIS WILL NEED TO BE INCREASED
C                                     BASED ON MODEL SIZE)
        PARAMETER (MNONP=50000)
C     MAXIMUM NUMBER OF SPECIES EQUATIONS + 1
        PARAMETER (MNOSE=16)
C     NO. OF COORDINATE DIMENSIONS (2 OR 3)
        PARAMETER (NOCD=3)
C     NO. OF VELOCITY COMPONENTS (2 OR 3)
        PARAMETER (NOVC=3)
        PARAMETER (MELEM=100)
        DIMENSION XYZ(MNONP*NOCD), UF(NOVC*MNONP), P(MNONP)
        DIMENSION NODE(27), IFLAGS(5), VAL(1000), RFLAGS(5)
        dimension nodef(27),geo(18),velo(18),sam(20)
        DIMENSION IDOS(MNONP), NELPAR(175)
        DIMENSION W3(3),S3(3),AN(3),ANS(3)
        DATA S3/-0.774596669241480,0.0,0.774596669241480/,
       $ W3/0.555555555555560,0.888888888888890,0.555555555555560/
        CHARACTER*20 ELMMAT,FDBASE,FDPOST
C
C     NEUTRAL FILE UNIT NUMBER
        INEUT = 10
C
        OPEN (20, FILE='name', FORM='FORMATTED')
        READ(20,*)FDBASE
        READ(20,*)FDPOST
        CLOSE(20)
        IERD = 0
        IDBOPE = 0
        ZRO = 0
C
C     ---------------------
C     O P E N   F I L E S
C     ---------------------
C
C     OPEN THE NEUTRAL FILE
C
C       OPEN (INEUT, FILE='FDNEUT', FORM='FORMATTED',position='append'
        OPEN (INEUT, FILE='FDNEUT', FORM='FORMATTED'
       - , ERR=100)
        GO TO 110
  100 CALL JDBERR ('FORTRAN OPEN', 1, 0)
C
C     INITIALIZE THE DATABASE SYSTEM
C
  110 IERD = JLMINI (0)
        CALL JDBERR ('JLMINI', IERD, 0)
C
C     SET NO. OF DATABASE PAGES
C
        NDBPGS = 500
```

```
      CALL FGTVAL (15, NDBFSV, ELMMAT)
      IF (NDBFSV.NE.-1) NDBPGS = MAX (500, NDBFSV)
      CALL DBPSMB ( NDBPGS, IERD )
      CALL JDBERR ('DBPSMB', IERD, 0)
C
C     CHECK FORMAT OF DATABASE
C        IDBCOM = 0    COMPRESSED
C               = 1    UNCOMPRESSED
C
      IERD = JLMUNC (FDBASE, IDBCOM)
      IF (IERD.NE.0) THEN
C        UNRECOGNIZED DATABASE
         CALL JDBERR ('JLMFUNC: UNRECOGNIZED MODEL DATABASE', IERD, 0)
      ENDIF
C
C     OPEN THE FIDAP MODEL DATABASE
C
      IF (IDBCOM.EQ.0) THEN
C        COMPRESSED FORMAT
         IERD = JLMO2E ('FDTMP1', 6, FDBASE, 2)
         CALL JDBERR ('JLMO2E', IERD, 0)
      ELSE
C        UNCOMPRESSED FORMAT
         IERD = JLMOPE (FDBASE, 6, 1, 2)
         CALL JDBERR ('JLMOPE', IERD, 0)
      ENDIF
C
C
C     ------------------------------------
C     C O N T R O L   I N F O R M A T I O N
C     ------------------------------------
C
C
C     READ CONTROL INFORMATION FROM NODE DATABASE
C
      CALL READCN (0, 0, 2, IERD)
      CALL JDBERR ('READCN', IERD, 1)

      IF (NUMNP .GT. MNONP) CALL JDBERR (
     1   'NUMBER OF NODES.  PLEASE INCREASE MNONP.', 1, 1)
C
      IF (NDFVL.EQ.0) THEN
         NDFVL = 2
         IF (IDIM.GE.2) NDFVL = 3
      ENDIF
C
C
C     ----------------------------------
C     N O D A L   C O O R D I N A T E S
C     ----------------------------------
C
C
      IF (NUMNP.EQ.0)
     1   CALL JDBERR (' NODES.   NO NODES IN THIS PROBLEM.', 1, 1)
C
C     GET THE MODEL COORDINATES
C
      IERD = JNGXYZ (1, NDFCD, NUMNP, XYZ, IDOS)
      CALL JDBERR ('JNGXYZ', IERD, 1)
C
C     SCALE COORDINATES
C
      DO 115 I=1,NDFCD
         NDBEG = NUMNP*(I-1)
         DO 115 N=1,NUMNP
            XYZ(NDBEG+N) = XYZ(NDBEG+N)*SCLDOF(I)
  115 CONTINUE
C
      DO 120 INODES=1,NUMNP
C
C        GET THE EXTERNAL NODE NUMBER FOR MODE NOD
C
         IERD = JNGITE (IDOS(INODES), NOD)
         CALL JDBERR ('JNGITE', IERD, 1)
C
```

```
  120 CONTINUE
C
C     OPEN THE RESULTS DATABASE
C        CHECK FORMAT OF DATABASE
C
      IERD = JLMUNC (FDPOST, IDBCOM)
      IF (IERD.NE.0) THEN
C        UNRECOGNIZED DATABASE
         CALL JDBERR ('JLMFUNC: UNRECOGNIZED RESULTS DATABASE', IERD, 0)
      ENDIF
      IF (IDBCOM.EQ.0) THEN
C        COMPRESSED FORMAT
         IERD = JLMO2R ('FDTMP2', 6, FDPOST, 2, IPST)
         CALL JDBERR ('JLMO2R', IERD, 0)
      ELSE
C        UNCOMPRESSED FORMAT
         IERD = JLMOPR (FDPOST, 6, 1, 2, IPST)
         CALL JDBERR ('JLMOPR', IERD, 0)
      ENDIF
C
C     --------------
C     R E S U L T S
C     --------------
C
C     S O L U T I O N   V E C T O R S
C
C
      NUMNPM = NUMNP
      CALL READCN (1, IPST, 2, IERD)
      IF (NUMNP.NE.NUMNPM)
     1    CALL JDBERR ('READCN.  INCOMPATIBLE MODEL AND RESULTS DBS',
     2                    1, 1)
C
C     GET THE NUMBER OF TIME STEPS
C
      IERD = JQGNTS (IPST, IDENTR, NSTEP)
      CALL JDBERR ('JQGNTS', IERD, 1)
      IF (NSTEP.EQ.0)
     1    CALL JDBERR ('JQGNTS.  0 TIME STEPS DETECTED.', 1, 1)
C
      ISEQ = 3
      DO 900 KSTP = 1, NSTEP
C
C        TIME STEP HEADER INFORMATION
C
         IERD = JQGHSE (IPST, ISEQ, IDENTR, KSTEP, TIME, DT, RNORM)
         CALL JDBERR ('JQGHDI', IERD, 1)
         ISEQ = 2
         WRITE (INEUT, 1070) KSTEP, TIME, DT
C
C        VELOCITY RECORDS
C        ----------------
C
C        UF:    VELOCITY VECTOR - VELOCITY COMPONENTS FOR NODE I ARE STORED
C               AS UF(2*I-1), UF(2*I) FOR NDFVL=2 AND
C               AS UF(3*I-2),UF(3*I-1),UF(3*I) FOR NDFVL=3.
C
C
C        GET THE VELOCITY SOLUTION
C
         K = 1
         IERD = JQGRBT (IPST, IDENTR, KSTEP, K, NUMNP, NDFVL,
     1                  1, 0, 0, UF)
         IF (IERD .EQ. -1) GO TO 400
         CALL JDBERR ('JQGRBT: VELOCITIES', IERD, 1)
C
C        PRESSURE RECORDS
C        ----------------
C
C        (P(I,I=1,NUMNP) IS THE PRESSURE AT NODE I.
C
C
C           GET THE PRESSURE SOLUTION
C
  400        K = 2
```

```
            IERD = JQGRBT (IPST, IDENTR, KSTEP, K, NUMNP,
     1                       1, 1, 0, 0, P)
            IF (IERD .EQ. -1) GO TO 900
            CALL JDBERR ('JQGRBT: PRESSURE', IERD, 1)
C
  900 CONTINUE
C
C     ---------------------------
C     E L E M E N T    G R O U P S
C     ---------------------------
C
C     ELMMAT:   ENTITY NAME TO WHICH ELEMENT GROUP BELONGS
C               (20 CHARACTERS)
C
C     LOOP OVER ELEMENT GROUPS
C
      obj=0.0
      NG = 0
      DO 290 NGG=1,NELGPS(1)
C
C         GET NEXT ELEMENT GROUP NUMBER
C
          IERD = JGGSEQ (NG)
          CALL JDBERR ('JGGSEQ', IERD, 1)
          IF (NG.EQ.0) GO TO 300
C
C         GET THE ELEMENT GROUP INFORMATION RECORD
C
          IERD = JGGELG (NG, NELPAR, ELMMAT)
          CALL JDBERR ('JGGELG', IERD, 1)
C
          NDP     = NELPAR(6)
          NELGP   = NELPAR(5)
          NFTYP   = NELPAR(4)
          IGEOM   = NELPAR(16)
C
          SLETH=0.0
          if(elmmat .eq. 'fluid')  then
          ngf=ng
          nelgpf=nelgp
          igeomf=igeom
c         nftypf=nftyp
c         write(*,*)"ngf",ngf,nelgpf,igeomf,nftypf
          endif
c         write(*,*) igeom
          sleth = 0.0
          if(elmmat .eq. 'outlet') then
C
C         ELEMENT CONNECTIVITY RECORDS
C         ----------------------------
C
          obj=0.0
          is = 0
           DO 280 NE=1,NELGP
C
C             NE:    GLOBAL ELEMENT NUMBER
C             NODE:  LIST OF NDP NODES DEFINING ELEMENT (SEE FIPREP
C                    USERS MANUAL, CHAPTER 12 FOR ORDERING CONVENTIONS)
C
              IERD = JGGEL2 (NG, NE, 1, NUMRET, NELNUM)
              CALL JDBERR ('JGGEL2', IERD, 1)
              IF (NUMRET.EQ.0)
     1            CALL JDBERR ('JGGEL2.  NUMRET=0', 1, 1)
C
C             GET THE ELEMENTS OF THE ELEMENT GROUP
C
              IERD = JEGELE (NELNUM, IGEOM, NDP, IFLAGS, NODE, NGRP,
     1                       ICOL, IVIS)
              CALL JDBERR ('JEGELE', IERD, 1)
          do 2040 nef=1,nelgpf
              ierd = jggel2 (ngf, nef, 1, NUMRET, NELNUMf)
              CALL JDBERR ('JGGEL2', IERD, 1)
              IF (NUMRET.EQ.0)
     1            CALL JDBERR ('JGGEL2.  NUMRET=0', 1, 1)
              IERD = JEGELE (NELNUMf, IGEOMf, NDPf, IFLAGS, NODEf, NGRP,
```

```
      1                               ICOL, IVIS)
                CALL JDBERR ('JEGELE', IERD, 1)
            ncount=0
            do 2010 i=1,ndpf
            do 2010 j=1,ndp
            if(nodef(i) .eq. node(j)) ncount=ncount+1
2010        continue
c
c   *** find the velocity gradient tensor, and calculate the probability
C       distribution function
c
            if(ncount .eq. 3) then
c           write(*,*) ncount
            geo(1)=xyz(nodef(4))
            geo(2)=xyz(nodef(5))
            geo(3)=xyz(nodef(6))
            geo(4)=xyz(nodef(4)+numnp)
            geo(5)=xyz(nodef(5)+numnp)
            geo(6)=xyz(nodef(6)+numnp)
            velo(1)=uf(2*nodef(4)-1)
            velo(2)=uf(2*nodef(4))
            velo(3)=uf(2*nodef(5)-1)
            velo(4)=uf(2*nodef(5))
            velo(5)=uf(2*nodef(6)-1)
            velo(6)=uf(2*nodef(6))
            call psi(geo,velo,sx,sy)
            is = is + 1
            sam(is)=sx
            tlong =dabs(xyz(nodef(6)+numnp)- xyz(nodef(5)+numnp))
c           obj=obj+sx*tlong
            sleth = sleth + tlong
            geo(1)=xyz(nodef(6))
            geo(2)=xyz(nodef(7))
            geo(3)=xyz(nodef(9))
            geo(4)=xyz(nodef(6)+numnp)
            geo(5)=xyz(nodef(7)+numnp)
            geo(6)=xyz(nodef(9)+numnp)
            velo(1)=uf(2*nodef(6)-1)
            velo(2)=uf(2*nodef(6))
            velo(3)=uf(2*nodef(7)-1)
            velo(4)=uf(2*nodef(7))
            velo(5)=uf(2*nodef(9)-1)
            velo(6)=uf(2*nodef(9))
            call psi(geo,velo,sx,sy)
            is = is + 1
            sam(is)=sx
            tlong =dabs(xyz(nodef(7)+numnp)- xyz(nodef(6)+numnp))
c           obj=obj+sx*tlong
            sleth = sleth + tlong
c            write(*,*)sleth
C
C*** EVALUATE OBJECTIVE FUNCTION
C sum of square error
            endif
2040        continue
280         continue
            avg = 0.0
            do 2050 i = 1, 2*nelgp
            avg = avg + sam(i)
2050        continue
            avg=avg/dble(nelgp)/2.
            do 2060 i = 1, 2*nelgp
            obj = obj + (avg-sam(i))*(avg-sam(i))
2060        continue
            obj=dsqrt(obj/20.)
            open(11,file='obj',status='unknown')
            write(11,*) obj
            close(11)
            else if(elmmat .eq. 'wall') then
              DO 285 NE=1,NELGP
                IERD = JGGEL2 (NG, NE, 1, NUMRET, NELNUM)
                CALL JDBERR ('JGGEL2', IERD, 1)
                IF (NUMRET.EQ.0)
      1           CALL JDBERR ('JGGEL2.  NUMRET=0', 1, 1)
                IERD = JEGELE (NELNUM, IGEOM, NDP, IFLAGS, NODE, NGRP,
```

```
     1                        ICOL, IVIS)
            CALL JDBERR ('JEGELE', IERD, 1)
C
        DO 285 INOD=1,NDP
         WRITE (INEUT, *) XYZ(NODE(INOD)), XYZ(NODE(INOD)+NUMNP)
285     continue
         endif
  290 CONTINUE
         write(*,*) 'OBJECTIVE: ', obj
  300 CONTINUE
  950 STOP
C
 1070 FORMAT ('TIMESTEP: ', I5, ' TIME:      ', E15.7,
     1           ' INCRMNT: ', E15.7)
        END
C
        SUBROUTINE READCN (IOPT, IPSTFL, INDEX, IERR)
C
C----------------------------------------------------------------------
C     GET CONTROL INFORMATION FROM DATABASE
C
C     IOPT = 0    READ FROM GEOMETRY DATABASE
C
C            1    READ FROM RESULTS DATABASE IPSTFL
C
C     INDEX = 0   IGNORE
C             1   FIPREP RECORD
C             2   FISOLV RECORD
C             3   MESH   RECORD
C----------------------------------------------------------------------
C
        INCLUDE 'IMPLCT.COM'
        INCLUDE 'CNTRLW.COM'
C
        IERD = 0
        LRDATA = 600
        LIDATA = 450
        LCDATA = 9*80
C
C     GET SIMULATION CONTROL INFO
C
        IF (IOPT.EQ.0) THEN
C
C        GET THE SIMULATION CONTROL INFO: MODEL
C
           IERD = JUGSC2 (INDEX, LRDATA, RDATA, LIDATA, IDATA, LCDATA,
     1                    CDATA)
        ELSE
C
C        GET THE SIMULATION CONTROL INFO: RESULTS
C
           IERD = JUGRS2 (IPSTFL, INDEX, LRDATA, RDATA, LIDATA, IDATA,
     1                    LCDATA, CDATA )
        ENDIF
        IF (IERD.NE.0) IERR = 1
        RETURN
        END
C
        SUBROUTINE JDBERR (TEXT, IERRNUM, ICDBF)
C
C----------------------------------------------------------------------
C     DB ERROR ROUTINE.
C
C     TEXT     THE TEXT TO PRINT IN CASE OF AN ERROR
C
C     IERRNUM  THE ERROR FLAG; POSSIBLY RETURNED FROM A DATABASE TOOL
C                      -1 = NO ERROR BUT REQUESTED INFO WAS NOT FOUND
C                       0 = NO ERROR
C                       1 = ERROR
C
C     ICDBF    THE CLOSE DATABASE FLAG
C                       0 = A DATABASE CLOSE DOES NOT NEED TO BE PERFORMED
C                       1 = A DATABASE CLOSE IS NECESSARY
C
C----------------------------------------------------------------------
```

```
C
      CHARACTER*(*) TEXT
C
      IF (IERRNUM .GT. 0) THEN
          WRITE (*, '(''*** ERROR IN '', A)') TEXT
          WRITE (*, '(''    RDBASE RUN ABORTED.'')')
          IF (ICDBF .EQ. 1) THEN
C
C             CLEAN UP THE DATABASE
C
              IERD = JLMCLE (0)
              IF (IERD .NE. 0) THEN
                  WRITE (*, '(''*** ERROR IN JLMCLE'')')
                  WRITE (*, '(''    RDBASE RUN ABORTED.'')')
              ENDIF
          ENDIF
          GOTO 100
      ENDIF
C
      IF (IERRNUM .LT. 0) THEN
          WRITE (*, '(''*** WARNING: NO'', A, '' IN THIS PROBLEM.'',
     2          A)') TEXT
          WRITE (*, '(''    RDBASE RUN ABORTED.'')')
          RETURN
      ENDIF
C
      RETURN
C
  100 STOP
      END


C######################################
C###############   SUBROUTINE QSHAPE
C######################################
      SUBROUTINE QSHAPE(S,AN,ANS)
C
C  CALCULATE THE DERIVATIVES OF
C  1). SHAPE FUNCTIONS FOR THREE-NODE EDGE ELEMENT W.R.T. S
C  2). X AND Y W.R.T. S , IN GAUSS INTEGRATION POINT
C          R --- NATURAL COORDINATE OF DIRECTION 1
C
      INCLUDE 'IMPLCT.COM'
      DIMENSION AN(3),ANS(3)
C
      AN(1) = 0.5*S*(S-1.)
      AN(2) = 1.-S*S
      AN(3) = 0.5*S*(1.+S)

      ANS(1) = S-0.5
      ANS(2) = -2.*S
      ANS(3) = S+0.5
C
      RETURN
      END

C######################################
C###############   SUBROUTINE LSHAPE
C######################################
      SUBROUTINE LSHAPE(S,AN,ANS)
C
C  CALCULATE THE DERIVATIVES OF
C  1). SHAPE FUNCTIONS FOR THREE-NODE EDGE ELEMENT W.R.T. S
C  2). X AND Y W.R.T. S , IN GAUSS INTEGRATION POINT
C          R --- NATURAL COORDINATE OF DIRECTION 1
C
      INCLUDE 'IMPLCT.COM'
      DIMENSION AN(3),ANS(3)
C
      AN(1) = 0.5*(1.-S)
      AN(2) = 0.5*(1.+S)
      AN(3) = 0.0

      ANS(1) = -0.5
      ANS(2) = 0.5
```

```
       ANS(3) = 0.
C
       RETURN
       END
```

psi.f

```
C********************     ABSTRACT     ********************************
C
C      THIS PROGRAM CALCULATES THE PROBABILITY DISTRIBUTION FUNCTION IN
C   THE GENERALIZED FLOW FIELD.
C   A TWO-DIMENSIONAL BOUNDARY VALUE PROBLEM.
C
C*********************     NOMENCLATURE     ***************************
C LAMBDA: TIME CONSTANT FOR THE RIGID DUMBELL
C ZETA:   Friction Coefficient of rigid dumbell
C L: LENGTH OF RIGID DUMBELL
C T: TEMPERATURE
C K: Boltzmann constant
C
C********************     INPUT DESCRIPTION     ***********************
C
C      INPUT IS PROVIDED TO THIS PROGRAM BY STATEMENTS AT BEGINING OF
C   THE PROGRAM.  PHYSICAL PARAMETERS AND NUMERICAL PARAMETERS ARE
C   PROVIDED IN SEPARATE SECTIONS.
C   FLOW FIELD Ux = VFC(1)*X + VFC(2)*Y + CONTANT
C             Uy = VFC(3)*X + VFC(4)*Y + CONTANT
C   VFC(5) = LAMBDA (TIME CONTANT, ZETA*L*L/(12*k*T)
C
      subroutine psi(geo,velo,totalx,totaly)
      PARAMETER (M = 41, N = 45)
      IMPLICIT DOUBLE PRECISION (A-H, O-Z)
      DIMENSION F(N*M),COE(N*M,N*M),XX(N*M)
      DIMENSION IPVT(N*M),VARC(5),VFC(5)
      dimension geo(6),velo(6),pm(6)
C*********************************************************************
C****                         INPUT DATA                       *****
C*********************************************************************
C*****************     SET PHYSICAL PARAMETERS
      call para(geo,velo,pm)

      VFC(1) = (pm(1)-pm(5))/2.
      VFC(2) = pm(2)
      VFC(3) = pm(4)
      VFC(4) = (pm(5)-pm(1))/2.
      VFC(5) = 0.1d0

c      write(*,*) "a,b,c,d",vfc
c      return
      second=4.*vfc(1)*vfc(1)+2.*(vfc(2)+vfc(3))**2.+4.*vfc(4)*vfc(4)
c      write(*,*) "second invariant",second
C*****************     SET NUMERICAL PARAMETERS
      PI=4.*ATAN(1.)
      THETA=PI/2.
C      THETA=PI
      DX=THETA/FLOAT(M-1)
      PHI=PI
      DY=PHI/FLOAT(N-1)
      DX2=DX*DX
      DY2=DY*DY
      NM=N-1
      MM=M-1
C*********************************************************************
C****                 INITIALIZE COEFFICIENT MATRIX            *****
C*********************************************************************
      NBM=N*M
      DO 10 I=1,NBM
      F(I) = 0.0
      DO 10 J=1,NBM
      COE(I,J)=0.0
10    CONTINUE
C
C*****************************************************
C Boundary conditon at  NORTH POLE, THETA = 0.0
C*****************************************************
      DO 20 J=1,N
      IJ = 1 + (J-1)*M
      COE(IJ,IJ)= 1.
```

```fortran
       F(IJ)=1.
  20 CONTINUE
C*******************************************************
C  Boundary conditon at EQUATOR, THETA = PI/2
C*******************************************************
       DO 30 J=1,N
       IJ = J*M
       COE(IJ,IJ)  =  3.
       COE(IJ,IJ-1)= -4.
       COE(IJ,IJ-2)=  1.
  30   CONTINUE
C*******************************************************
C  Boundary conditon at PHI = PI, PERIODIC
C*******************************************************
       DO 35 I=2,MM
       IJ = I + (N-1)*M
       J1 = I
       COE(IJ,J1) = 1.
       COE(IJ,IJ) = -1.
  35   CONTINUE
C*****************          INTERIOR POINTS
       DO 40 J=1,NM
       DO 40 I=2,MM
       IMJ = I-1+(J-1)*M
       IF(J.EQ.1) THEN
C       IJM = I +(N-1)*M
       IJM = I +(N-2)*M
       ELSE
       IJM = I +(J-2)*M
       ENDIF
       IJ =   I  +(J-1)*M
       IPJ = I+1+(J-1)*M
C      IF(J .EQ. N) THEN
C       IJP = I + M
C      ELSE
       IJP = I  +J*M
C      ENDIF
       X=DX*DBLE(I-1)
       Y=DY*DBLE(J-1)
       CALL VAR(X,Y,VFC,VARC)
       COE(IJ,IMJ)=(VARC(1) - VARC(3)*DX/2.)*DY2
       COE(IJ,IJM)=(VARC(2) - VARC(4)*DY/2.)*DX2
       COE(IJ,IJ)= -2.*VARC(1)*DY2 -2.*VARC(2)*DX2 + VARC(5)*DX2*DY2
       COE(IJ,IPJ)=(VARC(1) + VARC(3)*DX/2.)*DY2
       COE(IJ,IJP)=(VARC(2) + VARC(4)*DY/2.)*DX2
  40   CONTINUE
       CALL LINPAC(NBM,COE,F,XX,IPVT)

C*************************************************************************
C****            Normalize the probability distribution           *****
C*************************************************************************

       IF(MOD(N,2) .EQ. 0 .OR. MOD(M,2) .EQ. 0 ) THEN
         WRITE(*,*)"NEED ODD NUMBER FOR SIMPSON'S INTEGRATION"
       ENDIF
       TOTAL = 0.0
       DO 60 J=1,N
       SUM=0.0
       DO 50 I=1,M
       IJ=I+(J-1)*M
       if (XX(IJ) .lt. 0.) write(6,*)"warning! negative PDF",vfc
       IF(MOD(I,2).EQ.0) THEN
         FAC = 4.
       ELSE IF(I .EQ. 1 .OR. I .EQ. M) THEN
         FAC = 1.
       ELSE
         FAC = 2.
       ENDIF
       X=DX*DBLE(I-1)
       SUM=SUM+FAC*XX(IJ)*SIN(X)
  50   CONTINUE
       IF(MOD(J,2).EQ.0) THEN
         FAC = 4.
       ELSE IF(J .EQ. 1 .OR. J .EQ. N) THEN
         FAC = 1.
```

```
      ELSE
        FAC = 2.
      ENDIF
      SUM= SUM*DX/3.
      TOTAL = TOTAL + FAC*SUM
60    CONTINUE
      TOTAL= TOTAL*DY/3.
C
C****************************************************************************
C****            PRINT OUT THE PROBABILITY DISTRIBUTION            *****
C****************************************************************************
C
c     WRITE(6,302)
c     WRITE(*,304)  TOTAL
      DO 70 J=1,N
c     WRITE(6,*)
      DO 70 I=1,M
      IJ = I+(J-1)*M
c     X=DX*DBLE(I-1)*180./PI
c     Y=DY*DBLE(J-1)*180./PI
      XX(IJ)=XX(IJ)/TOTAL/2.
c     XX(IJ)=XX(IJ)
c     WRITE(6,*)X,Y,XX(IJ)
70    CONTINUE
  302 FORMAT(/)
  304 FORMAT( "# TOTAL =",E14.7)
C
C****************************************************************************
C****          CALCULATE THE PROJECTION ON THE X AND Y DIRECTION    ****
C****************************************************************************
C
      TOTALX = 0.0
      TOTALY = 0.0
      DO 90 J=1,N
      SUMX=0.0
      SUMY=0.0
      DO 80 I=1,M
      IJ=I+(J-1)*M
      IF(MOD(I,2).EQ.0) THEN
        FAC = 4.
      ELSE IF(I .EQ. 1 .OR. I .EQ. M) THEN
        FAC = 1.
      ELSE
        FAC = 2.
      ENDIF
      Y=DY*DBLE(J-1)
      X=DX*DBLE(I-1)
      SUMX=SUMX+FAC*XX(IJ)*SIN(X)*SIN(X)*abs(COS(Y))
      SUMY=SUMY+FAC*XX(IJ)*SIN(X)*SIN(X)*SIN(Y)
80    CONTINUE
      IF(MOD(J,2).EQ.0) THEN
        FAC = 4.
      ELSE IF(J .EQ. 1 .OR. J .EQ. N) THEN
        FAC = 1.
      ELSE
        FAC = 2.
      ENDIF
      SUMX= SUMX*DX/3.
      SUMY= SUMY*DX/3.
      TOTALX = TOTALX + FAC*SUMX
      TOTALY = TOTALY + FAC*SUMY
90    CONTINUE
      TOTALX= TOTALX*DY/3.
      TOTALY= TOTALY*DY/3.
c     write(*,*) "Sx,Sy", totalx, totaly
      RETURN
      END

C################################################################################
C#####  SUBROUTINE FOR EVALUATE VARIABLE COEFICIENTS OF DIFFUSION EQUATION
C################################################################################
      SUBROUTINE VAR(X,Y,VFC,VARC)
      IMPLICIT DOUBLE PRECISION (A-H, O-Z)
      DIMENSION VARC(5),VFC(5)
      S2X = SIN(X)*SIN(X)
```

```
      S2Y = SIN(Y)*SIN(Y)
      C2Y = COS(Y)*COS(Y)
      SCY = SIN(Y)*COS(Y)
      VARC(1) = S2X/12./VFC(5)
      VARC(2) = 1./12./VFC(5)
      VARC(3) = COS(X)*SIN(X)/12./VFC(5) - (VFC(1)*C2Y+
     &    (VFC(2)+VFC(3))*SCY+VFC(4)*S2Y)*SIN(X)**3.*COS(X)
      VARC(4) = ((VFC(1)-VFC(4))*SCY+VFC(2)*S2Y-VFC(3)*C2Y)*S2X
      VARC(5) = (-(VFC(1)*C2Y+(VFC(2)+VFC(3))*SCY+VFC(4)*S2Y)
     &    *(1.+3.*COS(2*X))/2.+(VFC(1)-VFC(4))*(C2Y-S2Y)
     &    +(VFC(2)+VFC(3))*SIN(2.*Y))*S2X
      RETURN
      END


      subroutine para(geo,velo,pm)
      IMPLICIT DOUBLE PRECISION (A-H, O-Z)
      dimension geo(6),velo(6),am(3,3),bm(3),xm(3),ipvt(3)
      dimension x(3),y(3),ux(3),uy(3),pm(6)
c
c Node numbering in this program.
c
      x(1) = geo(1)
      x(2) = geo(2)
      x(3) = geo(3)

      y(1) = geo(4)
      y(2) = geo(5)
      y(3) = geo(6)

      Ux(1) = velo(1)
      Uy(1) = velo(2)
      Ux(2) = velo(3)
      Uy(2) = velo(4)
      Ux(3) = velo(5)
      Uy(3) = velo(6)

c     write(*,*)"x",x
c     write(*,*)"y",y
c     write(*,*)"Ux",ux
c     write(*,*)"Uy",uy

      am(1,1) = x(1)
      am(1,2) = y(1)
      am(1,3) = 1.
      bm(1) = ux(1)
      am(2,1) = x(2)
      am(2,2) = y(2)
      am(2,3) = 1.
      bm(2) = ux(2)
      am(3,1) = x(3)
      am(3,2) = y(3)
      am(3,3) = 1.
      bm(3) = ux(3)
      CALL LINPAC(3,Am,Bm,Xm,IPVT)
      pm(1)=xm(1)
      pm(2)=xm(2)
      pm(3)=xm(3)

      am(1,1) = x(1)
      am(1,2) = y(1)
      am(1,3) = 1.
      bm(1) = uy(1)
      am(2,1) = x(2)
      am(2,2) = y(2)
      am(2,3) = 1.
      bm(2) = uy(2)
      am(3,1) = x(3)
      am(3,2) = y(3)
      am(3,3) = 1.
      bm(3) = uy(3)
      CALL LINPAC(3,Am,Bm,Xm,IPVT)
      pm(4)=xm(1)
      pm(5)=xm(2)
      pm(6)=xm(3)
```

```
c        write(*,*)pm
         return
         end
```

VITA

Tsung-Chieh Tsai

Candidate for the Degree of

Doctor of Philosophy

Thesis: MODELING AND OPTIMIZATION OF FLOW-INDUCED CRYSTALLIZATION IN POLYMER PROCESSING

Major Field: Chemical Engineering

Biographical:

Personal Data: Born in Tainan, Taiwan, August 27, 1964, the son of Chao-Chan Tsai and Chin-Ying Tsai-Hu.

Education: Graduated from Kung Shan Institute of Technology, Tainan, Taiwan in June 1984; received Bachelor of Science Degree in Chemical Engineering from National Taiwan Institute of Technology at Taipei in June, 1989; received Master of Science Degree in Chemical Engineering from Oklahoma State University at Stillwater in July, 1992; completed requirements for the Doctor of Philosophy Degree at Oklahoma State University in May, 1997.

Personal Experience: Maintenance Engineer, Jang-Dah Nylon Inc., Process control engineer, Department of Computer & Control Engineering, Advanced Control & Systems Inc., October, 1989, to July, 1990. Teaching Assistant, School of Chemical Engineering, Oklahoma State University, August, 1990 to May, 1991. Research Assistant, School of Chemical Engineering, Oklahoma State University, August, 1991, to May, 1997.